

ENCAPSULATION AND RELEASE OF CALCEIN FROM HERCEPTIN-
CONJUGATED E-LIPOSOMES

by

Mah Noor Zafar

A Thesis presented to the Faculty of the
American University of Sharjah
College of Engineering
In Partial Fulfilment
of the Requirements
for the Degree of

Master of Science in
Biomedical Engineering

Sharjah, United Arab Emirates

June 2023

Declaration of Authorship

I declare that this thesis is my own work and, to the best of my knowledge and belief, it does not contain material published or written by a third party, except where permission has been obtained and/or appropriately cited through full and accurate referencing.

Signed Mah Noor Zafar

Date 23rd June, 2023

The Author controls the copyright for this report.

Material should not be reused without the consent of the author. Due acknowledgement should be made where appropriate.

© Year 2023

Mah Noor Zafar

ALL RIGHTS RESERVED

Approvals

We, the undersigned, approve the Master's Thesis written by: Mah Noor Zafar.

Thesis Title: Encapsulation and Release of Calcein from Herceptin-conjugated eLiposomes.

Date of Defence: 22/06/2023

Name, Title and Affiliation

Signature

Dr. Ghaleb Husseini
Professor,
Department of Chemical and Biological Engineering
Thesis Advisor

Dr. Karnail Singh
Senior Lecturer,
Department of Chemical and Biological Engineering
Thesis Committee Member

Dr. Wael Abuzaid
Associate Professor,
Department of Mechanical Engineering
Thesis Committee Member

Accepted by

Dr. Fadi Aloul
Dean
College of Engineering

Dr. Mohamed El-Tarhuni
Vice Provost for Research and Graduate Studies
Office of Research and Graduate Studies

Acknowledgements

I want to thank my advisor and mentor, Dr. Ghaleb Husseini, for not only sharing his vast knowledge and expertise but also investing and dedicating his time to understanding my strengths and aspirations. His constructive feedback has helped me think critically. I want to thank Prof. William Pitt for his valuable guidance and support. I also want to thank all the professors who taught me master-level courses, especially Dr. Abdulrahim Shamayleh, Dr. Vian Ahmed, and Dr. Mohamed Abdelgawad, for their commitment to my growth and their faith in me, that inspired me to push my limits and achieve more than I thought was possible.

Dedication

To my loving and supportive husband, Farhan Qadir Baksh...

Abstract

Cancer is one of the deadliest diseases afflicting humanity with no definitive cure. Its heterogeneous nature poses significant challenges. Currently, available cancer treatments such as; chemotherapy, radiation therapy, surgery, etc., have successfully addressed specific types of cancer. However, their side effects reduce the quality of patient life. Fortunately, new approaches involving triggered site-specific delivery of therapeutic drugs using nanoparticles are being devised to provide a personalized and definitive cure for all types of cancer. Surface modification of liposomes with targeting moieties specific to the receptors on the surface of cancer cells enhances the selectivity of the drug delivery systems and reduces off-target effects. Furthermore, external triggers, such as ultrasound, have surfaced as a promising tool to foster triggered and controlled release of the encapsulated drug. The application of low-frequency ultrasound can induce various mechanical and thermal effects that help disrupt liposomal membranes and trigger the release of encapsulated drugs. This study assessed liposomal encapsulation of sono-sensitive phase-changing perfluoro pentane (PFC5) nanoemulsion droplets alongside Herceptin (Trastuzumab) as a targeting moiety. Four liposomal formulations, namely; NH₂ liposomes, emulsion liposomes (eLiposomes), Herceptin-conjugated liposomes, and Herceptin-conjugated eLiposomes, were synthesized, and characterization tests and assays were conducted throughout the thesis to evaluate the properties of different liposomal-formulations. The size was assessed using dynamic light scattering, whereas the lipid and protein content of the liposomes was assessed using the Stewart and bicinchoninic acid assays, respectively. Low-frequency ultrasound (20kHz) at power densities (6.2, 9, and 10 mW/cm²) was then used to trigger the release of the encapsulated drug from liposomes. Herceptin-conjugated emulsion liposomes showed significantly higher release than the rest of the formulations at all three power densities investigated. Furthermore, the zero-order kinetic model was observed to be the best fit for all the liposomal formulations used in this study. Conjugating an antibody to a nanocarrier encapsulating a chemotherapeutic agent and triggering the latter's release using ultrasound show promise in the quest for a magic bullet that reduces the side effects of chemotherapy.

Keywords: Drug Delivery, Ultrasound, targeted therapy, e-liposomes, emulsion liposomes.

Table of Contents

Abstract.....	6
List of Figures.....	10
List of Tables.....	17
List of Abbreviations.....	18
Chapter 1. Introduction.....	19
1.1 Overview.....	19
1.2 Causes of cancer.....	20
1.3 Cancer cell characteristics.....	21
1.3.1 Hypoxic and Acidic Microenvironment.....	21
1.3.2 Cancer cells' ability to spread.....	22
1.3.3 Shape and Size.....	22
1.4 Statistics about the different types of cancers.....	23
1.5 Cancer treatments.....	24
1.5.1 Surgery.....	24
1.5.2 Chemotherapy.....	24
1.5.3 Radiation therapy.....	25
1.5.4 Hormonal therapy.....	25
1.5.5 Targeted therapy.....	26
1.5.6 Immunotherapy.....	26
1.6 Thesis Objectives.....	27
1.7 Research Contribution.....	27
1.8 Thesis Organization.....	28
Chapter 2 Background and Literature Review.....	29
2.1 Nanoparticles (NPs) as drug delivery system.....	29
2.2 Characteristics of NPs.....	29
2.3 Types of NPs.....	30
2.3.1 Polymeric Micelles.....	30
2.3.2 Dendrimers.....	31

	2.3.3 Liposomes	32
2.4	Ultrasound (US) as an external trigger	54
	2.4.1 US-induced effects on liposomes	54
	2.4.2 Advantages and disadvantages of ultrasound.....	57
	2.4.3 Enhancing liposomal sensitivity to ultrasound.....	58
Chapter 3	Methodology	70
3.1	Materials	70
3.2	Procedures	70
	3.2.1 Preparation of PFC5 nanoemulsion droplets.....	70
	3.2.2 Preparation of calcein-encapsulated DSPE-PEG-NH ₂ control liposomes.....	71
	3.2.3 Preparation of emulsion liposomes (eLiposomes)	71
	3.2.4 Preparation of Trastuzumab-conjugated liposomes	72
	3.2.5 Preparation of Trastuzumab-conjugated eLiposomes	73
	3.2.6 Size and polydispersity evaluation using Dynamic Light Scattering (DLS).....	73
	3.2.7 Quantification of Lipid content of the prepared liposomal formulations using Stewart Assay.....	74
	3.2.8 Quantification of antibody conjugation using bicinchoninic acid (BCA) assay	76
	3.2.9 Cryogenic transmission electron microscopy (Cryo-TEM).....	77
	3.2.10 Low-frequency ultrasound release of calcein	78
	3.2.11 Statistical analysis.....	79
	3.2.12 Kinetic modeling of drug release.....	79
Chapter 4	Results and Analysis	82
4.1	Estimation of size using Dynamic Light Scattering (DLS).....	82
4.2	Quantification of total lipid concentration using the Stewart Assay	85
4.3	Estimation of protein content through BCA assay	85
4.4	Cryogenic electron microscopy (Cryo-TEM) images:	87
4.5	Stimulation of drug release from liposomal formulations using low-frequency ultrasound (LFUS):	87

4.6	Kinetic Modeling:	95
4.6.1	Control liposomes release modeling	95
4.6.2	eLiposomes release modeling	96
4.6.3	HER-conjugated liposomes release modeling.....	96
4.6.4	HER-conjugated eLiposomes release modeling.....	97
Chapter 5. Conclusion and Future Work		100
References.....		101
Appendix A: Control Liposomes Kinetic Modeling.....		102
Appendix B: eLiposomes kinetic Modeling		119
Appendix C: HER-conjugated liposomal kinetic modeling		128
Appendix D: HER-conjugated eLiposomal kinetic modeling.....		137
Vita.....		146

List of Figures

Figure 1-1 Difference between cancer cells and normal cells [10]	22
Figure 2-1 Schematic illustration of a polymeric micelle [20]	30
Figure 2-2 Schematic illustration of a dendrimer [18].....	31
Figure 2-3 Classification of liposomes based on size and number of lamellae [27] ...	33
Figure 2-4 Structural illustrations of components of liposomes a) structure of glycerophospholipid b) structure of sphingomyelin. c) structure of cholesterol [27]	34
Figure 2-5 A schematic diagram of an amphiphilic liposome with a hydrophilic (red) drug in its core and a lipophilic (green) drug encapsulated in the phospholipid bilayer [16].	35
Figure 2-6 Schematic representation of conventional and surface-modified liposomes [27].....	37
Figure 2-7 Graphical representation of uptake of DOX liposomes as a function of folate targeting content [32]	38
Figure 2-8 Tf transports ferric iron to the TfR1 receptor via receptor-mediated endocytosis, where Tf and ferric iron disassemble in the endosome, with ferric iron reduced to ferrous iron, which enters the cytosol [33].....	39
Figure 2-9 Graphical representation of Tf-CPP conjugated liposomes for targeting brain through BBB, with kFGF-Tf showing the superior ability in overcoming the BBB [39].....	41
Figure 2-10 Schematic illustrating the active and passive targeting techniques of liposomes into specific tumor tissues for enhanced efficacy of therapeutic agents	43
Figure 2-11 Different active loading techniques employing pH and ion concentration gradients [25].	47
Figure 2-12 Liposomal bilayer phase transition from gel phase to liquid crystalline phase under the influence of temperature [25].....	50
Figure 2-13 Schematic illustration showcasing a liposome-based drug delivery system for the treatment of tumors.....	52
Figure 2-14 Active targeting strategies using nanoparticles [49]	53
Figure 2-15 Ultrasound-induced thermal effects [49]	55

Figure 3-1 Structural illustration of Conjugation of Herceptin to DSPE-PEG-NH ₂ with cyanuric chloride as a coupling agent [35]	72
Figure 3-2 Dynamic Light Scattering machine set up	74
Figure 4-1 Size distribution of control liposomes, emulsions, eLiposomes, HER-conjugated liposomes and HER-conjugated eLiposomes	84
Figure 4-2 The difference in color intensity observed between control liposomes (left) and Herceptin-conjugated liposomes (right)	86
Figure 4-3 Cryo-TEM images for liposomes encapsulated with nanoemulsions	87
Figure 4-4 Comparison of Cumulative Fractional Release from control liposomes, eLiposomes, HER-conjugated liposomes and HER-conjugated eLiposomes at 6.2mW/cm ² power density	87
Figure 4-5 Comparison of Cumulative Fractional Release from control liposomes, eLiposomes, HER-conjugated liposomes and HER-conjugated eLiposomes at 9mW/cm ² power density	87
Figure 4-6 Comparison of Cumulative Fractional Release from control liposomes, eLiposomes, HER-conjugated liposomes and HER-conjugated eLiposomes at 10mW/cm ² power density	88
Figure 4-7 Comparison of cumulative fractional release from control liposomes after four pulses at different power densities	91
Figure 4-8 Comparison of cumulative fractional release from control liposomes after four pulses at different power densities	91
Figure 4-9 Comparison of cumulative fractional release from control liposomes after four pulses at different power densities	91
Figure 4-10 Comparison of cumulative fractional release from control liposomes after four pulses at different power densities	92
Figure 4-11 Comparison of differential fractional release from control liposomes after individual pulses at different power densities	98
Figure 4-12 Comparison of differential fractional release from eLiposomes after individual pulses at different power densities	98
Figure 4-13 Comparison of differential fractional release from Her-liposomes after individual pulses at different power densities	99
Figure 4-14 Comparison of differential fractional release from HER-eLiposomes after individual pulses at different power densities	99

Figure A-1 Calcein release from control Liposomes (Batch 1) at 6.2 mW/cm ² fitting Zero-order Model	114
Figure A-3 Calcein release from control Liposomes (Batch 1) at 6.2 mW/cm ² fitting First-order Model.....	114
Figure A-4 Calcein release from control Liposomes (Batch 2) at 6.2 mW/cm ² fitting First-order Model.....	115
Figure A-5 Calcein release from control Liposomes (Batch 3) at 6.2 mW/cm ² fitting Zero-order Model	115
Figure A-6 Calcein release from control Liposomes (Batch 3) at 6.2 mW/cm ² fitting First-order Model.....	116
Figure A-7 Calcein release from control Liposomes (Batch 1) at 9 mW/cm ² fitting Zero- order Model	116
Figure A-8 Calcein release from control Liposomes (Batch 1) at 9 mW/cm ² fitting First- order Model	117
Figure A-9 Calcein release from control Liposomes (Batch 2) at 9 mW/cm ² fitting Zero- order Model	117
Figure A-10 Calcein release from control Liposomes (Batch 2) at 9 mW/cm ² fitting First-order Model.....	118
Figure A-11 Calcein release from control Liposomes (Batch 3) at 9 mW/cm ² fitting Zero-order Model	118
Figure A-12 Calcein release from control Liposomes (Batch 3) at 9 mW/cm ² fitting First-order Model.....	119
Figure A-13 Calcein release from control Liposomes (Batch 1) at 10 mW/cm ² fitting Zero-order Model	119
Figure A-14 Calcein release from control Liposomes (Batch 1) at 10 mW/cm ² fitting First-order Model.....	120
Figure A-15 Calcein release from control Liposomes (Batch 2) at 10 mW/cm ² fitting Zero-order Model	120
Figure A-16 Calcein release from control Liposomes (Batch 2) at 10 mW/cm ² fitting First-order Model.....	121
Figure A-17 Calcein release from control Liposomes (Batch 3) at 10 mW/cm ² fitting Zero-order Model	121

Figure A-18 Calcein release from control Liposomes (Batch 3) at 10 mW/cm ² fitting First-order Model.....	122
Figure B-1 Calcein release from eLiposomes (Batch 1) at 6.2 mW/cm ² fitting First-order Model	122
Figure B-2 Calcein release from eLiposomes (Batch 1) at 6.2 mW/cm ² fitting Zero-order Model	123
Figure B-3 Calcein release from eLiposomes (Batch 2) at 6.2 mW/cm ² fitting First-order Model	123
Figure B-4 Calcein release from eLiposomes (Batch 2) at 6.2 mW/cm ² fitting Zero-order Model	124
Figure B-5 Calcein release from eLiposomes (Batch 3) at 6.2 mW/cm ² fitting First-order Model	124
Figure B-6 Calcein release from eLiposomes (Batch 3) at 9 mW/cm ² fitting Zero-order Model.....	125
Figure B-7 Calcein release from eLiposomes (Batch 1) at 9 mW/cm ² fitting First-order Model.....	125
Figure B-8 Calcein release from eLiposomes (Batch 1) at 9 mW/cm ² fitting Zero-order Model.....	126
Figure B-9 Calcein release from eLiposomes (Batch 2) at 9 mW/cm ² fitting First-order Model.....	126
Figure B-10 Calcein release from eLiposomes (Batch 2) at 9 mW/cm ² fitting Zero-order Model.....	127
Figure B-11 Calcein release from eLiposomes (Batch 3) at 9 mW/cm ² fitting First-order Model.....	127
Figure B-12 Calcein release from eLiposomes (Batch 3) at 10 mW/cm ² fitting Zero-order Model	128
Figure B-13 Calcein release from eLiposomes (Batch 1) at 10 mW/cm ² fitting First-order Model	128
Figure B-14 Calcein release from eLiposomes (Batch 1) at 10 mW/cm ² fitting Zero-order Model	129
Figure B-15 Calcein release from eLiposomes (Batch 2) at 10 mW/cm ² fitting First-order Model	129

Figure B-16 Calcein release from eLiposomes (Batch 2) at 10 mW/cm ² fitting Zero-order Model	130
Figure B-17 Calcein release from eLiposomes (Batch 3) at 10 mW/cm ² fitting First-order Model	130
Figure B-18 Calcein release from eLiposomes (Batch 3) at 10 mW/cm ² fitting First-order Model	131
Figure C-1 Calcein release from Herceptin-conjugated liposomes (Batch 1) at 6.2 mW/cm ² fitting First-order Model.....	131
Figure C-2 Calcein release from Herceptin-conjugated liposomes (Batch 1) at 6.2 mW/cm ² fitting Zero-order Model	132
Figure C-3 Calcein release from Herceptin-conjugated liposomes (Batch 2) at 6.2 mW/cm ² fitting First-order Model.....	132
Figure C-4 Calcein release from Herceptin-conjugated liposomes (Batch 2) at 6.2 mW/cm ² fitting Zero-order Model	133
Figure C-5 Calcein release from Herceptin-conjugated liposomes (Batch 3) at 6.2 mW/cm ² fitting First-order Model.....	133
Figure C-6 Calcein release from Herceptin-conjugated liposomes (Batch 3) at 9 mW/cm ² fitting Zero-order Model	134
Figure C-7 Calcein release from Herceptin-conjugated liposomes (Batch 1) at 9 mW/cm ² fitting First-order Model.....	134
Figure C-8 Calcein release from Herceptin-conjugated liposomes (Batch 1) at 9 mW/cm ² fitting Zero-order Model	135
Figure C-9 Calcein release from Herceptin-conjugated liposomes (Batch 2) at 9 mW/cm ² fitting First-order Model.....	135
Figure C-10 Calcein release from Herceptin-conjugated liposomes (Batch 2) at 9 mW/cm ² fitting Zero-order Model	136
Figure C-11 Calcein release from Herceptin-conjugated liposomes (Batch 3) at 9 mW/cm ² fitting First-order Model.....	136
Figure C-12 Calcein release from Herceptin-conjugated liposomes (Batch 3) at 10 mW/cm ² fitting Zero-order Model	137
Figure C-13 Calcein release from Herceptin-conjugated liposomes (Batch 1) at 10 mW/cm ² fitting First-order Model.....	137

Figure C-14 Calcein release from Herceptin-conjugated liposomes (Batch 1) at 10 mW/cm ² fitting Zero-order Model	138
Figure C-15 Calcein release from Herceptin-conjugated liposomes (Batch 2) at 10 mW/cm ² fitting First-order Model.....	138
Figure C-16 Calcein release from Herceptin-conjugated liposomes (Batch 2) at 10 mW/cm ² fitting Zero-order Model	139
Figure C-17 Calcein release from Herceptin-conjugated liposomes (Batch 3) at 10 mW/cm ² fitting First-order Model.....	139
Figure C-18 Calcein release from Herceptin-conjugated liposomes (Batch 3) at 10 mW/cm ² fitting First-order Model.....	140
Figure D-1 Calcein release from Herceptin-conjugated eLiposomes (Batch 1) at 6.2 mW/cm ² fitting First-order Model.....	140
Figure D-2 Calcein release from Herceptin-conjugated eLiposomes (Batch 1) at 6.2 mW/cm ² fitting Zero-order Model	141
Figure D-3 Calcein release from Herceptin-conjugated eLiposomes (Batch 2) at 6.2 mW/cm ² fitting First-order Model.....	141
Figure D-4 Calcein release from Herceptin-conjugated eLiposomes (Batch 2) at 6.2 mW/cm ² fitting Zero-order Model	142
Figure D-5 Calcein release from Herceptin-conjugated eLiposomes (Batch 3) at 6.2 mW/cm ² fitting First-order Model.....	142
Figure D-6 Calcein release from Herceptin-conjugated eLiposomes (Batch 3) at 9 mW/cm ² fitting Zero-order Model	143
Figure D-7 Calcein release from Herceptin-conjugated eLiposomes (Batch 1) at 9 mW/cm ² fitting First-order Model.....	143
Figure D-8 Calcein release from Herceptin-conjugated eLiposomes (Batch 1) at 9 mW/cm ² fitting Zero-order Model	144
Figure D-9 Calcein release from Herceptin-conjugated eLiposomes (Batch 2) at 9 mW/cm ² fitting First-order Model.....	144
Figure D-10 Calcein release from Herceptin-conjugated eLiposomes (Batch 2) at 9 mW/cm ² fitting Zero-order Model	145
Figure D-11 Calcein release from Herceptin-conjugated eLiposomes (Batch 3) at 9 mW/cm ² fitting First-order Model.....	145

Figure D-12 Calcein release from Herceptin-conjugated eLiposomes (Batch 3) at 10 mW/cm ² fitting Zero-order Model	146
Figure D-13 Calcein release from Herceptin-conjugated eLiposomes (Batch 1) at 10 mW/cm ² fitting First-order Model.....	146
Figure D-14 Calcein release from Herceptin-conjugated eLiposomes (Batch 1) at 10 mW/cm ² fitting Zero-order Model	147
Figure D-15 Calcein release from Herceptin-conjugated eLiposomes (Batch 2) at 10 mW/cm ² fitting First-order Model.....	147
Figure D-16 Calcein release from Herceptin-conjugated eLiposomes (Batch 2) at 10 mW/cm ² fitting Zero-order Model	148
Figure D-17 Calcein release from Herceptin-conjugated eLiposomes (Batch 3) at 10 mW/cm ² fitting First-order Model.....	148
Figure D-18 Calcein release from Herceptin-conjugated eLiposomes (Batch 3) at 10 mW/cm ² fitting First-order Model.....	149

List of Tables

Table 1-1 The statistics of the total deaths caused by the U.S.'s top three leading causes of death [2]	19
Table 3-1 The sample preparation of the Stewart Assay	75
Table 3-2 BCA assay sample preparation.....	77
Table 4-1 DLS results for control and HER-conjugated liposomes	82
Table 4-2 DLS results for emulsions, eLiposomes and HER-conjugated eLiposomes	83
Table 4-3 Stewart Assay results for control liposomes and HER-conjugated liposomes	85
Table 4-4 BCA assay results for control liposomes and HER-conjugated liposomes.	86
Table 4-5 Statistical comparison of cumulative fractional release values at different power densities after the first pulse	93
Table 4-6 Statistical comparison of cumulative fractional release values at different power densities after the second pulse	94
Table 4-7 Comparison of the average fractional release values at different power densities after first pulse.....	94
Table 4-8 Comparison of the average fractional release values at different power densities after first pulse.....	95
Table 4-9 R ² values for calcein release from control liposomes.....	95
Table 4-10 R ² values for calcein release from eLiposomes.....	96
Table 4-11 R ² values for calcein release from HER-conjugated liposomes.....	97
Table 4-12 R ² values for calcein release from HER-conjugated eLiposomes.....	97

List of Abbreviations

DLS	Dynamic Light Scattering
EPR	Enhanced Permeability and Retention
HER	Herceptin
LFUS	Low-frequency ultrasound
DSPE-PEG-NH ₂	1,2-Distearoyl-sn-glycero-3-phosphorylethanolamine- polyethylene-glycol-Amine
DPPC	Dipalmitoylphosphatidylcholine

Chapter 1. Introduction

2.1 Overview

Humanity's never-ending fight against cancer and recent advances in nanotechnology has led to considerable interest in providing researchers to devise ways to tackle this fatal disease. Recent statistics show that cancer is the second leading cause of death globally, following cardiovascular disease. One out of six people dies of cancer. A total of 3,383,729 deaths occurred in the U.S. in the year 2020. The coronavirus disease 19 (COVID-19) pandemic is considered one of the worst health disasters. It is ranked third among the leading causes of death, following cancer which secures the second rank among leading causes of death. According to projections made by the American Cancer Society, it is estimated that in 2023, there will be 1,958,310 new cancer cases and 609,820 cancer-related deaths[1]. Table 1-1 [2] shows the statistics of the total deaths caused by the US's top three leading causes of death.

Table 1-1 The statistics of the total deaths caused by the U.S.'s top three leading causes of death [2]

Death causes	Total number of deaths	% of total deaths
Heart disease	696,962	20.6%
Cancer	602,350	17.8%
COVID-19	350,831	10.4%

In the UAE, cancer falls in third place, with a death rate of 10.26 per 100,000 people, preceded by cardiovascular disease and trauma. Breast cancer is the most commonly occurring cancer amongst the population in the UAE, specifically affecting women, and ranked first among cancer deaths with 110 deaths [3].

Tumors can be further classified into benign tumors, localized masses of cells that do not spread, and malignant tumors that grow uncontrollably, spreading to different body parts. Moreover, a malignant tumor may lead to other threatening events called tumor metastasis. Cancer cells can spread (i.e., metastasize) to other body parts via the bloodstream or lymphatic system, relocating and causing secondary malignant tumor

sites in the lungs, liver, bone, and brain. This, however, will require early detection of the tumor along with proper cancer treatment [2], [4]-[5].

Symptoms of cancerous cells depend on the location of cell growth; nevertheless, they do not show any signs during the early development stage. The local signs of cancer depend on the site of the mass of over-growing cells and ulceration. A tumor mass in the brain may affect and interfere with brain function, or a growing mass of lung cells may obstruct the bronchus leading to respiratory failures [6].

2.2 Causes of cancer

As stated earlier, cancer is the rapid growth of cells; moreover, this intractable growth of cells is caused due to genes undergoing mutations within the DNA. DNA holds genetic information that is a map of protein production in the body. Proteins are responsible for cell division and growth, whereas other proteins are responsible for suppressing growth. Mutations are modifications in the DNA gene sequence, and this change in genotype results in a changed phenotype and abnormal production or abnormally functioning proteins. The root cause of this genetic defect could be hereditary, i.e., inherited from parents known as “Germline mutations” or external factors that interact with genetic factors, increasing the risk of developing cancer by exposure to these factors. These factors involve physical carcinogens such as; ionizing radiation and ultraviolet radiation, chemical carcinogens; such as alcohol, tobacco smoke components, arsenic (a drinking water contaminant), aflatoxin (a food contaminant), etc., as well as factors that increase the risk of developing cancer, i.e., acquired by exposure to mutagens such as; sunlight, chemicals, carcinogens, radiation, nitrites, etc., called “acquired mutations.” [7].

Cells undergo hundreds of mutations every day. Apoptosis is a beneficial programmed cell death (cell suicide) that clears out the old or damaged cells and replaces them with new ones. If this biologically healthy cell death mechanism is disrupted, it may lead to the formation of solid tumors (non-solid tumors, in the case of lymphoma). Moreover, cancer proliferation may lead to other threatening events called stage IV cancer or tumor metastasis, spreading malignant cancerous cells to other parts of the body and causing secondary malignant tumor sites. To avoid this, early tumor detection along with proper cancer treatment are desperately needed [2].

Cancer cells form as a result of the following cell physiology alterations:

- Undergoing pathological mitosis due to the activation of oncogenes.
- Becoming unresponsive to growth-inhibitory signals by deactivating tumor suppressor genes, such as Rb.
- Suppressing and deactivating genes that enable apoptosis.
- Activating specific gene pathways which allow unlimited replication and makes them immortal.
- Producing their blood vessels through tumor angiogenesis.
- Relocating and invading other tissues and cells and multiplying in these tissues, hence spreading throughout the body [5].

2.3 Cancer cell characteristics

Cancer cells show different characteristics compared to normal healthy cells (see Figure 1-1), which will be discussed in the upcoming sections.

2.3.1 Hypoxic and Acidic Microenvironment

Tumor cells may undergo enhanced cell proliferation into late stages, and these rapidly growing cells require an oxygen-rich environment and nutrients to meet their demand due to increased metabolism; however, such an environment does not exist within the body to fulfill this demand. This leads to an imbalance between the available amounts of oxygen and the metabolic needs of cancer cells, also known as hypoxia. To meet this demand, tumor cells, with their chemical signaling processes, employ growth factors such as Vascular Endothelial Growth Factors (VEGF) to form new blood vessels. This process is called tumor angiogenesis (generating new blood vessels to feed and grow the tissue). Unlike healthy cells, Cancer cells' abnormal signaling pathways lead to an unnecessary, imbalanced, disorganized, and uneven arrangement, poorly forming vascular system and capillary growth, leaky endothelial cells, and increased vascular permeability due to pores. The vascular system also includes the development of an abnormal lymphatic system (tumor lymph angiogenesis), which instead of draining lymph fluid, retains it and accumulates waste particles within the infected tumor tissue [2], [8].

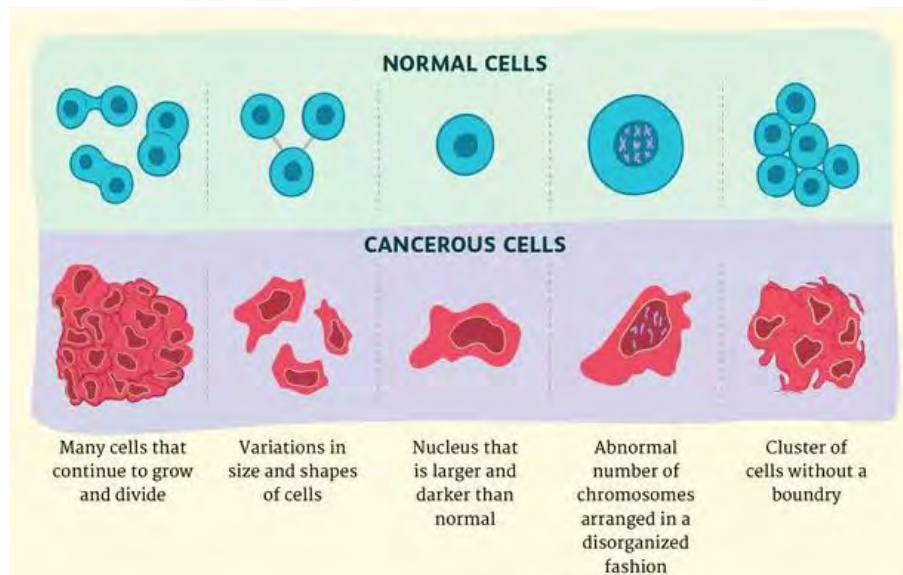


Figure 1-1 Difference between cancer cells and normal cells [10]

Due to a hypoxic state, cancer cells demonstrate a metabolic shift to compensate for increased oxygen and metabolic demands. Consequently, mutations in oncogenes and overexpression of Hypoxia Inducible Factor (HIF) enable cancer cells to adopt glycolysis as a respiring anaerobically instead of aerobic oxidative phosphorylation method. Glycolysis leads to excess lactic acid production and protons due to ATP hydrolysis, leading to a lower pH value, making them acidic compared to healthy cells. Reduced nutrients and waste accumulation create a hypoxic and acidic microenvironment [8], [9].

2.3.2 Cancer cells' ability to spread

Unlike normal cells, cancer cells lack adhesion molecules that stick cells to nearby cells. As discussed earlier, this helps cancer cells get free, detach from their original location, and travel to various body parts. This detached cancer cell colonizes other body parts by further dividing and growing in its new location, forming new tumors far away from the original tumor [8], [9].

2.3.3 Shape and Size

Normal cells have a fixed shape and size; however, unlike normal cells, cancer cells and their nuclei exhibit an abnormal shape and variability in size. The nucleus of cancer cells also appears to be darker than the normal cell nucleus due to the

overabundance of DNA enclosed with an unorganized and atypical number of chromosomes [10], [11]-[13].

Ability to escape the immune system

Normal damaged cells are removed by being tagged and engulfed by the immune system (lymphocytes). However, cancer cells can trick the immune system by secreting chemicals that deactivate the patrolling immune cells [10].

2.4 Statistics about the different types of cancers

As elaborated earlier, there are more than 100 types of existing cancers, depending on the tissue or organ undergoing abnormal growth of cells. However, depending on the cells that undergo this genetic anomaly, cancer can be classified into the following major types: carcinomas, sarcomas, melanomas, lymphomas, and leukemias [2], [14].

- Carcinomas are initiated in the epithelial cells, which enclose the lining (outside and inside) of body surfaces, including organs, glands, etc.
- Sarcomas are tumors that begin in connective tissues such as; muscles, tendons, ligaments, blood vessels, lymph vessels, fat, bone, etc.
- Leukemia begins in the bone marrow, within the tissue that forms blood. It leads to abnormal growth of leukemia cells, i.e., white blood cells that outnumber the rest of the blood cells, inhibiting other blood cells' development.
- Lymphoma initiates in lymphocytes (T and B cells), which play a significant role in the immune system against fighting foreign antigens and diseases. In this type of cancer, abnormal lymphocytes accumulate in lymph nodes, lymph vessels, and other organs such as the breast and brain.
- Myeloma is a cancerous growth of plasma cells which are immune cells, building up in the bone marrow and forming bone tumors throughout the body.
- Melanoma is a type of cancer that begins in melanocytes (skin pigment cells) that make melanin, a pigment that gives skin its color. Melanomas can form on the skin and pigmented tissue, like in the eyes [2], [14].

2.5 Cancer treatments

Cancer treatments vary according to the nature or type of cancer and the stage to which the cancerous cell may have advanced. Many cancer treatment strategies are currently being used in clinics, including chemotherapy, radiotherapy, surgery, hormonal therapy, targeted therapy, immunotherapy, or a combination of these methods. Some treatments may also involve various combinations of the below-mentioned treatments to maximize the effect of the treatment [6], [15], [16]. However, these treatments are associated with side effects, as discussed below.

2.5.1 Surgery

A surgical operation aims to extract or altogether remove the locally grown mass of cancerous cells or a complete organ; it can also serve as a partial or complete cure for the tumor. These include; mastectomy of the breast, neurosurgery for the brain, treating prostate cancer through prostatectomy, etc. However, surgical procedure is limited to small-sized or locally spread cancers. Even if a minute-sized invisible cancerous cell were left behind during the procedure, it would lead to a new tumor. Surgery is impossible for blood or bone marrow-related cancers, i.e., hematological ones. Another limitation involves metastasis, where cancer spreads to different parts of the body, and hence the complete removal of cancer cells becomes impossible [6], [18].

2.5.2 Chemotherapy

Chemotherapy uses “Chemo” – chemicals administered intravenously to intervene with cancer cell division and cell growth and kill these fast-growing cells. It is considered an effective cancer treatment method. Combination chemotherapy can also be employed by administering two or more drugs for cancer treatment. However, these anticancer drugs have demonstrated severe toxic effects and kill both cancerous and healthy cells, or any fast-growing cell in the body such as; hair cells (hence the reason behind the hair fall), as they do not specifically target cancer cells [6], [13], [19]-[22]. Anti-neoplastic agents for chemotherapy induce toxic side effects such as cardiotoxicity, tissue necrosis, and secondary malignancies in the case of doxorubicin (DOX), nephrotoxicity, hepatotoxicity, etc., among others. Moreover, healthy cells demonstrated a faster reproduction rate than cancerous cells post-chemotherapy [12].

Mudd TW Jr. and colleagues studied the cardiotoxic side effects induced by anticancer drugs, such as anthracyclines, like DOX, which cause cardiotoxicity via topoisomerase II inhibition, resulting in heart failure [11].

2.5.2.1 Drug cocktail chemotherapy

A drug cocktail is a treatment method that uses multiple drugs instead of one during chemotherapy, also called combination chemotherapy delivery, depending on the drug's pharmacokinetics [11].

Multi-Drug Resistance (MDR): Cancer cells develop resistance against a wide range of anticancer drugs, rendering the chemotherapeutic drug ineffective. Tumor tissue is an intelligent group of cells that starts working against the anticancer drug by decreasing the anticancer drug uptake, increasing the extrusion of the drug, evading drug-induced apoptosis, and activating detoxifying and DNA repair mechanisms against the chemotherapeutic drug [23],[24]-[26]. To combat this, the drug must be instantly released into the tumor cells using trigger mechanisms such as light, ultrasound, etc. [27].

2.5.3 Radiation therapy

This method employs a very high dose of ionization radiation, such as X-rays, to destroy cancer cells by directly harming their DNA or by generating free radicals within cancer cells to damage the DNA. Radiation therapy can be used for different cancers, including leukemia and lymphoma. However, some of the disadvantages of radiation therapy include; that it induces side effects on nearby organs and tissues; hence it cannot be used if the tumor is located in a highly vulnerable location. It cannot be used on children or when cancer has progressed to an advanced stage[6].

2.5.4 Hormonal therapy

This technique intervenes with cancer cell growth by altering body hormones that may be important for developing specific cancer types. However, this treatment is only limited to cancers associated with the reproductive system, breast, or prostate. Side effects depend on the type of drug used in this method, type of cancer, patient age, sex, etc. [6].

Cancer therapeutic methods can also be combined to enable synergistic effects; for example, radiation and chemotherapy can significantly drop cancerous cells' growth rates by increasing cell apoptosis, as studied by Wagner & Yang [12]. However, it can lead to toxicity and severe side effects, limiting chemotherapeutic drug doses.

2.5.5 Targeted therapy

Targeted therapy targets specific receptors overexpressed on the surface of cancer cells to increase effectiveness. This involves targeting and interfering with the function of specific proteins and genes resulting from a genetic mutation that helps in the growth and survival of cancerous cells. It confines and localizes the drug and its effect on specific tumor cells without affecting nearby regions. This helps improve the efficiency and efficacy of the drug, meanwhile reducing the side effects on other cells and tissues. For instance, targeted therapy delivers the medication to targeted tissue instead of circulating in the body and damaging other cells; this method requires lesser doses of the economically preferable therapeutic drug and reduces the side effects. However, unlike chemotherapy, which induces cell death, targeted therapy prevents cell division and growth [28].

2.5.6 Immunotherapy

An example of target therapy is immunotherapy which stimulates and improves the body's natural defense mechanism and helps target and fight cancer cells. Since cancer cells are the body's mutated cells, it is hard for the immune system to recognize them. To aid the immune system, immune therapy marks the cancer cells so that the immune system can locate and kill them. However, cancer cells may become resistant to targeted therapy, and another disadvantage involves the difficulty of developing drugs based on specific target structures, target functions within a cell, etc. [28].

Researchers have introduced smart drug delivery systems to overcome the side effects associated with conventional cancer treatments, e.g., chemotherapy. It provides targeted delivery of therapeutic drugs directly to cancer cells, thus reducing systemic side effects and minimizing damage to healthy cells. These smart drug delivery systems utilize several techniques to enhance drug efficacy and improve patient outcomes. Examples include; nanoparticle-based drug delivery, stimuli-responsive drug delivery, antibody-drug conjugates (ADCs), and implantable drug delivery. The early smart drug

delivery system used in cancer treatment is the liposomal formulation of doxorubicin, which was approved by the Food and Drug Administration (FDA) in 1995 called “Doxil” or Caelyx.” It is an early milestone in developing SDDS for improved cancer therapy. It offers several advantages over conventional doxorubicin, as the tiny lipid vesicles contain and protect doxorubicin from degrading, thus improving its circulation time in the bloodstream and providing a controlled release at the tumor site[4], [29].

2.6 Thesis Objectives

This research aims to devise an enhanced approach for administering anticancer therapeutic agents via ligand-conjugated liposomes in conjunction with ultrasound as an external stimulus. To realize these objectives, the following aims were established:

1. Synthesize non-targeted control liposomes using the thin-film hydration method.
2. Synthesize emulsion liposomes (eLiposomes).
3. Synthesize Herceptin-conjugated liposomes and e-Liposomes.
4. Conduct characterization tests and assays on all the liposomal formulations through dynamic light scattering, Stewart, and BCA assays to determine their respective size, phospholipid content, and extent of ligand attachment, respectively.
5. Employ cryogenic transmission electron microscopy (cryo-TEM) to affirm the encapsulation of emulsions within liposomes, providing a detailed examination of the structural integrity of the resulting liposomal formulations.
6. Investigate the acoustic discharge of the model drug calcein from the categories above by utilizing 20kHz LFUS at power densities of 6.2, 9, and 10 mW/cm².
7. Conduct a mathematical analysis to model the drug release kinetics of the developed drug delivery system, employing appropriate statistical techniques to analyze the data.

2.7 Research Contribution

The contributions of this research work can be summarized as follows:

- Propose schemes to release the encapsulated drug more quickly than conventional liposomes by encapsulating liposomes with phase-shifting emulsion droplets that instantly burst upon encountering ultrasound negative peak pressure wave.

- Propose schemes to improve cancer treatment efficacy by employing Herceptin-loaded emulsion encapsulated liposomes to treat HER2-positive breast cancer and reduce side effects compared to conventional liposomes.

2.8 Thesis Organization

The rest of the thesis is organized as follows: Chapter 2 provides background on cancer and its treatments. Chapter 3 discusses the applications of nanotechnology in drug delivery systems and the recent techniques used for improvising current cancer treatment methods and rendering them more humane by mitigating their side effects. Chapter 4 presents the characterization tests, assays, and performance evaluation for different liposomal formulations. Finally, Chapter 5 concludes the thesis and outlines future work.

Chapter 2 Background and Literature Review

2.1 Nanoparticles (NPs) as drug delivery system

Due to the concerns associated with the release and side effects of chemotherapeutic drugs, nanocarriers are being explored. These nanoparticles are vesicles whose cavities serve as a vehicle to confine and carry the drug to the target tumor tissue. Due to their nano-size (15-200 nm), they can be quickly taken up by cells and induce controlled release to the target tumor site, permitting efficient drug delivery, increasing chemotherapeutic drug efficacy, reducing off-target effects, and minimizing the side effects and toxicity. The evolution in nanotechnology and its application to drug delivery offers the potential to upgrade and enhance medical treatments. Nanocarriers have been designed to overcome these limitations offered by conventional cancer therapies. In a study by Ayub & Wettig, nanocarrier-based systems have led to promising results, especially for treating numerous types of cancer, especially brain cancer [30].

Many types of nanocarriers have been developed for various applications, including drug delivery applications. For example, NPs can be fabricated from organic materials such as lipids, polymers, or inorganic materials assembled into nanocrystals of metallic oxides, gold nanoparticles, etc., polymeric NPs such as micelles, liposomes, and dendrimers. These nanomaterials are designed for target-specific drug delivery and can be zero-dimensional nanoparticles, one-dimensional, e.g., nanotubes, or two-dimensional, e.g., nanoplates [31].

2.2 Characteristics of NPs

For a nanoparticle (NP) to be effective as a drug delivery system, the efficacy of these structures depends on the following characteristics:

- A NP must be biocompatible, i.e., non-toxic and safe to interact with living cells. It must be biodegradable into safe and non-toxic components to be eliminated from the body.
- The stability of NP in a physiological environment up to the intended period determines the effectiveness of drug delivery systems.

- The size of nanoparticles and the surface morphology play a significant role in determining the targeting capability and distribution of the nanoparticle in the body. For example, NPs with a diameter above 200nm are more rapidly cleared from the blood than NPs below 200 nm.
- The surface charge of NPs determines the uptake of NPs by the cells; e.g., positively charged NPs experience higher cellular uptake than NPs with a negative charge. NPs must have a high drug loading capacity; however, the nature of the drug impacts the loading capacity depending on the nature of the NP [31].

2.3 Types of NPs

2.3.1 Polymeric Micelles

Micelles are amphiphilic copolymer vesicles that allow the loading of one of the hydrophobic or hydrophilic drugs into their core (at any time), making them flexible vehicles for chemotherapy. Micelles are small-sized (ranging between 10 to 100 nm) and spherical. They are self-assembled, and their colloidal arrangement of hydrophobic tails separates from the hydrophilic heads, leading to an inner hydrophobic core and an outer hydrophilic head layer[32]. Figure 2-1 shows a structural schematic of a polymeric micelle.

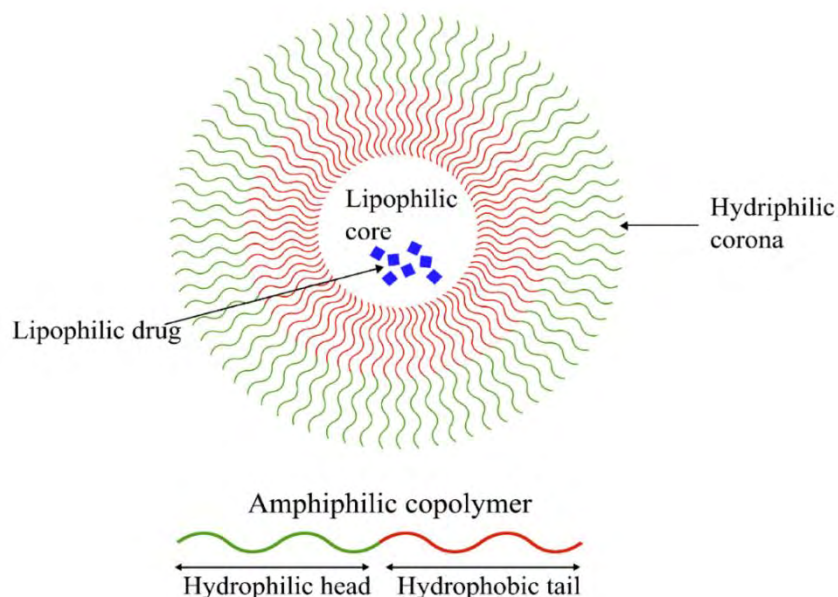


Figure 2-1 Schematic illustration of a polymeric micelle [31]

This arrangement allows them to be stable in physiological environments. It helps retain them in the blood circulatory system for extended periods to enable their reach to the target tumor tissue. Moreover, it allows them to be employed in different medical applications; these include diagnostic medical imaging, gene delivery, and Transdermal Delivery Systems (TDD). Micelles are biocompatible, have a long blood circulation time, and have good stability. Additionally, they can accumulate at the targeted site via the EPR effect. Moreover, their surfaces can be conjugated with targeting ligands to actively target and increase their distribution in the targeted tumor sites and trigger drug release via various stimuli[32].

The FDA has approved pluronics, and pluronic micelles that have been extensively utilized for tumor-targeted delivery. Zhao et al. synthesized pluronic micelles made up of block-copolymers PPO-PEO-PPO (size 68.2 nm) composed of Pluronic (P123) and Pluronic (F68) as a medium to encapsulate curcumin, which enhanced the encapsulating efficiency (EE) by 86.93% and drug loading capacity by 6.996% [33].

2.3.2 Dendrimers

These polymeric NPs are highly branched and referred to as “starburst” polymers. They are spherical and consist of repeating units, each repeating subunit called a generation. They consist of three main components, i.e., an initiator core, interior layers (dendrons/generations), and terminals[30], as shown in Figure 2-2.

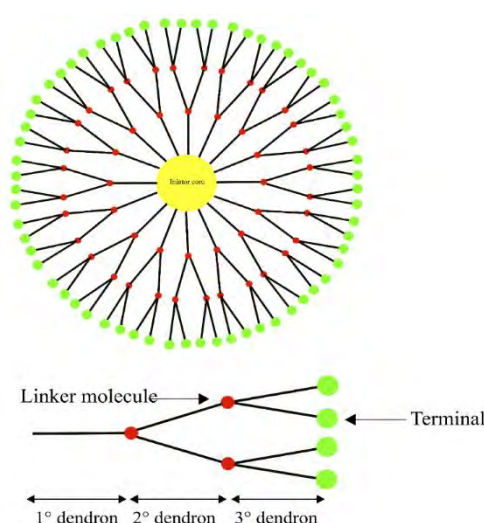


Figure 2-2 Schematic illustration of a dendrimer [30]

Dendrons are repeating subunits radially connected to the initiator core, whereas terminals perform most functionalization and drug loading. Hence, the dendrimer's size and the drug's loading capacity can be controlled easily. In addition, dendrimers' extensive branches allow them to quickly conjugate proteins and antibodies onto their surface[30]. Polyamidoamine (PAMAM) dendrimers have been extensively used for drug and gene delivery, along with targeting ligands to help improve therapeutic efficacy [34].

2.3.3 Liposomes

Liposomes are nanoscale, versatile spherical vesicles made up of one or more lipid bilayers similar to the cell membrane; they can be referred to as artificial cells, previously called Banghasomes, discovered by Alec D. Bangham in the 1960s, and were later named liposomes originating from the Greek words “lipos” meaning fat and “soma” meaning body.” They are made of natural substances, sometimes made out of synthetic surfactants that entrap molecules such as vaccines, plasmid DNA, hormones, antibodies, etc. Liposomes are amphiphilic molecules that consist of a hydrophilic head (water-loving) and a hydrophobic/lipophilic (water-repelling) tail [35], [36].

2.3.3.1 Classification of liposomes

Liposomes can be classified based on lamellarity, size, and preparation method. Based on their structure or lamellarity, as shown in Figure 2-3, liposomes can be classified as a unilamellar vesicle (UV) with a single phospholipid bilayer structure and multilamellar vesicle (MUV) with several lipid bilayer membranes enclosing the other with ones smaller in size, resembling an onion-like structure. Unilamellar vesicles can be further classified into small unilamellar vesicles (SUV, with a diameter of 20-100 nm, large unilamellar vesicles (LUV, diameter 100 nm – 1 μ m), and giant unilamellar vesicles (GUV diameter > 1 μ m[34], and multivesicular vesicle (MVV, 1.6 - 10.5 μ m) that demonstrates a honeycomb-like structure with multiple vesicles covered by a single lipid bilayer structure [36], [37]. The size of liposomes can range from 20 nm to 1 μ m [31]; however, for medical applications, liposomes ranging between 50 to 450 nm³ in volume are used [38]. Figure 2-3 depicts the classification of liposomes based on their lamellarity and size.

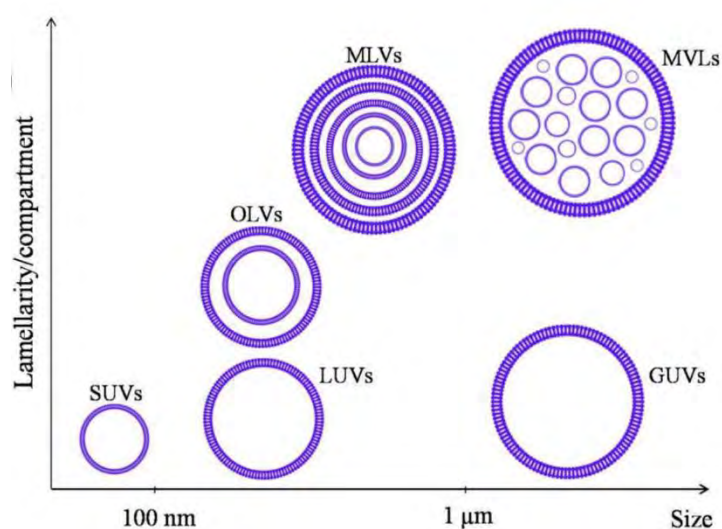


Figure 2-3 Classification of liposomes based on size and number of lamellae [39]

Based on the therapeutic efficacy, the second generation of liposomes has been modulated based on their composition, size, surface charge, and organization [39].

2.3.3.2 Formation of liposomes

In an aqueous solution, lipid molecules self-assemble due to hydrophobic interactions, forming a bilayer sphere with lipophilic/hydrophobic tails facing each other and directed inwards, acting as a permeability barrier and hydrophilic heads facing outwards with hydrogen bonds and polar interactions between water molecules and the polar heads and an internal aqueous core respectively as shown in Figure 2-5. This is due to their extremely low solubility and low critical micelle concentration values of lipids forming the bilayer structure. However, this enabled them to simultaneously encapsulate lipid-soluble and aqueous-soluble drugs and was known as the potential universal drug carrier. Liposomes are extensively researched nanocarriers due to their drug encapsulation, protection from clearance of the drug, and its controlled release that leads to remarkable therapeutic effects with minimum toxic side effects [37], [40]-[42]. These advantages are further discussed in the following sections.

2.3.3.3 Main components of liposomes

Liposomes are lipid bilayer structures, with phospholipids being the most widely found lipids, which are major components that form the cell membrane structures. They consist of glycerol which links the hydrophobic chains and hydrophilic head group (consisting of phosphate and organic group), also known as glycerophospholipid,

illustrated in Figure 2-4. However, instead of glycerol, sphingomyelin derived from sphingosine can be used as a basic component, with two hydrocarbon chains of saturated or unsaturated fatty acids. The factors determining phospholipid bilayers' elasticity and phase behavior of phospholipid bilayers are the nature of fatty acids and the number of double bonds in the chain [39].

The incorporation of organic molecules to the phosphate group generates various kinds of phospholipids, such as; Phosphatidylcholine (PC), Phosphatidylethanolamine (PE),

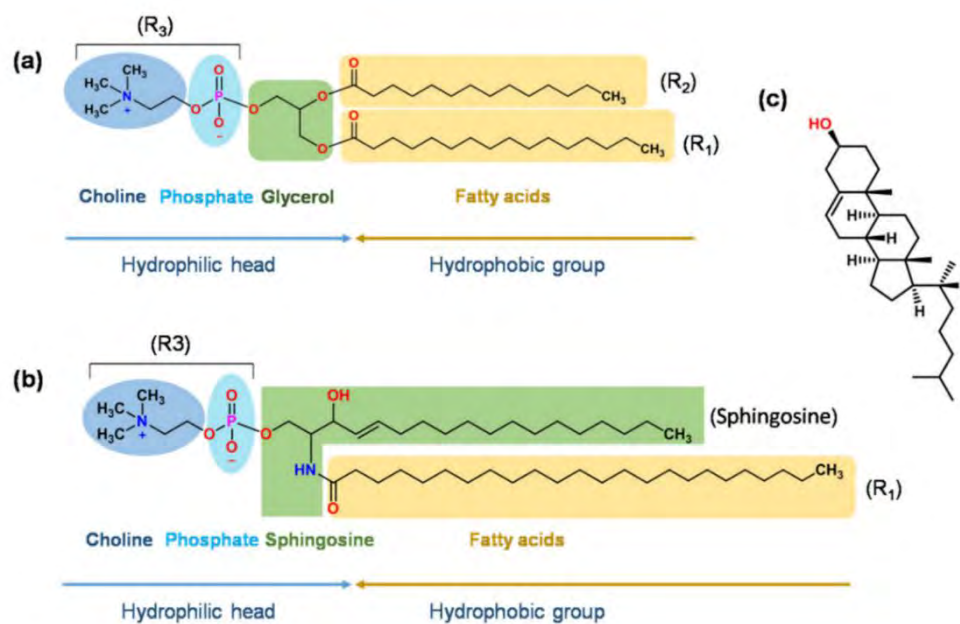


Figure 2-4 Structural illustrations of components of liposomes a) structure of glycerophospholipid b) structure of sphingomyelin. c) structure of cholesterol [39]

Phosphatidylserine (PS), with PC or lecithin being the most commonly used phospholipids for the formation of liposomes (“Lecithin is derived from the Greek word Lekithos, meaning egg yolk”). Phospholipids occur abundantly in nature; however, their synthetic derivatives also exist; some examples are 1,2-Dimyristoyl-sn-glycero-3-phosphocholine (DMPC) and 1,2-Dipalmitoyl-sn-glycero-3-phosphocholine (DPPC) as derivatives of PC, and 1,2-Dimyristoyl-sn-glycero-3-phosphoethanolamine (DMPE) as a derivative of PE, etc. [43] [44], [45], [46], [43], [40].

2.3.3.4 Liposomal surface modification for enhanced pharmacokinetics

Liposomes are the most researched nanoparticles partly because of the ease of their surface modification and functionalization to better fit the application as per the tumor pathophysiology. Functionalized liposomes showed significant improvement in

physiological behavior when compared with conventional liposomes. Molecules used to manipulate the liposome surface are discussed in the following sections [47].

2.3.3.4.1 Cholesterol

To enhance liposomal physical stability in the bloodstream and increase their shelf-life, sterols are incorporated into the nanocarrier's structure to adjust the liposomal membrane composition. The most commonly and naturally occurring sterol in the cell membrane is cholesterol, a hydrophobic molecule that interacts with the core of the liposomal membrane and helps reduce its permeability to water. This, in turn, increases the liposomal membrane micro-viscosity and fluidity by making them less rigid, preventing crystallization of the phospholipid acyl chains, and increasing their stability in the presence of blood/plasma, *in-vivo* and *in-vitro*. Cholesterol can also anchor or attach PEG to the liposomal surface to render them stealth drug carriers. In addition, Phosphatidylcholine with saturated fatty acyl chains increases the transition temperature beyond the physiological temperature, i.e., 37°C, to prolong the *in-vivo* circulation of liposomes [43], [48].

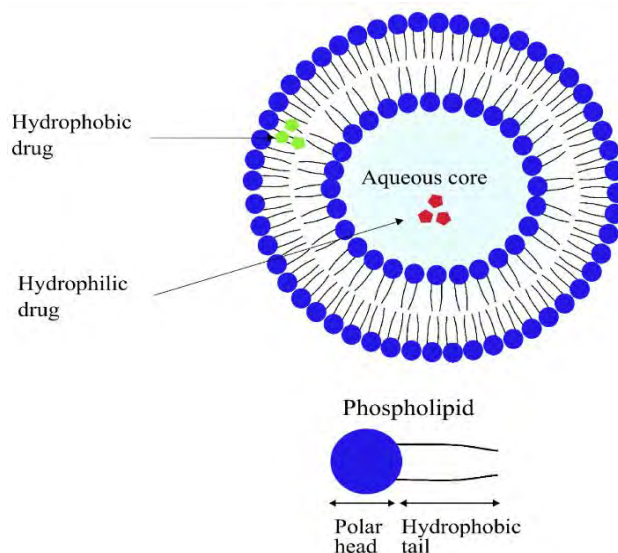


Figure 2-5 A schematic diagram of an amphiphilic liposome with a hydrophilic (red) drug in its core and a lipophilic (green) drug encapsulated in the phospholipid bilayer [16].

2.3.3.4.2 Polyethylene Glycol (PEG)

When liposomes are administered in the bloodstream, they face an extremely short half-life in the circulatory system. The immune system (mononuclear phagocyte system)

identifies them as foreign particles and removes them by the opsonization process. In this process, a protein (an opsonin) binds to the liposomes. Opsonin proteins are adsorbed onto the surface of the liposomes based on their size and surface properties, signaling the reticuloendothelial system (RES) cells to phagocytose and clear these particles from the bloodstream rapidly. Liposomes are detected, captured, and removed from the bloodstream via phagocytosis. Hence, rendering the liposome an ineffective drug delivery vehicle. In order to increase liposomal circulation half-life in the bloodstream, flexible hydrophilic polymers such as; Polyethylene Glycol (PEG) chains are attached to the surface of the liposomes that form a barrier and demonstrate repulsive forces that prevent opsonin proteins from interacting and being adsorbed onto the surface of liposomes, thus shielding them, and rendering them thermodynamically, and sterically stable [43], [49].

In 1995, FDA (USA) approved Doxil (the first injectable Doxorubicin HCl liposome), whose surface has PEG chains attached.

2.3.3.4.3 Targeting Ligands

Liposomes are functionalized by binding single or multiple ligands to liposomes for selectively binding to the cell, improving drug efficacy and reducing side effects. Ligands are moieties that contain one or more functional groups to bind to another molecule or ion (in this case, biological receptors) to form a coordination complex for biological purposes, triggering a cascade of events that invaginate and take in the ligands and NPs within the cell (receptor-mediated endocytosis). Examples of specific receptors that may be overexpressed by tumor cells include folic acid (FA), integrins, epidermal growth factor (EGF), Vascular endothelial growth factor (VEGF), etc. To use liposomes in active targeting, targeting moieties or ligands specific to these receptors, such as monoclonal antibodies or their fragments (Herceptin), small molecules (folic acid), carbohydrates (galactose), nucleic acids (aptamers), polypeptides (iRGD), proteins (transferrin, albumin), hormones, etc. are attached to liposomal surfaces, to specifically bind to their corresponding cellular receptors at the cancer sites rather than targeting the healthy cells. Thus, limiting the interaction of NPs with healthy cells. Antibody ligands may trigger a specific immune response in the cancer cells; however, molecular ligands encourage receptor-mediated endocytosis

without affecting the activity or the ability of NPs they are conjugated to [31], [49], [50]. Figure 2-6 shows a schematic representation of conventional and surface-modified liposomes.

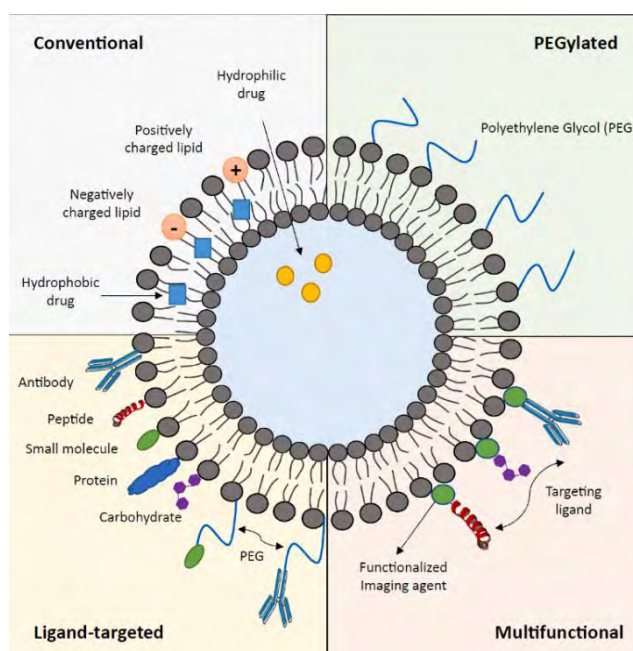


Figure 2-6 Schematic representation of conventional and surface-modified liposomes [27]

As discussed earlier, rapidly growing cancer cells express a high demand for oxygen, vitamins, and nutrients due to increased metabolism, hence the reason behind their over-expression of specific receptors such as folate receptors, transferrin receptors, biotin, EGF, etc.

2.3.3.4.3.1 Folate-mediated targeting

Folic acid (pteroyl-L-glutamic acid) is a member of the vitamin B family, widely found in green vegetables, and is responsible for cell growth and development. Folic acid (FA) is used as a ligand to target folate receptors overexpressed in cancers such as; cervical, ovarian, colorectal, breast and other cancers, and delivers anticancer drugs to the cancer cells. Another *in vitro* study by Lu et al. revealed that folate conjugated to IOP (inositol) liposomes were responsible for the selective delivery and enhanced tumor cell uptake while showing excellent therapeutic efficacy and minimum toxicity toward healthy cells [51]. Another study by Haftcheshmeh and colleagues revealed that modification of passive Doxil liposomes to SS-02 peptide targeted Doxil liposomes significantly enhanced toxicity due to the higher density of targeted ligand and positive

surface charge that enhanced uptake by cancer cells and hence the therapeutic efficacy of DOX [52].

A cell uptake study carried out by Lohade et al. demonstrated that folate-conjugated DOX liposomes showed an enhanced intracellular uptake in A549 human lung cancer cell lines and B16F10 murine lung carcinoma cell lines compared to conventional DOX liposomes. However, when the folate concentration on the surface of liposomes was varied, as shown in the Figure 2-7, an increase in the uptake of DOX was recorded when the folate content increased from 0.5 mol% - 1.0 mol%; however, no significant increase was recorded when folate content was further increased from 1.0 mol% - 1.5 mol%, this may be due to the saturation of folate receptors on the surface of tumor cells [53]. Dual ligand targeting was tested to solve this issue and will be summarized in the upcoming sections.

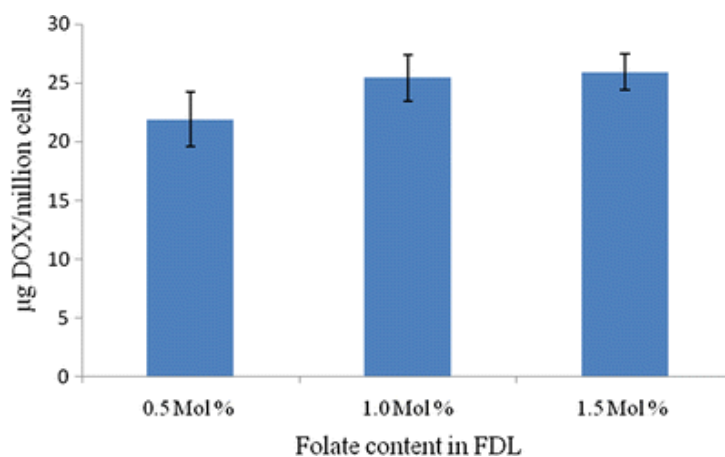


Figure 2-7 Graphical representation of uptake of DOX liposomes as a function of folate targeting content [32]

2.3.3.4.3.2 Transferrin-mediated targeting

Transferrin is a glycoprotein secreted primarily by the liver and is responsible for the transport of iron from the digestive system and red blood cells (erythrocytes) degradation to tissues via the transferrin receptor (TfR) through receptor-mediated endocytosis, where the endo-lysosomes' low pH helps in the release of iron into the cytosol. Iron helps in cell vitality, cellular proteins, and metabolism. [54] hence, modifying liposomes on the surface with transferrin moieties will help target TfR tumor cells and deliver the drug, Figure 2-8.

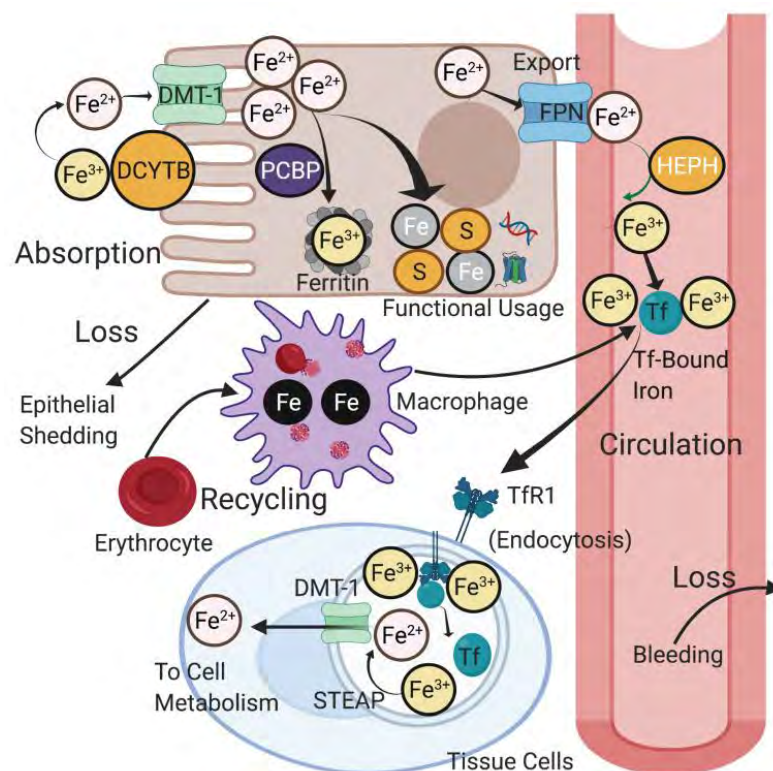


Figure 2-8 Tf transports ferric iron to the TfR1 receptor via receptor-mediated endocytosis, where Tf and ferric iron disassemble in the endosome, with ferric iron reduced to ferrous iron, which enters the cytosol [33].

Jhaveri et al. investigated the effects of conventional resveratrol (RES) liposomes, free RES, and Tf-targeted RES liposomes by comparing tumor growth inhibition and survival in mice. The study showed that Tf-RES liposomes exhibited higher cytotoxicity and cell survival rate than RES liposomes and free RES, confirming Tf-RES liposomes' selective targeting, intracellular binding, and effective anticancer agent delivery [55]. In another study conducted by Alsawaftah et al., Tf-PEG liposomes showed significantly higher calcein uptake by HeLa cells compared to conventional liposomes, and the uptake further increased after the application of low-frequency ultrasound (at 35kHz), rendering Tf-PEG liposomes highly sono-sensitive. However, it was also noted that both types of liposomes showed a decrease in size under the influence of US; this may be due to the alterations in phospholipid structure due to sonoporation and hence the size reduction [56].

2.3.3.4.3.3 Trastuzumab (Herceptin®)-mediated targeting

Human Epidermal growth factor Receptor 2 (HER2) is a transmembrane receptor tyrosine kinase responsible for functions such as, cell growth, differentiation and the

survival of epithelial cells. In cancer cells, HER2 gene overexpression leads to the high-level production of HER2 protein responsible for the rapid growth and multiplication of cancer cells in HER2+ cancer cells, including breast, ovarian, prostate, pancreatic, bladder, and stomach cancers [57], [58]. HER2 gene is overexpressed in over 20 – 30% of breast cancer patients. Herceptin is a monoclonal antibody used against HER2 receptors by binding to them, similar to the lock-and-key mechanism. This blocks the cell from receiving the growth and multiplication signals and thus leads to cell apoptosis. Furthermore, Herceptin can be used for immune-targeted therapy by binding to the cancer cells and alerting the immune system to destroy these diseased cells. Lee et al. studied the anticancer effects of Herceptin-conjugated pegylated liposomes encapsulating with Metformin (MET), both *in-vitro* and *in-vivo*. It was observed that the conjugation of Herceptin to the MET-encapsulated liposomal assembly had significantly enhanced the anticancer efficiency of the nanocarrier [59].

2.3.3.4.3.4 Dual Ligand mediated targeting

Liposomes functionalized with two ligands on their surface showed positive synergistic effects by targeting multiple cancer cell receptors, thus improving the selectivity and enhancing uptake and cytotoxicity compared to single ligand targeting. In a study conducted by Rodrigues et al., dual-targeted liposomes were functionalized with Tf and cell-penetrating peptide (CPP) to treat neurodegenerative diseases for efficient gene delivery, encapsulating plasmid DNA as a model drug. Among the three types of CPPs tested with Tf, Tf-kFGF conjugated liposomes showed higher potential for overcoming the blood-brain barrier (BBB) and improving drug delivery into the brain, as shown in Figure 2-9 [60].

Tf helps the uptake of NPs from the blood into the brain; however, the receptor saturation phenomenon may interfere with Tf, which is when CPP comes into play and overcomes the saturation phenomenon, aiding NPs transport into the brain cells [60].

2.3.3.5 Advantages of Liposomes:

Since the structure of cell membranes resembles a phospholipid bilayer structure, allowing exceptional interaction between the cell membrane and liposomes. Hence, they are regarded as highly biocompatible, biodegradable, and nonimmunogenic as they

are composed of phospholipids and cholesterol, rendering them good candidates for nanoparticulate drug delivery systems [30], [48], [50].

Furthermore, liposomal surfaces can be modified with poly(ethylene glycol) (PEG), to render liposomes less immunogenic, increase the bloodstream circulation time by protecting them from degrading in the plasma, and conjugate with targeting ligands to bind to specific receptors on tumor cells aiding them to be endocytosed by cancer cells [31], [61]. Liposomes were first employed in drug delivery systems in 1971 [2], [49], and now they are being utilized as delivery vehicles to improve patient compliance via various administration routes that include; oral, transdermal, parenteral, pulmonary, nasal, and ophthalmic routes, which allows them to aid in medical imaging as well by delivery imaging agents to targeted sites [39].

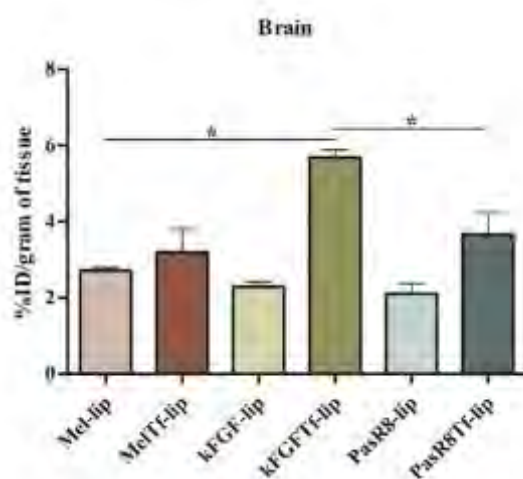


Figure 2-9 Graphical representation of Tf-CPP conjugated liposomes for targeting brain through BBB, with kFGF-Tf showing the superior ability in overcoming the BBB [39]

2.3.3.6 Targeting mechanisms

Targeting cancer cells and increasing the efficiency of drugs while reducing their toxic side effects is one of the biggest challenges. To do so, three general methods, passive, active, and triggered drug delivery, are employed.

2.3.3.6.1 Passive Targeting

Passive drug delivery allows the localization of NPs and the accumulation of the drug within the tumor cell's microenvironment by making use tumor's physiological features. Tumors with leaky vasculature and pores allow the passage and permeability of nanocarriers, typically < 200nm. The poor lymphatic drainage in tumors enables the accumulation and retention of these nanocarriers within cancer cells. This effect is

known as the enhanced permeation and retention (EPR) effect, which helps the tumor cells' passive targeting. However, healthy tissues do not allow the passage of these NPs through their tight junctions, leading to a high concentration and accumulation of the drug in tumor cells compared to the rest of the body. Liposomes and other macromolecules are typically used for passive delivery, without the targeting ligands [62]. Figure 2-10 illustrates a schematic representation of active and passive targeting mechanisms.

2.3.3.6.2 Active Targeting

The EPR effect may result in a slower uptake of NPs and delayed drug pharmacokinetics; slow drug release would not allow the drug to reach the desired therapeutic concentration; moreover, passive targeting is limited to certain solid tumors that are larger than approximately 4.6 mm, with porosity depending on the type and location of the tumor. Furthermore, non-vascularized sites are questionable when taking advantage of the EPR effect. Therefore, facilitating the uptake of NPs by the tumor cells and protecting healthy cells becomes essential [62]. Active targeting improves uptake by tumor cells by conjugating ligands to the NPs surface (e.g., antibodies, hormones, fusogenic proteins, polypeptides, etc.) to target specific receptors or antigens overexpressed on tumor cell membranes; these include;

- **Targeting tumor's angiogenesis**, which targets tumor angiogenic factors such as vascular endothelial growth factors (VEGF) by specific targeting receptors with an affinity for VEGF, such as vascular endothelial growth factor receptors (VEGFR) [50].
- **Targeting overexpressed uncontrolled cell division receptors** to target cancer cells; these include Human Epidermal Receptors (HER), transferrin receptors (for iron transport proteins), and folate receptors (for folic acid) [50].
- **Target tumor-specific receptors** depending on the tumor's nature and type of malignancy, e.g., breast cancer overexpresses HER-2, folate receptors inorganic anion transporting peptides (OATPs), that can easily bind to ligands anti-HER-2 monoclonal antibody, folic acid, and estrone-3-sulfate ligands respectively [50].

The EPR effect has to be attained to localize the NPs in the tumor microenvironment to aid the active targeting process and be effective. Once localized, binding interactions between the ligand and the cell receptors (called receptor-mediated endocytosis)

uptake the NPs, leading to the accumulation of anticancer drugs within the tumor cells. Once endocytosed into the tumor cells, carriers need a release mechanism to release their content into the tumor cells. Thus, targeting the cancerous cells and minimizing side effects corresponding to these enclosed drugs. [50], [61], [50], [61], [63],[64]

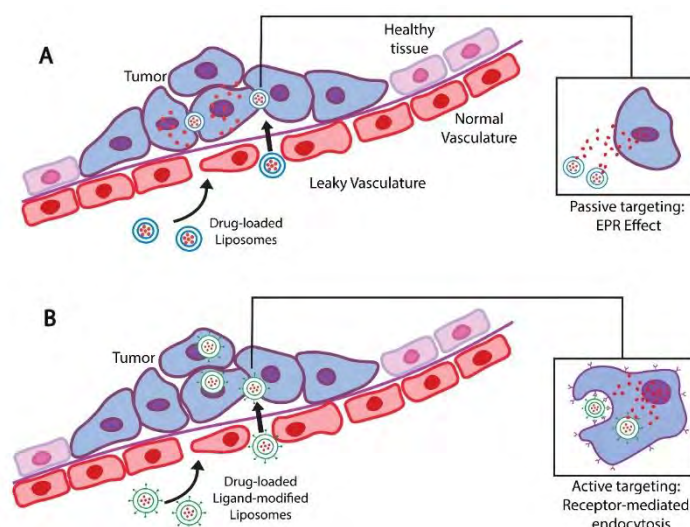


Figure 2-10 Schematic illustrating the active and passive targeting techniques of liposomes into specific tumor tissues for enhanced efficacy of therapeutic agents

2.3.3.7 Triggered-release mechanism

NPs can be designed in such a way to make use of the changes in the NPs' environment to release its cargo; these changes are both internal tumor environment such as; temperature, pH, enzymes, redox reactions, etc. or external stimuli such as; ultrasound, magnetism, light, temperature increase (wax bath, water bath, microwaves), electric field, etc. [50], [61]. These mechanisms will be elaborated on in the upcoming section: stimuli-responsive liposomes.

2.3.3.8 Commercially available liposomes

Liposomes have been approved as a drug delivery system by the Food and Drug Administration (FDA) and the European Medicines Agency (EMA) and are undergoing clinical therapy, where they are commonly loaded with chemotherapeutic drugs such as; doxorubicin (DOX), paclitaxel, cisplatin derivatives, and daunorubicin. The majority of the commercial products marketed is SUVs. The first one to be approved by the FDA is Doxil (US)/ Caelyx (EU), which are passively targeted liposomes encapsulating DOX and are SUVs with the main lipid composition of HSPC, MPEG-

DSPE, and Cholesterol. Other examples of commercially available liposomes approved for the treatment of various types of cancer are shown in Table. 2-1.

Table. 2-1 Approved by FDA EMA for delivery of anticancer agents [31], [39], [48], [65]-[68]

Liposomal product	Encapsulated drug	Administration route	Approved year	Size and Structure	Indication (Cancer)
Doxil/ Caelyx	Doxorubicin hydrochloride (DOX-HCl)	Intravenous (IV)	1995	SUVs (100 nm)	Ovarian cancer, breast cancer, myeloid melanoma, and Kaposi's sarcoma
DaunoXome	Daunorubicin	IV	1996	SUVs (45-80 nm)	Kaposi's sarcoma
Myocet	DOX-HCl	IV	2000	MLVs (80-90 nm)	Breast cancer
Mepact	MTP-PE	IV	2012	MLVs (2.0-3.5 μ m)	Osteosarcoma
Marqibo	Vincristine sulfate, Irinotecan	IV	2012	SUVs (130-150 nm)	Acute lymphoblastic leukemia
Onivyde	Hydrochloride trihydrate	IV	2015-2016	SUVs (110 nm)	Pancreatic adenocarcinoma

Myocet is mainly composed of EPC, Cholesterol, Arikaye are considered as LUVs due to their large diameter ranging from 200 – 300 nm and are primarily composed of DPPC and Cholesterol, Shingrix (SUVs 50 - 100 nm formed of DOPC and Cholesterol, and DaunoXome (SUVs ranging from 45 – 80 nm mainly composed of DSPC, cholesterol). Commercially available liposomes also range in micron diameters; e.g., Mepact, Depocyt, DepoDur, and Exparel, with Mepact being an MLV, whereas the rest are classified as MVVs. Doxil or doxorubicin liposomes are used in cancer therapy such as; ovarian cancer, multiple myeloma, etc. [31], [39], [38], [69], [70].

2.3.3.9 Preparation of liposomes

2.3.3.9.1 Synthesis of liposomes

There are various techniques to synthesize liposomes, and they influence lamellarity, size, and even the efficiency of drug encapsulation. These techniques include the thin-film hydration method, the double emulsification method, reverse-phase evaporation, solvent injection techniques, detergent removal, etc. New procedures are being looked into for their large-scale production by modifying conventional methods, such as the modification of the ethanol injection method to cross-flow injection or the Wagner method and improving the detergent removal method to cross-flow filtration method; however, each technique has pros and cons. The Wagner method is a simple, sterile process; however, the residual organic solvents cause instability. Compared to other methods, the thin-film hydration technique or Bangham method is the most widely used laboratory synthesis of liposomes. This technique begins with dissolving the main liposome components, such as; phospholipids and cholesterol, in an organic solvent, i.e., chloroform, methanol, etc.; the lipid-solvent solution is evaporated by the rotation of a round-bottomed flask under vacuum, leaving behind a thin film of dry lipid onto the walls of the round-bottomed flask. The dried cake left behind is re-hydrated using an aqueous solvent to form spherical liposomal vesicles with a different organizational structure, creating large and multilamellar liposome vesicles. To adjust the lamellarity and size of liposomes, they must undergo sonication, which helps break and reform liposomes into unilamellar vehicles. Extrusion through a filter ensures liposomal size distribution favors the EPR effect. However, the drawbacks of this technique are low encapsulation efficiency, production of large and diverse liposomes, and its difficulty in scaling-up [48].

2.3.3.9.2 Drug loading methods

As discussed earlier, liposomes are universal drug-encapsulating vesicles that can load hydrophilic and hydrophobic drugs. The encapsulation of drugs is carried out during or after the formation of liposomes. It is highly influenced by liposome composition, liposome production technique, solubility, encapsulation efficiency (EE), drug/ lipid ratio, stability of liposomes, leakage, retention of the drug, etc. Drug encapsulation consists of two techniques, namely, active and passive drug loading [48],[39].

2.3.3.9.2.1 Passive drug loading

In the passive drug loading method, drugs are encapsulated during the formation of the liposomal vesicle. The encapsulated drug is either confined within the hydrophilic core or implanted within the hydrophobic bilayer with the help of covalent, ionic, electrostatic, and hydrophobic interactions, etc. However, this method results in low encapsulation efficiency with high leakage for the drugs permeable to the liposome membrane, resulting in a large volume of unencapsulated drugs. Nonetheless, this can be fixed by the active loading method, which improves the encapsulation efficiency compared to passive loading [39], [48], [71].

2.3.3.9.2.2 Active drug loading

Active or remote drug loading is applied after the formation of liposomal vesicles and requires the establishment of transmembrane pH or ion concentration gradient inside the core and in the aqueous solution outside the liposome where the drug is solubilized; this would promote driving the uncharged drug through the bilayer, where their protonation and low solubility inhibits them from diffusing out of the liposome, this may take up to 30 min and result up to a 100% loading of various drugs with enhanced EE and retention within the liposomes [39],[48],[71].

In the Figure 2-11, the transmembrane gradient of ammonium sulfate $(\text{NH}_4)_2\text{SO}_4$ is established where its concentration outside is much higher compared to the core of liposomes; this increases the permeability of neutral DOX- NH_2 molecules and enables their diffusion across the bilayer into the core of liposomes where it precipitates into $(\text{DOX}-\text{NH}_3)_2\text{SO}_4$, which is a fiber-like crystalline structure that possesses low solubility and hence minimizes the osmotic pressure within the liposome [39],[53].

A combination of both passive and active drug loading methods has also been adopted in approved liposomes such as; Vyxeos, where a variety of drugs (cytarabine is loaded passively and daunorubicin is remotely loaded in non-antagonistic molar ratios) has proven to be helpful within the same liposome vesicles for the treatment of hematologic cancers [72].

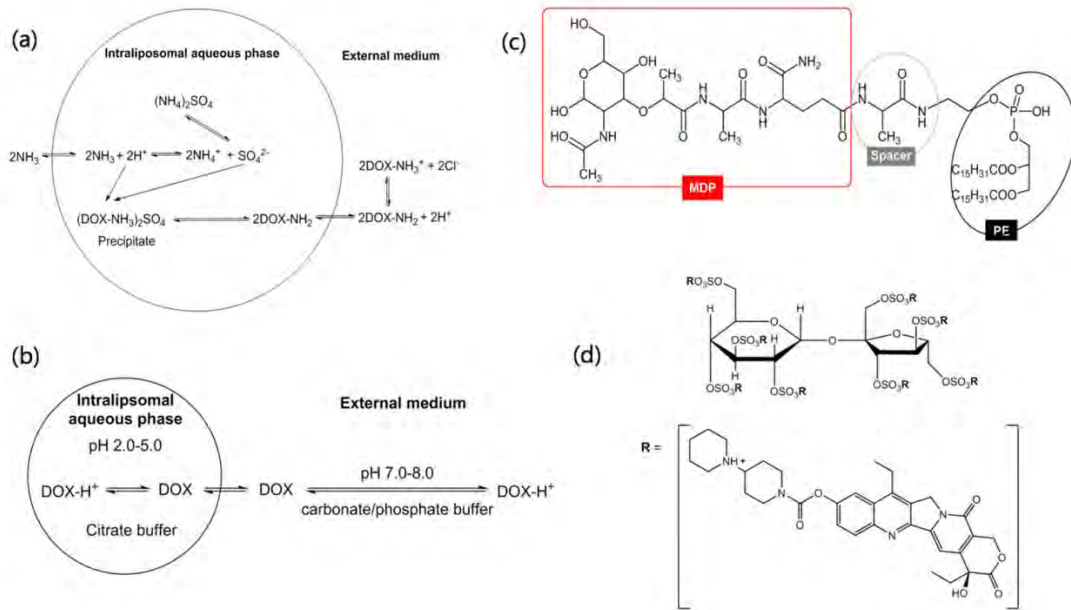


Figure 2-11 Different active loading techniques employing pH and ion concentration gradients [25].

2.3.3.10 Liposomal characterization

Intensive characterization of liposomes post-production is a crucial requirement and a prerequisite before applying liposomes. It enables the evaluation and assurance of the physicochemical properties and performance of liposomes *in-vitro* and *in-vivo*. These properties involve; liposome size, size distribution, surface charge, shape, lamellarity, phase behavior, encapsulation efficiency EE, and *in vitro* release. The techniques used for the assessment of the properties mentioned above are summarized in the following sections:

2.3.3.10.1 Size and polydispersity

Size and polydispersity index (PDI) play a crucial role in drug delivery applications. Liposomes' size ranging between 50 and 200 nm is advisable for drug delivery, as small-sized liposomes easily circulate in the bloodstream for extended periods, in contrast, large-sized liposomes are rapidly eliminated from the bloodstream. Small size also aids processes such as, parenteral administration, systemic circulation, extravasation into the tumor tissue, cell uptake efficacy, and determination of circulation half-life of liposomes [39]. Singh and his colleagues investigated the immune response as a function of particle size and determined that small-sized particles ranging from 10 – 200 nm are efficiently taken up by dendritic cells; however, large particles are phagocytosed by the macrophages [39], [73].

PDI value, on the other hand, measures the variability in the sample, revealing the monodisperse or polydisperse behavior of the liposomes within the sample. Polydispersity is an arbitrary quantity and ranges from 0 – 1; however, for drug delivery applications, a lower PDI value of below or equal to 0.3 is considered acceptable, as it measures the narrow size distribution and demonstrates the homogeneity of the sample. The most commonly used technique for measuring the size and PDI is Dynamic Light Scattering (DLS), which analyzes the Brownian motion of the dispersed particles in a liquid medium and measures the scattered light, which correlates with the diffusion level of the liposomes in the liquid suspension [48],[39].

2.3.3.10.2 Zeta Potential

Zeta potential is a physical property that determines the liposomes' overall charge or surfaces electric charge to predict their stability and behavior in the surrounding medium. Liposomes can be classified as anionic, cationic, or neutral. Low zeta potential or uncharged liposomes are preferable in drug delivery applications, as they have a higher probability of aggregation. High zeta potential with a large positive or negative charge will offer repulsive forces that may prevent the aggregation of the liposomes within the medium. The most commonly used laboratory technique for the measurement of the surface charge is Laser Doppler electrophoresis (LDE), which involves the illumination of the sample from the middle using a laser as a light source and measuring the alterations in the scattered light intensity due to particle movement, under the influence of electric current. The rate of mobility of the particles is directly proportional to the charge of the liposomes [28], [31].

Due to negatively charged particles on tumor endothelial cells, cationic liposomes undergo electrostatic interactions and target tumor cells, thus accumulating and releasing the drug at the targeted site. Cationic liposomes have also been extensively used to deliver negatively charged nucleic acids, sequestering them to prevent enzymatic degradation of DNA or endosome by interacting with the negatively charged plasma membrane. However, limitations concerning cationic liposomes exist, and one of them is the toxicity at high dosages [43], [60].

2.3.3.10.3 Shape

The shape of liposomes is analyzed by directly observing the nanoparticle images under the electron microscopes such as TEM and cryo-TEM. Cryo-TEM is preferred for nanometer-sized liposomes because it preserves the native state of liposomes and minimizes their shape distortion by flash-freezing via liquid nitrogen, followed by direct visualization under controlled conditions. Atomic force microscopy (AFM) is quick, powerful, and very high-resolution microscopy that enables direct sample observation [48].

2.3.3.10.4 Number of lamellae

Liposomal lamellarity directly influences the encapsulation efficiency of the drug. The most commonly employed method to analyze lamellarity is cryo-TEM. It enables visualization of the phospholipid bilayer and the distance between the adjacent bilayers; however, other techniques include Nuclear Magnetic Resonance (NMR), Small-angle X-ray scattering (SAXS), and Differential Scanning Calorimetry (DSC) [48].

2.3.3.10.5 Phase behavior

One of the crucial parameters that determine the stability and the fluidity of liposomes is the phase transition temperature (T_c), which is the temperature that causes phospholipids to shift their phase from the gel phase (lower fluidity) to the liquid crystalline phase (high fluidity). T_c depends on the length and saturation of hydrocarbon chains. It is directly proportional to the chain's length and is inversely proportional to the number of double bonds in the hydrocarbon chain [48].

Phase behavior is necessary for predicting the performance of liposomes. Liposomes must be stored in the gel phase and change into the liquid phase when administered at the cancer site. This phase change enhances permeability and allows *in-vivo* release of the drugs [39]. Figure 2-12 shows the transition of the liposomal bilayer from an ordered gel crystalline phase to a disorganized liquid crystalline phase under the influence of temperature. The fluidity and permeability of the membrane increase when the temperature increases above the melting point. The most commonly used technique for thermal analysis of phase behavior is Differential Scanning Calorimetry (DSC) [43],[48], [39],[74].

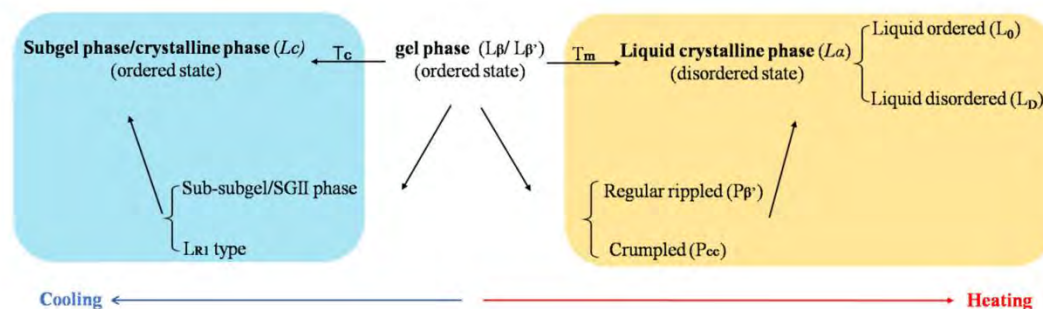


Figure 2-12 Liposomal bilayer phase transition from gel phase to liquid crystalline phase under the influence of temperature [25].

2.3.3.10.6 Encapsulation Efficiency

In drug delivery applications, loading an optimal dose of drugs is one of the main factors that help achieve therapeutic efficacy. Encapsulation efficiency (EE) is the percentage of the encapsulated drug compared to the amount of non-encapsulated or free drug used during the preparation. The amount of encapsulated drug is quantified, either indirectly assessing the encapsulated drug by subtracting the free drug concentration from the total drug concentration used or measured directly by completely disrupting the liposomes and quantifying the encapsulated drug. It is given by the equation:

$$EE\% = \frac{\text{mass of encapsulated drug}}{\text{mass of free drug}} * 100 \quad (2.1)$$

Size exclusion chromatography is one of the most extensively used techniques for measuring EE. It measures the size differences between the loaded liposomes and the free drug; However, the free drug must be separated from the drug-encapsulated liposomes before measuring EE. This can be achieved by dialysis membrane or ultracentrifugation methods. Other techniques such as UV-vis, fluorescence spectroscopy, and NMR are also used to quantify the EE [43],[48], [39].

2.3.3.11 Stimuli-responsive liposomes

One key advantage liposomes offer is the ability to alter their physicochemical properties by modifying their surface, which consequently changes the behavior of liposomes *in-vivo* to enhance therapeutic efficacy. Altering liposomal design enables triggered drug release that helps target the tumor tissue and release its cargo in response to a specific stimulus. This stimulus can be either intrinsic (from inside the body), i.e., pH, temperature, pressure, enzymes, redox reactions, or extrinsic (from outside the

body), such as light, magnetism, electric fields, ultrasound, etc. [39]. Figure 2-13 illustrates a schematic of liposome-based drug delivery system for the treatment of tumors.

2.3.3.11.1 Temperature responsive liposomes

Liposomes can be made temperature-sensitive by altering the phospholipid composition (mainly composed of DPPC) that makes them responsive to the increase in local temperature, hence providing an efficient method for the site-specific delivery of the anticancer drugs at the tumor site. Temperature-sensitive liposomes respond to high internal tumor temperatures and release maximum cargo at 41°C. Additionally, an external trigger can be applied to increase the local temperature. External stimuli include, hyperthermia, ultrasound, microwave, radiofrequency ablation, etc.[43], [60].

2.3.3.11.2 pH responsive liposomes

The targeting efficiency of the liposomes is improved by rendering them sensitive to changes in the pH in the tumor microenvironment, i.e., low acidic (pH < 6) in the tumor cells. It enables liposomes to alter their bilayer structure and promote site-specific drug release. Liposomes composed of phospholipid PE, such as DOPE or ligands sensitive to changes in pH, are examples of pH-sensitive liposomes [60].

2.3.3.11.3 Magnetic responsive liposomes

Liposomes synthesized of PC phospholipid, cholesterol, and magnetic iron oxide or encapsulated with metallic ions render liposomes sensitive to magnetism. In this phenomenon, NPs are targeted on-site by an external magnetic field, causing the immediate rupture and release of their cargo [60].

2.3.3.11.4 Ultrasound responsive liposomes

Ultrasound (US) is chosen as a stimulus of choice for this research. Ultrasound waves are mechanical and longitudinal pressure waves with frequencies higher than the human audible range (> 20 kHz) and can propagate through different media. The US is a physical phenomenon that possesses the physical properties of any wave, such as reflection, refraction, absorption, scattering, etc. The most important parameters that are used to modulate US waves are frequency, power intensity, velocity, and wavelength. US waves are for diagnostic purposes such as ultra-sonography, which

employs high-frequency sound waves to view images of the body's internal structures and diagnose infection. Some of the therapeutic applications of the US are; physiotherapy and lithotripsy (breaking kidney stones via shockwaves), and hyperthermia (for cancer therapy). Ultrasound is a theranostic (therapeutic and diagnostic) tool and offers both therapeutic and diagnostic functions by high-frequency ultrasound (HIFU) and sonography, respectively [2], [49], [50], [75]. Moreover, it is safe and penetrates body tissues without causing any harmful or adverse effects; thus, this technique can be used to monitor a developing baby (fetus) in pregnant women.

To image internal body organs or monitor a developing fetus, an ultrasound transducer probe is placed on the patient's skin or inserted through an opening, for example, the vaginal tract. A water-based gel is used to couple the US waves and eases the transmission of the US waves between the transducer probe and the patient. Ultrasound utilizes the phenomenon of acoustic impedance (AI), i.e., the resistance offered to the US beam by the tissue media. The US probe detects the reflected US wave penetrating the tissues with different AI. AI is dependent on the density of body tissues and the velocity of the US wave through the tissue. Ultrasound frequency used for medical purposes ranges from 2 – 10 MHz [2], [49], [50].

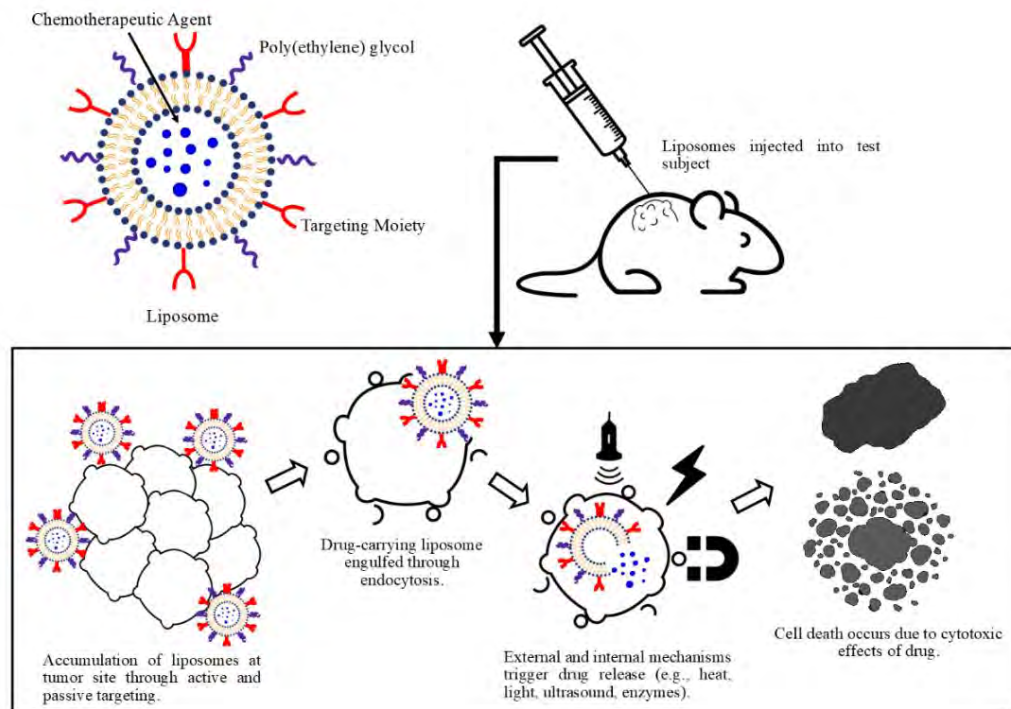


Figure 2-13 Schematic illustration showcasing a liposome-based drug delivery system for the treatment of tumors

Ultrasound uses a piezoelectric (piezo-pressure) crystal enclosed in an ultrasound transducer probe to focus the sound waves. It is a bi-directional crystal that can transform an electric signal into a pressure wave and vice versa. The generation of ultrasound relies on the pulse-echo principle, which employs an electric pulse to initiate the deformation in the piezoelectric crystal, and causes it to vibrate. These vibrations result in the transmission of high-frequency sinusoidal/ acoustic compression waves that propagate through the medium, which in this case are the body tissues [76]. Figure 2-14 represents a schematic of active targeting strategies employing nanoparticles.

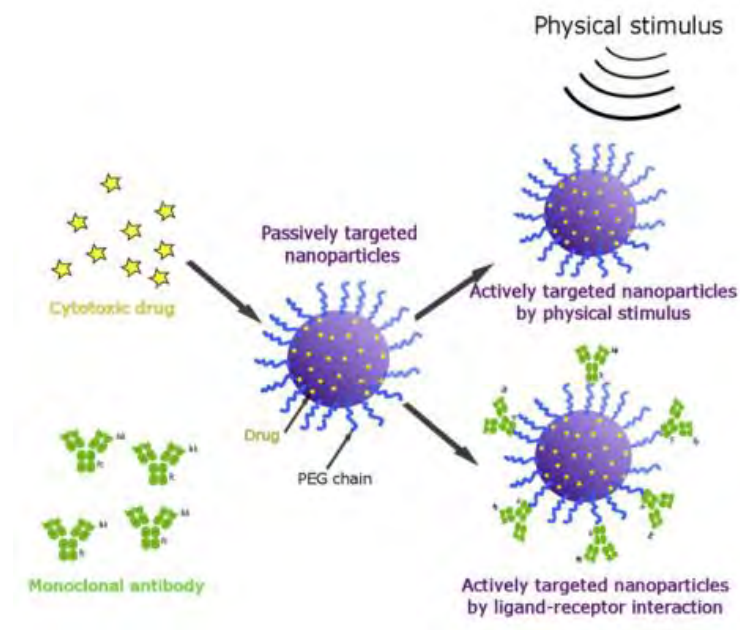


Figure 2-14 Active targeting strategies using nanoparticles [49]

Frequency, power density, and pulse duration are three crucial parameters of ultrasound waves. Frequency is the number of cycles per second (Hz), and power density is the amount of power applied per cross-sectional area of the US beam (W/cm^2). The transducer emits ultrasound waves in pulses of a specific duration at a certain rate, known as pulse repetition frequency, which determines the duty cycle of the US. Parameter selection depends on the medical applications, such as imaging requires the low-frequency US, whereas the high-frequency US is used to image superficial organs, e.g., skin. Drug delivery systems employ high-intensity focused ultrasound (HIFU) or low-intensity focused ultrasound (LIFU) to induce synergistic effects in the controlled release of antineoplastic drugs at the tumor site [76].

The duty cycle determines the time of US exposure to the tissues. The application of ultrasound for medical purposes employs the Doppler principle, with a continuous-wave (CW) doppler or a pulsed-wave (PW) doppler; However, for medical purposes, exposure of body tissue to continuous wave ultrasound is undesirable, as the US energy accumulation may overheat the body tissues and kill them. To combat this limitation, the US is applied as a pulsed wave to allow the energy to dissipate between successive pulses [76].

2.4 Ultrasound (US) as an external trigger

2.4.1 US-induced effects on liposomes

Ultrasound-induced biological effects; thermal and mechanical effects (such as cavitation) are used as a stimulus to trigger drug release from liposomes. Since the US is a physical phenomenon, it physically shakes the liposomes to render them unstable and induce the release of the encapsulated drug [77].

In drug delivery applications, the US is used as a stimulus to trigger drug release from liposomes once they accumulate at the tumor site. it allows time and location-specific release of encapsulated antineoplastic drugs, which helps minimize the side effects caused by conventional chemotherapy [78].

2.4.1.1. Thermal effects

Upon exposure to high-frequency ultrasound (HIFU), body tissues absorb thermal energy and elevate the local tissue temperature. Ultrasound-induced hyperthermia enables the temperature-sensitive NPs to release their content or kill cancer cells by heating. Mild hyperthermia (40 –43°C) causes vasodilation (increased blood flow), improves the accumulation of NPs at the tumor site, and induces protein denaturation in cancer cells due to increased sensitivity to hyperthermia compared to normal body tissues. In contrast, high hyperthermia > 43°C ceases the blood flow to the tissues leading to rapid cell death, i.e., necrosis. High-intensity focused ultrasound (HIFU) may prove an effective anti-cancer therapy by increasing local tissue temperature up to 50 – 80°C [78], [79]. Figure 2-15 shows a schematic of ultrasound-induced thermal effects.

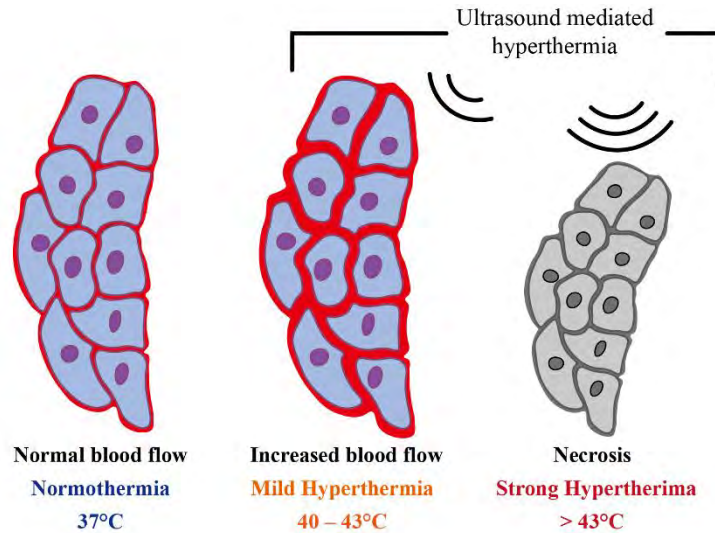


Figure 2-16 Ultrasound-induced thermal effects [49]

2.4.1.2 Mechanical effects and mechanical index

Cavitation: Mechanical index (MI) is the ability of the ultrasound acoustic beam to induce inertial cavitation effects on the body tissues. Mechanical effects of the US trigger drug delivery systems by oscillating bubbles, acoustic cavitation, acoustic streaming, and pressure waves. Mechanical Indices of up to 1.9 are considered acceptable by the FDA.

Mechanical Index (MI) is given by the following equation:

$$MI = \frac{P_-}{\sqrt{f}} \quad (2.2)$$

F is the US acoustic frequency, whereas P- is the peak negative or rarefaction pressure measured in megapascals and depends on the acoustic impedance of water (Z) and the intensity (I) of LFUS. P- is expressed by the equation below;

$$P_- = \sqrt{2ZI} \quad (2.3)$$

As the LFUS propagates through a medium, it induces non-thermal effects or pressure changes in that medium. As discussed earlier, ultrasound is a physical phenomenon; it transfers the energy to the particles of the medium through which it propagates. These mechanical waves transmit through a medium as high-pressure or compression waves and low-pressure waves or rarefactions/decompression waves. Figure 2-16 represents

a schematic diagram of mechanical effects of ultrasound. When the US propagates to a targeted site through a medium, it produces small gas pockets called acoustic cavitation. The US transfers its energy to pockets of gas, and variations in the pressure of US waves cause the gas bubbles to oscillate. These oscillating bubbles expand at low or rarefaction waves and contract at high-pressure waves without disintegrating or collapsing. This constant oscillation of gas bubbles due to linear oscillations is known as stable cavitation, which occurs at low-intensity US waves. Stable cavitation creates shear forces that are strong enough to break particles or permeabilize cells. [78].

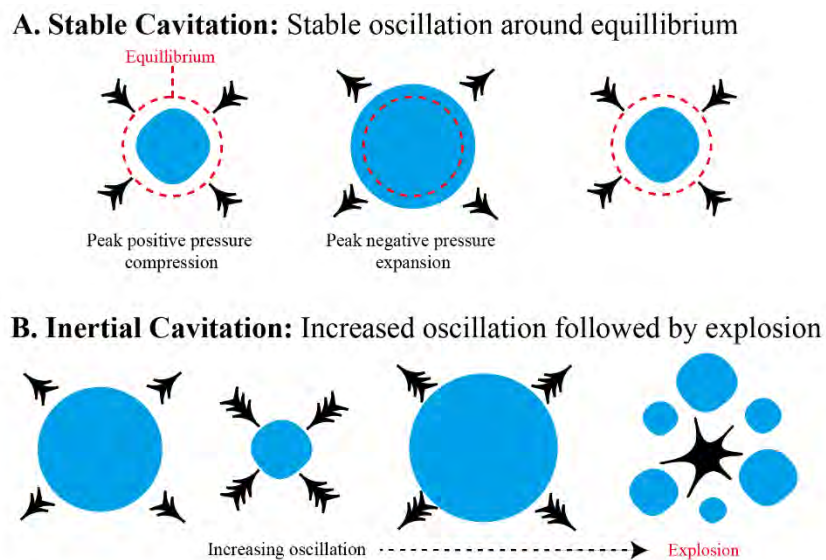


Figure 2-16 Mechanical effects of ultrasound, with microbubbles undergoing stable cavitation or inertial cavitation

However, as the intensity of the US wave increases, oscillations become non-linear leading to the rapid growth of gas bubbles until it reaches a point where it has enough inertia and keeps growing until the bubble finally explodes; and is called inertial or collapse cavitation of gas bubbles [78]. Figure 2-17 depicts a representation of effect of

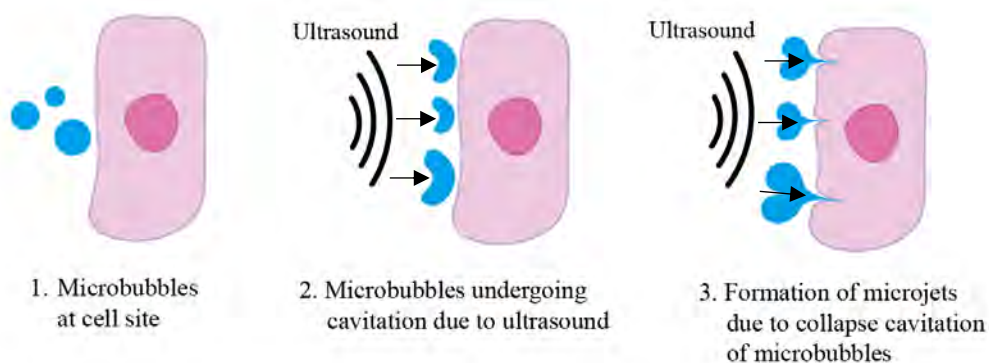


Figure 2-17 Microbubbles creating a micro jet as an effect of collapse cavitation and are directed towards the nearby solid surface

collapse cavitation of gas bubbles in the fluid/ tissue that occurs at high US intensity. The implosion of a bubble due to collapse cavitation accompanies two biological effects depending on the bubble's location.

Bubbles located at a distance from a solid body gives way to spherical, symmetrical, and high-pressure shock waves in the surrounding; however, if the bubble explosion occurs close to a solid object, the implosion will lead to the production of a sonic jet or jet stream of liquid that tends to pierce the solid particle and create pores on the cell membrane. In 1996, FDA revised the guidelines concerning the diagnostic US and regulated output based on the biological effect of US, such as thermal and mechanical indices and their significance, to avoid any over-exposure to the biological effects caused by the US [31], [50], [78].

Ultrasound is safe, non-invasive, and practical, used to see the insides of the human body without causing any adverse effects, and is based on non-ionizing radiation that eliminates the risks and cell toxicity associated with ionizing radiation such as; X-rays and other imaging modalities. However, US can slightly heat the tissues, primarily when used as a continuous wave (CW), and can produce gas pockets or bubbles (cavitation) inside the body; they are used as contrast agents in US imaging and are used to enhance the resolution in US diagnostic imaging and reduce noise. However, the former can be taken care of using a pulsed US wave instead of CW [32].

2.4.2 Advantages and disadvantages of ultrasound

Ultrasound is safe, non-invasive, and practical, used to see the insides of the human body without causing any adverse effects, and is based on non-ionizing radiation that eliminates the risks and cell toxicity associated with ionizing radiation such as; X-rays and other imaging modalities. However, US can slightly heat the tissues, primarily when used as a continuous wave (CW), and can produce gas pockets or bubbles (cavitation) inside the body; they are used as contrast agents in US imaging and are used to enhance the resolution in US diagnostic imaging and reduce noise. However, the former can be taken care of using a pulsed US wave instead of CW [32].

2.4.3 Enhancing liposomal sensitivity to ultrasound

Liposomes are naturally insensitive to US stimulus alone; however, liposome sensitivity to the US can be enhanced for drug delivery by introducing microbubbles or gas phase into liposomes (known as echogenic liposomes or bubble liposomes) or nanoemulsions droplets of perfluorocarbons (PFC) liquids inside the liposomes (eLiposomes), to increase the drug efficacy [31], [61].

2.4.3.2 Microbubbles

Microbubbles are micron-ranged structures composed of phospholipid shells filled with a gas such as perfluorocarbons. Perfluorocarbons have been used as oxygen carriers in the blood and as contrast agents in ultrasound diagnostic imaging. Recently microbubbles have gained the attention of researchers to be used in drug delivery systems. These gas bubbles are introduced into the liposomes with other therapeutic compounds to promote cavitation and sonoporation (pore formation by applying acoustic ultrasound) and release the drug at the tumor site. In a study done by Ingram and colleagues showed a significant increase in the efficacy of cytotoxic low-dose medicines, irinotecan, and SN38, by triggering microbubbles using the US in colorectal cancer mouse models [80].

Olsman et al. investigated the effect of focused ultrasound (FUS) and microbubbles on the transferrin (Tf) targeted liposomes in enhancing the permeability of the blood-brain barrier (BBB) in rats, overexpressing TfR in the BBB. The study revealed that FUS and microbubbles helped safely increase blood-brain barrier permeability and recorded a 40% increase in the accumulation of Tf-targeted liposomes in the brain hemisphere compared with isotype immunoglobulin G (IgG) liposomes. However, the size of microbubbles, i.e., 1 μm or above, limits them within the tumor vasculature and prevents microbubbles from penetrating the tumor cells. Thus, they have been used as intra-vascular agents to actively target endothelial markers such as VEGFR2 and $\alpha\text{v}\beta\text{3}$ integrin. The size restriction of microbubbles introduced nano-scale-sized nanobubbles and nanoemulsions that would easily extravasate into the tumor tissues and get endocytosed into the tumor cells [81],[82].

2.4.3.3 Nanobubbles (NBs)

NBs contain a colloidal gas center enclosed in a shell of surfactants (phospholipids, polymers, and enzymes). Surfactants help reduce the surface tension and increase the kinetic stability of the emulsions, keeping NBs stable [83].

They boost liposomes' sensitivity to the US by causing a rapid explosion of gas bubbles by cavitation, as shown in Figure 2-18.

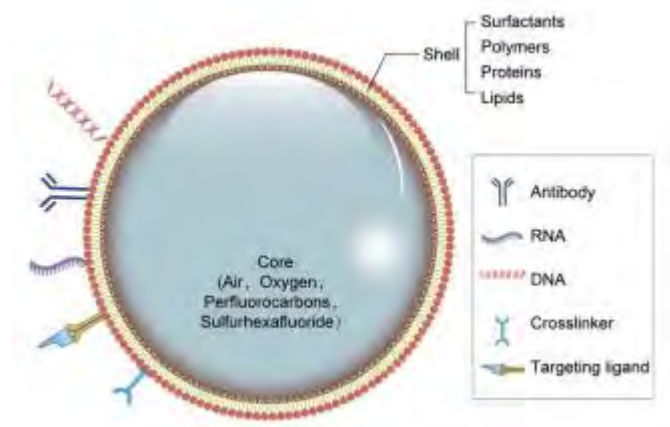


Figure 2-18 Structural illustration of a Nanobubble [62]

2.4.3.4 Nanoemulsions

Emulsions are a mixture of immiscible or insoluble liquids; a mix of oil and water is a perfect example. Emulsions on a nano-scale are called nano-emulsions, and they have nano-droplets of liquid dispersed through another immiscible liquid. Figure 2-19 shows the schematic structure of a liposome encapsulated with nano-emulsions. Liposomes

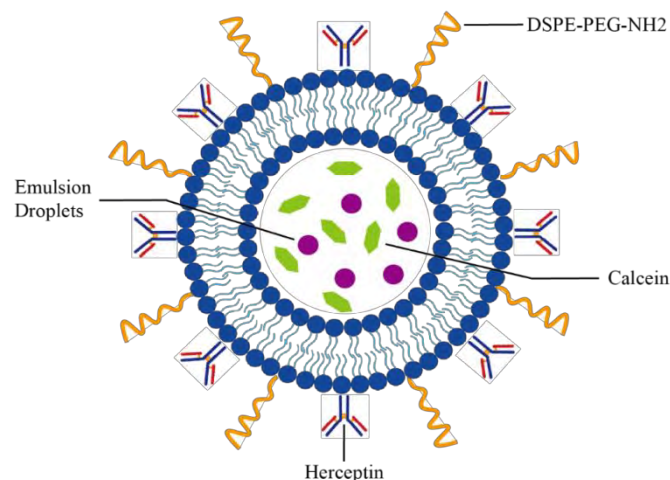


Figure 2-19 Structural illustration of Herceptin (Trastuzumab) conjugated-DSPE-PEG-NH₂ calcein encapsulated eLiposomes

encapsulate phase shift nano-sized liquid droplets such as perfluorocarbons (PFCs, with a low boiling point) for drug delivery applications. PFCs enhance the sensitivity of liposomes to the US waves. Upon exposure to the US, during the low-pressure wave, the pressure around emulsion droplets falls below the vapor pressure, and they vaporize, resulting in the expansion and explosion of the liposome. Lipid bilayer liposomes can only undergo 3% expansion in their structure before they break or puncture; this aids in releasing the encapsulated drug at the tumor site [31], [61], [84]. Figure 2-20 shows a schematic of nanobubbles cell membrane permeability via US.

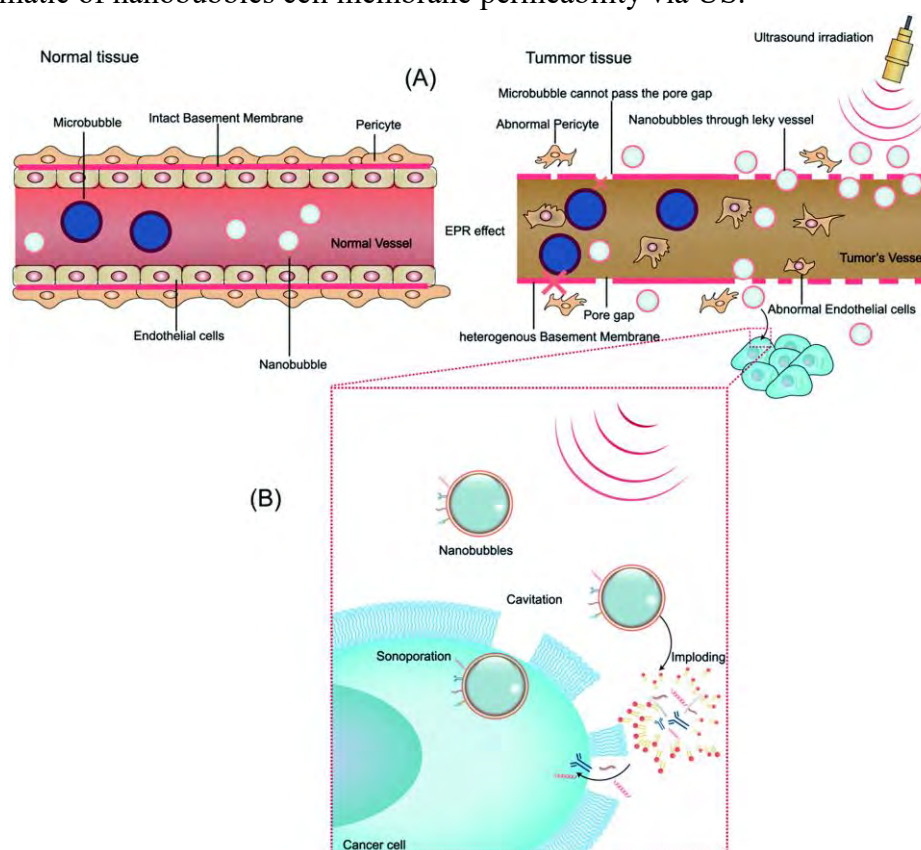


Figure 2-20 Nanobubbles passing through the endothelial pore in tumor tissue and increasing cell membrane permeability via US [53]

2.4.3.4.1 Acoustic droplet vaporization (ADV)

It is a phenomenon in which a liquid droplet changes its emulsion droplet's phase from liquid to gaseous, i.e., vapor, under acoustic US waves. This transition in phase leads to expansion and increase in NPs volume, consequently rupturing the liposome coat and resulting in the drug being set free [61],[85].

Perfluorocarbons (PFCs) are considered excellent candidates for emulsions in drug delivery applications due to their biocompatibility, non-toxicity, and hydrophobic behavior; hence, they have a very low solubility in aqueous solutions or even blood. In

medicine, PFCs find their application as ultrasound imaging contrast agents and oxygen carriers in blood substitutes [31], [61],[86],[87].

In a study by Lattin et al., the behavior of PFC₅ emulsion droplets upon exposure to the US demonstrates that only tiny emulsion droplets were visible before the application of US; however, upon exposure to the US, even the tiny emulsion droplets had vaporized into bubbles as observed in Figure 2-21(b) [87].

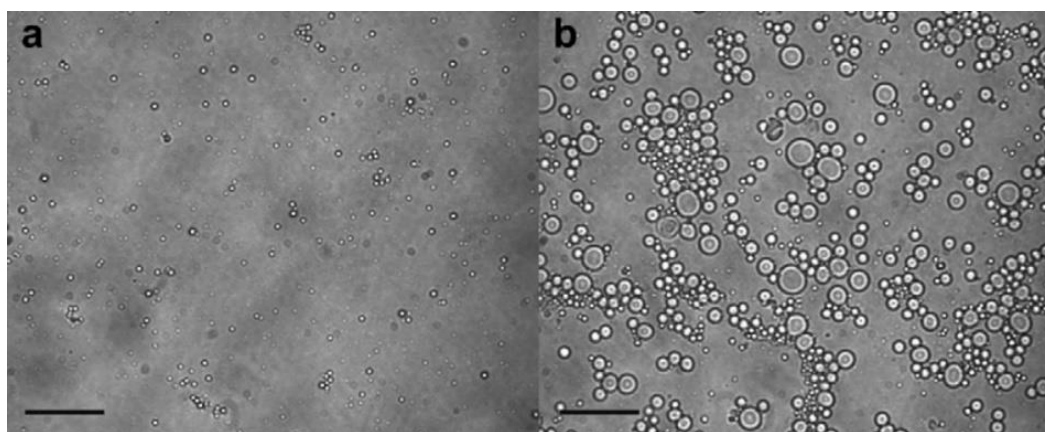


Figure 2-21 State of PFC₅ emulsion droplets (a) before the application of US VS (b) after the application of US. Scale bars represent 50 μm [87].

In a study by Ahmed and his colleagues, US was utilized as a trigger to release calcein from stealth and non-stealth liposomes. The thermal and mechanical disturbances by the US caused collapse cavitation, consequently piercing the liposomes and releasing calcein into the aqueous surrounding. The study showed that the release was inversely proportional to the frequency; however, at a constant frequency, increasing the power density led to an increase in calcein release. The study also compared the release from stealth and non-stealth liposomes at different pH values under constant frequency and power density. It revealed that at higher pH, the release from non-stealth liposomes was significantly higher than that observed from stealth liposomes [88].

Lattin and Pitt designed a series of experiments to analyze the release of calcein (used as a model drug) from eLiposomes as a function of temperature, size, and ultrasound frequency. Figure 2-22 represents Cryo-TEM images of eLiposomes encapsulated with PFC₅ emulsion. The research group designed ultrasound-responsive eLiposomes using perfluoropentane (PFC₅) and perfluorohexane (PFC₆) with different vapor pressures and boiling points. The DPPC lipid layer (5mg) encloses and stabilizes PFC₅ and PFC₆ emulsion droplets (0.2 g) to 1.5ml of water. 167 μL of hydrated DPPC is sonicating at a power density of 1W/cm² on an ice bath for 1 minute. Using an Avanti Mini Extruder,

the suspension was extruded through 100-nm and 450-nm polycarbonate filters. Whereas the eLiposome vesicles are synthesized using the dry film hydration method by hydrating DPPC (30 g/ml) sheets with PFC emulsions (0.2 ml) and calcein solution (0.2 ml of 30 mM) and heated to the lipid transition temperature of 50°C to form emulsion encapsulated eLiposomes [89].

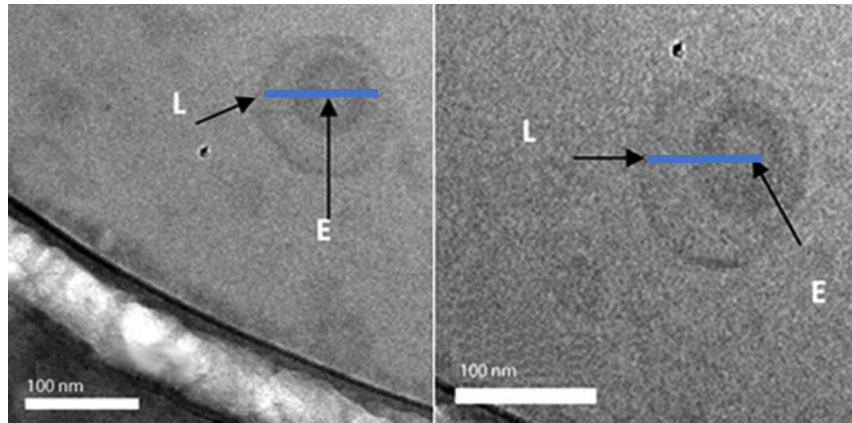


Figure 2-22 Cryo-TEM images of eLiposomes encapsulated with PFC5 emulsion droplets about 50nm in size [40].

Control liposomes were synthesized with the same lipid and calcein concentrations ignoring the emulsions. Liposomes and eLiposomes were extruded through 200-nm and 800 nm filters to compare the size effect. Figure 2-23 verifies the size using DLS data after the extrusion of eLiposomes through a 200-nm filter, showing a bimodal distribution with a peak at 80 nm corresponding to the emulsion and a peak at 200-nm corresponding to the liposome lipid membrane [89].

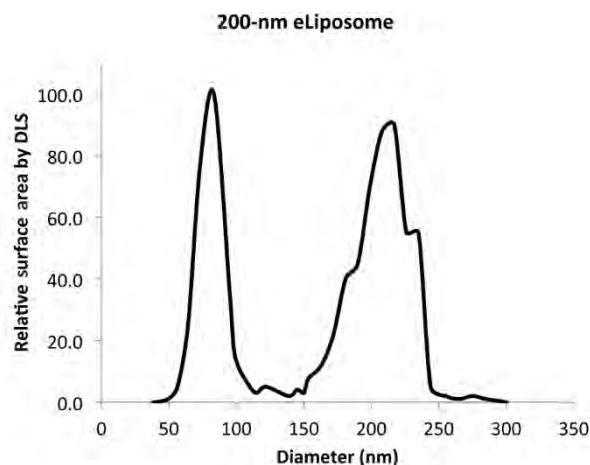


Figure 2-23 DLS measurement depicting a smaller diameter of emulsion peak and a larger diameter liposomal peak encapsulating the emulsion [57]

In order to measure the release of calcein, baseline fluorescence was recorded for 10 seconds when calcein was self-quenched and did not contribute to fluorescence; after

the application of US, calcein was released into the external solution, and fluorescence was measured; finally, 100% release of calcein was measured by lysing liposomes using 25 μL of 5% Triton X-100. Finally, the release was calculated using the following equation:

$$\%Release = \frac{F_{US} - F_i}{F_{tot} - F_i} * 100 \quad (2.4)$$

where F_i is the initial fluorescence at the baseline, F_{us} is the fluorescence after US application or sonication, and F_{tot} is the total release of calcein using Triton-X [89]. Figure 2-24a shows calcein release from small conventional liposomes (green circles), small eLiposomes with 100 nm PFC₅(red squares), and small eLiposomes with 100-nm PFC₆ droplets when exposed to the US at 20 kHz for 100 ms with intensity varying between 0.5 – 5 W/cm^2 , whereas, Figure 2-24b shows a comparison between release from small and their large counterparts (800-nm) vesicles with similar emulsions droplets of 100-nm [89].

Another study by Lattin et al. demonstrates a significantly higher release from 800-nm diameter eLiposomes than their small-sized counterparts, 200-nm eLiposomes. The study conducted that size significantly affects the release, possibly due to small eLiposomes being less susceptible to the US disturbances. Large eLiposomes, as seen in Figures 2-23 a and b, tend to encapsulate more than one emulsion or a large emulsion, respectively [87]. Small PFC₅ and large PFC₅ showed a release of 13% and 31%, respectively, whereas small PFC₆ and large PFC₆ showed a release of 13% and 22%, respectively; moreover, large and small control liposomes showed a 10% and 4% release, upon exposure to ultrasound at 20kHz for 100 ms. Figure 2-25a and b show the

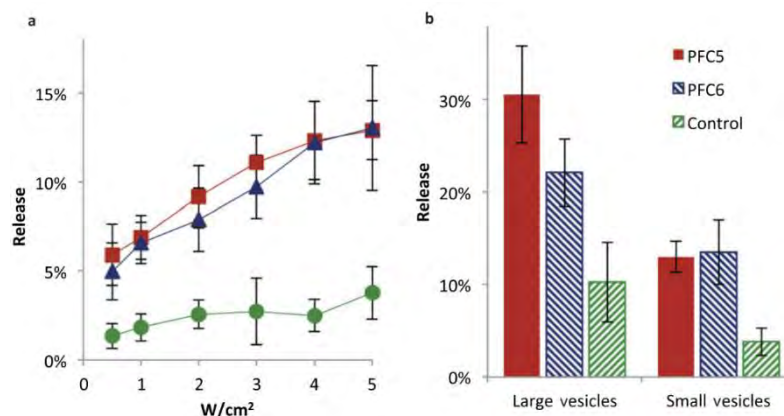


Figure 2-24 Percent calcein release results observed from Lattin and Pitt experiments (a) Percent release from eLiposomes as a function of power density b) Percent release as a function of eLiposome size [57]

percent calcein release from eLiposomes VS control liposomes as a function of increasing US intensities and insonation time. It depicts that PFC₅ eLiposomes showed a significantly higher calcein release that increased upon increasing insonation time and power intensities from 0.5, 1, and 2 W/cm².

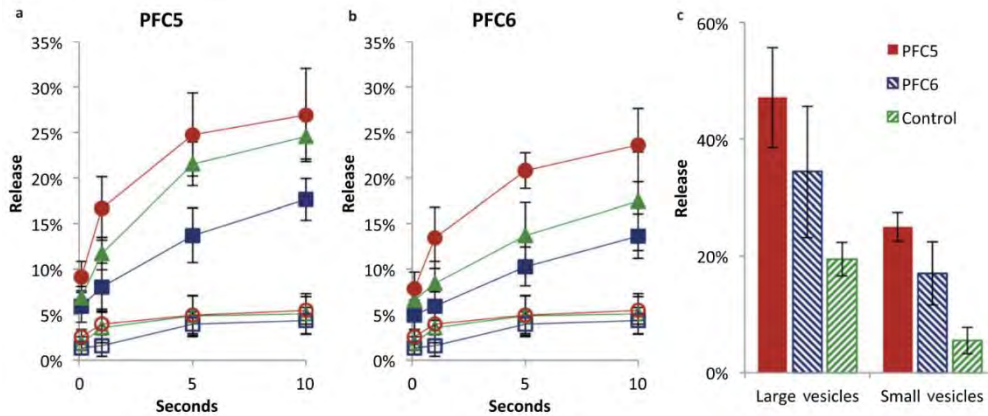


Figure 2-25 a) Percent calcein release from small PFC₅ eLiposomes solid shapes compared to control liposomes hollow shapes shows a significant difference between the percent release from these two carriers b) with small PFC₆ eLiposomes solid shapes compared to control liposomes hollow shapes at varying US intensities of 0.5W/cm² (blue squares), 1W/cm² (green triangles) and 2W/cm² (red circles) c) Percent release from PFC₅, PFC₆ and control liposomes as a function of size, shows that PFC₅ has been outperforming the other two carriers in terms of percent release [57]

However, there was no significant difference in the release from control liposomes, showing less calcein release at a statistical level. A similar trend is seen for PFC₆ liposomes, only that PFC₅ showed much higher release than PFC₆ at longer insonation times. It was also observed that large eLiposomes and control liposomes showed a much higher calcein release upon exposure to the US at 1 W/cm² for 10 seconds. The difference in release between PFC₅ and PFC₆ emulsion liposomes could have been due to their vapor pressure, as PFC₅ has a higher vapor pressure of 135.05kPa compared to PFC₆ of 48.09kPa, at 1 atm and 37°C [86]. Hence, these droplets have weaker intermolecular forces than compared to PFC₆, with a vapor pressure of 28kPa. Thus, a lower threshold value and low US amplitude would suffice to reduce the vapor pressure and induce acoustic droplet vaporization [87].

Lattin and Pitt designed experiments to investigate the performance of eLiposomes and liposomes at physiological temperatures (37°C); experiments revealed the stability and capability of eLiposomes to sequester drugs at physiological temperatures. Experiments employed a fluorometer that measured fluorescence in a heated water bath at incubation times of 3, 10, 20, and 30 minutes. They repeated the process for both eLiposomes with

large (450 nm) and (100 nm) emulsions. No calcein release was observed from the samples mentioned above, signifying that heating alone cannot render eLiposomes unstable. Finally, Triton-X was used to lyse the eLiposomes, which released all calcein sequestered throughout the heating process, thus indicating that eLiposomes are very stable at physiological temperatures [87]. Figure 2-26 depicts % drug release obtained from large and small-sized eLiposomes in comparison to conventional liposomes.

The calcein release from eLiposomes (large and small) and control liposomes upon exposure to the US at 20kHz for 100 ms at physiological temperature 37°C and varying intensities showed that large samples released significantly higher calcein (PFC₅-49%, PFC₆-31%, and control-12%) than small samples (PFC₅-15%, PFC₆-12%, and control-5%). The experiments deduced that eLiposomes are thermally stable, and increasing the temperature above the emulsions' boiling point, did not affect the calcein release. PFC₅ and PFC₆ eLiposomes demonstrated similar release at room temperatures; the release was significantly different at physiological temperatures for both large and small eLiposomes [87]. The above parameters provided good insight into the performances of liposomes and eLiposomes; however, assessing their behavior as a

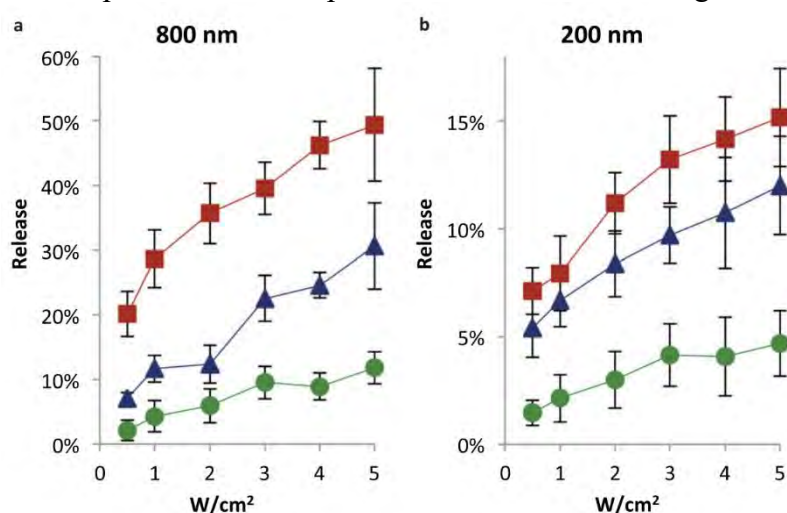


Figure 2-26 Percent calcein release from large eLiposomes (800 nm vesicles with 450 nm emulsions) and small liposomes (200 nm vesicles with 100 nm emulsions), PFC₅ (red squares), PFC₆ (blue triangles) and control liposomes (green circles) [55]

function of ultrasound frequency is equally essential. Lattin and Pitt studied the behavior of PFC₅ eLiposomes and control liposomes as a function of US frequency (varying from 20 kHz to 525 kHz) and mechanical indices (MI = 0.53 at 5W/cm² and MI=1.41 corresponding to 35W/cm²). In this study, PFC₅ eLiposomes and control liposomes are exposed to PW ultrasound for 2 to 30 seconds with 525kHz at 20kHz

pulse repetition frequency. Figure 2-27 depicts a representation of calcein release from eLiposomes in comparison with conventional liposomes, at varying power density and exposure times. The study demonstrates that frequency significantly affects the evaporation of emulsion droplets. Since lower frequency offers a long window of negative peak pressure, allowing more time for nucleating and gas expansion, thus it

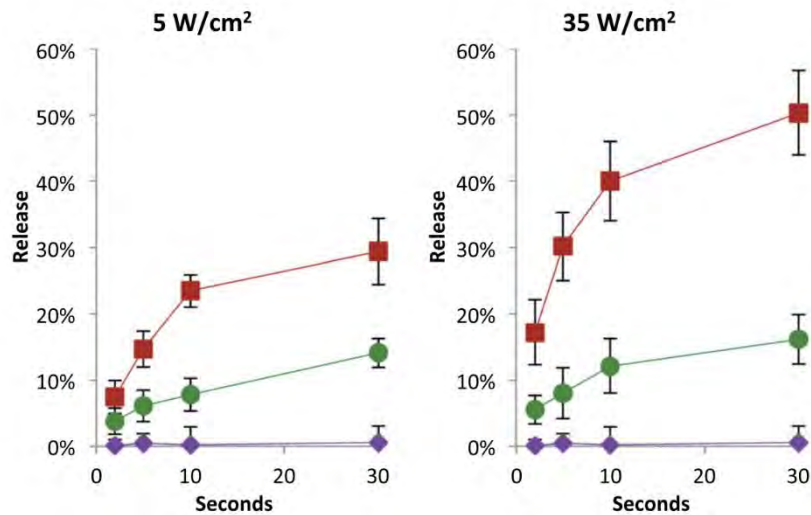


Figure 2-27 Calcein release PFC₅ eLiposomes (red squares) and control liposomes (green circles) at 525kHz US frequency by varying power density from 5 W/cm² to 35 W/cm² and exposure time from 2-30 seconds [55].

can be concluded that increasing the frequency, decreases the threshold of acoustic vaporization. PFC₅ eLiposomes showed a significant difference in their release compared to control liposomes, which are 2-3 times and 3-5 times more when exposed to 5W/cm² and 35W/cm², respectively; however, the study shows no significant release in control liposomes with the change in intensities [87].

The study revealed that identical mechanical indices at 20kHz and 525kHz did not produce a significant difference in the release, as shown in Figure 2-28 a. However, at similar power intensities (see Figure 2-28b), 20kHz frequency produced a significantly higher release than 525kHz. The study by Lattin et al. confirmed that the emulsions were effective and enhanced liposome sensitivity to ultrasound only when encapsulated within liposomes instead of submerging outside the liposomes to induce maximum release upon exposure to ultrasound [87]. Figures 2-29 a and b depict that PFC₅ and PFC₆ eLiposomes show the highest % calcein release than control liposomes and liposomes with emulsions on the outside; however, PFC₅ eLiposomes show a 10% higher release than PFC₆ eLiposomes. Similar trends were observed regardless of increasing intensity or varying insonation times. The study by Lattin et al. revealed that

the sensitivity of pure liposomes to ultrasound dramatically relies on the cavitation effects caused by the surrounding air bubble; however, formulating eLiposomes, which, unlike conventional liposomes, contain nano-sized emulsion droplets made of liquids with high vapor pressure, allowed passive targeting and increased sensitivity to ultrasound [87].

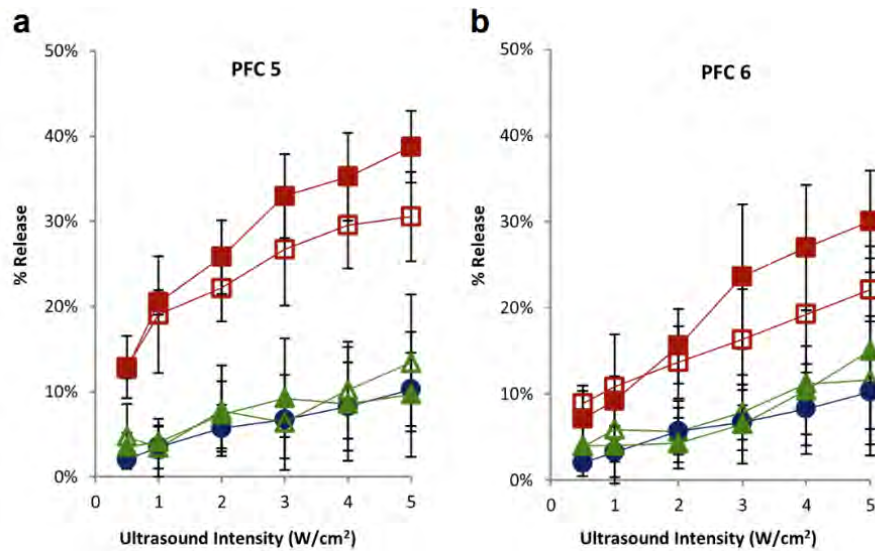


Figure 2-28 (a) Percent calcein release from PFC₅ eLiposomes, and (b) Percent calcein release from PFC₆ eLiposomes upon exposure to the Us at 20 kHz for 100 ms at varying intensities. eLiposomes with large (solid red block) and small (hollow red block) emulsions, conventional liposomes (blue circle), empty lipid vesicles with large emulsions droplets to its outside environment (solid green triangle), and small emulsions to the outside (hollow green triangle) [87]

Lattin and colleagues compared the ultrasound-induced release of the encapsulated model drug, calcein, from eLiposomes (PFC₅ and PFC₆) with the two negative controls (without the droplets and with droplets outside the liposomes vesicle). eLiposomes showed significantly higher calcein release than both control groups due to emulsion droplets inside the liposome vesicles, disrupting its membrane structure from within the

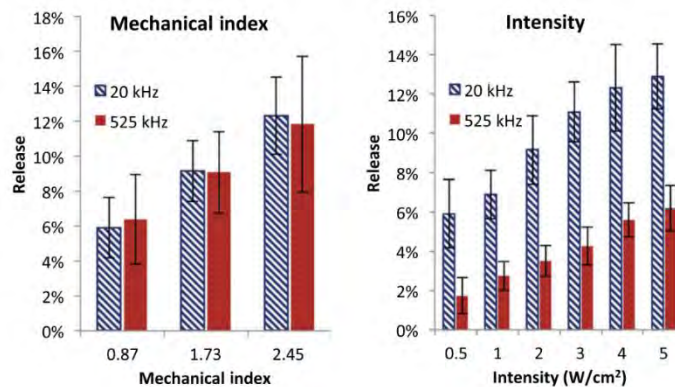


Figure 2-29 Calcein release from PFC₅ eLiposomes when exposed to short burst cycles of frequency 20 and 525 kHz for 100 ms to avoid heating and damaging of tissues, a) with identical mechanical indices and b) with identical intensity [55].

eLiposomes and aiding calcein release. eLiposomes showed 3- 4 times more calcein release than the control groups, which increased further upon increasing ultrasound power intensity and time of exposure. However, after a certain eLiposomes became saturated, no further increase was observed upon increasing the power intensity.

The study also reported that an increase in power density resulted in an increased tissue temperature; however, this increase in temperature was not responsible for the significantly higher release from eLiposomes compared to pure liposomes [87]. Another study on eLiposomes conducted by Javadi and co-workers successfully prepared two types of eLiposomes using the one-step method and ultra-method by encapsulating PFC₅ and PFC₆ emulsion droplets, having boiling points closer to physiological temperature, i.e., 29°C and 57°C, respectively that may cause a change in the emulsion's phase from liquid to gas and consequently expanding the liposome and breaking it open. Figure 2-30 represents the calcein release from eLiposomes in comparison with conventional liposomes at a fixed power density but varying periods.

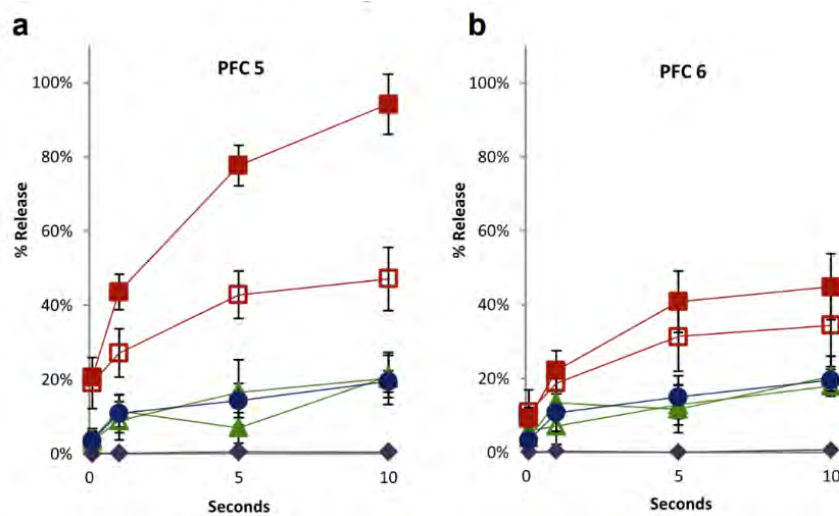


Figure 2-30 (a) % Calcein release from PFC₅ eLiposomes, and (b) % Calcein release from PFC₆ eLiposomes with exposure to 20kHz US at 1W/cm² at varying periods. ELiposomes with large (red solid block) and small (red hollow block) emulsions, conventional liposomes (blue circle), empty lipid vesicles with large emulsions droplets to their outside environment (green solid triangle), and small emulsions to the outside (green hollow triangle) [87].

eLiposomes synthesized using the ultra-method were conjugated with folate-targeting ligands and used to deliver calcein to HeLa cells. These eLiposomes were small enough to make the most of the EPR effect and extravasate through the leaky blood vessels into the tumor cells. The study revealed that encapsulated emulsions and folate-targeting ligands were essential for ultrasound-mediated calcein release [61], [90]-[93].

Husseini and colleagues tested and confirmed the absence of untimely breakage of eLiposomes by varying temperatures. The study monitored calcein release from PFC₅ eLiposomes in the absence of acoustic ultrasound for an hour and confirmed that they are stable at a physiological temperature of 37°C, which is above its boiling point, i.e., 20°C; however, the release of calcein was significantly high at temperatures higher than lipids transition temperature, i.e., 49°C; this may have been due to the thermal transition of lipids or vaporization of emulsion droplets contained within eLiposomes. Hence it was confirmed that eLiposomes are stable at physiological temperatures and are triggered at the target site upon exposure to the US [94].

Work done by Husseini and colleagues demonstrates that the non-actuated release of calcein at higher temperatures may have occurred due to the impurity leading to heterogeneous nucleation of gas [95]. Williams and co-workers further investigated and studied the delivery of DOX to multidrug-resistant cancer cells and found that ultrasound did not play a significant role in triggering the drug release when using folate-targeted eLiposomes, aiding its ingestion into cancer cells. Heterogeneous nucleation caused by the DOX sulfate fibers while loading DOX led to gas-phase transformation. At the same time, the eLiposome was taken in and endocytosed, proving the occurrence of vaporization without the actuated trigger, i.e., ultrasound [96].

Chapter 3 Methodology

In this chapter, materials and methods used to formulate the four different liposomal formulations are discussed in detail.

3.1 Materials

The phospholipids used to synthesize the liposomes, namely; 1,2-dipalmitoyl-sn-glycero-3-phosphocholine (DPPC) and 1,2-distearoyl-sn-glycero-3-phosphoethanolamine-*N*-[amino(polyethyleneglycol)-2000] (ammonium salt) (DSPE-PEG₍₂₀₀₀₎-NH₂) are purchased from Avanti Polar Lipids Inc. (Alabaster, AL, U.S.A, supplied by Labco LLC. Dubai, UAE). On the other hand, calcein disodium salt (C₃₀H₂₄N₂Na₂O₁₃), cholesterol, bicinchoninic acid kit, Sephadex G-100, Triton X-100, Ammonium Ferrothiocyanate (AF) are purchased from Sigma Aldrich (St. Louis, Missouri, USA), supplied by LABCO L.L.C. (Dubai, UAE). Trastuzumab (Herceptin) was purchased from a local pharmacy. The 0.2- μ m and 0.05- μ m polycarbonate membrane filters and filter support were purchased from Whatman PLC (Maidstone, England, U.K.).

3.2 Procedures

3.2.1 Preparation of PFC₅ nanoemulsion droplets

Ten mg of DPPC is dissolved in 1 mL of chloroform and dried onto the walls of a round-bottomed flask at 50°C for 15 min under vacuum using a rotary evaporator (rotovap). Subsequently, 2 mL of PBS was added to hydrate the dried film, followed by the addition of 0.6 ml of PFC₅. During the subsequent ultrasonic mixing process, an iced bath was utilized to minimize the evaporation of PFC₅ and effectively reduce the potential loss of PFC₅ during the emulsification process and maintain stability. Sonication was carried out using a sonication bath at 35 kHz (Elma D-78224, Melrose Park, Illinois, USA) for five times, 10 seconds each with a 1-minute pause between sonications. The size of emulsion droplets was reduced by extruding through 0.05- μ m polycarbonate membrane filters.

3.2.2 Preparation of calcein-encapsulated DSPE-PEG-NH₂ control liposomes

Liposomes were prepared using the lipid-film hydration technique. For each batch of liposomes prepared using this approach, 19.2 mg of DPPC (with a transient temperature of 41°C) along with lipid-soluble compounds to be incorporated into the liposomes such as; DSPE-PEG₂₀₀₀-NH₂ (5.6 mg) and cholesterol (4.7 mg) are added at 65:30:5 molar ratios and dissolved in 4 ml of organic solvent chloroform in a 250 mL round bottom flask. The chloroform was evaporated using a rotary evaporator above the transition temperature of the lipids, i.e., 50°C, for 15 min in a round-bottomed flask under vacuum using a roto-vap (80 rpms) until a dried film was observed onto the walls of the flask. First, the flask is inspected to ensure no chloroform is present, as this could compromise liposome stability while increasing exposure to toxicants.

The dried thin film of lipid makes liposome sphere formation easy by hydrating the film using 2 ml of 50 mM calcein solution (calcein - 40 mg, PBS – 1.87 ml, NaOH – 130 µl) with pH adjusted to 7.4 at 60 °C in a rotatory bath without vacuum at 120 rpm for 50 – 60 mins. Since PBS is aqueous, it forms a bilayer liposome encapsulating calcein via self-assembly resulting in a small volume of multilamellar vesicles (MLVs) resembling an onion-like structure. To acquire unilamellar liposomes, sonicate the suspension using a sonication bath at 35 kHz (Elma D-78224, Melrose Park, Illinois, USA) for 2 mins. The size of the liposomes is adjusted to a diameter <200 nm (80-100 nm radius) using high-pressure extrusion (100-1000 psi) with a polycarbonate Nuclepore Whatman filter with a fixed pore size of 200 nm (Avanti Polar Lipids, Inc., Alabaster, AL, USA). Gel exclusion chromatography using Sephadex G-100 column is used to purify liposomes from any free calcein.

3.2.3 Preparation of emulsion liposomes (eLiposomes)

In this method, 0.5 mL of nanoemulsion droplets previously formed are added to 0.5 mL calcein-encapsulated control liposomes in a similar ratio of 1:1; the mixture is sonicated on an ice bath for 10:60 (10 seconds on and 60 seconds off) for three times, encapsulating nanoemulsions into liposomes, thus forming eLiposomes. Gel exclusion chromatography using Sephadex G-100 column is used to purify eLiposomes from the liposomes and free nanoemulsion droplets.

3.2.4 Preparation of Trastuzumab-conjugated liposomes

The conjugation process for Trastuzumab to control liposomes involved two distinct steps. Figure 3-1 illustrates the overall process. First, liposomes needed to be modified using 2,4,6 trichloro-1,3,5 triazine (cyanuric chloride) as a coupling agent to initiate conjugation. Subsequently, the monoclonal antibody was added at a pH of 8.5. Cyanuric chloride was first dissolved into acetone to produce a 10 (mg/ml) solution. Next, 9.23 μ l of the prepared cyanuric chloride solution was diluted in de-ionized water to avoid rupturing of liposomes. The resulting solution was added to liposomes (1 ml) in a vial, to achieve a 1:1 molar ratio between cyanuric chloride and DSPE-PEG-NH₂. The reaction was carried out by stirring at 80 rpm in an iced bath for three hours. This allowed for the nucleophilic substitution of the proton on the NH₂ group located on the surface of the liposomes with chloride sites present in cyanuric chloride. Following this initial conjugation step and three-hour incubation, 1 mg of Trastuzumab was dissolved in 0.5 mL of borate buffer with a pH of approximately 8.5 and introduced into the liposome mixture and left to stir at 80 rpm overnight to ensure the completion of conjugation. This prolonged stirring facilitated the binding of trastuzumab to the modified liposomes. To purify liposomes, a Sephadex G-100 column was prepared and equilibrated with a PBS solution. The liposomal solution was then passed through this column, purified, and subsequently stored at 4°C until further use.

Step 1: Nucleophilic substitution of Chloride



Step 2: Conjugation reaction to obtain immunoliposome

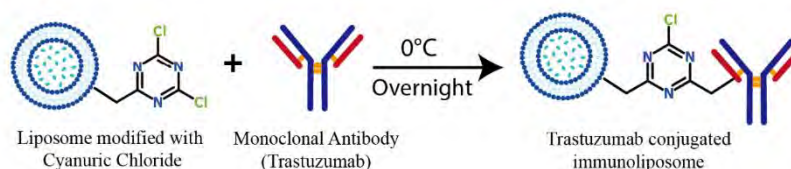


Figure 3-1 Structural illustration of Conjugation of Herceptin to DSPE-PEG-NH₂ with cyanuric chloride as a coupling agent [35]

3.2.5 Preparation of Trastuzumab-conjugated eLiposomes

In this method, the previously formulated nanoemulsion droplets (0.5 mL) are added to 0.5 mL Trastuzumab-conjugated immunoliposomes to achieve the proper ratio (1:1), the mixture is sonicated on an ice bath for 10:60 (10 seconds on and 60 seconds off) for three times, encapsulating nanoemulsions into liposomes, thus forming eLiposomes. Gel exclusion chromatography using a Sephadex G-100 column is used to purify eLiposomes from the liposomes and free nanoemulsion droplets.

3.2.6 Size and polydispersity evaluation using Dynamic Light Scattering (DLS)

The average size and polydispersity index (PDI) of liposomes and eLiposomes were assessed using Dynamic Light Scattering (DLS) using Dynapro® NanoStar™ equipment provided by Wyatt Technology Corp., Santa Barbara, CA, USA. This is a powerful technique that reveals the dynamics of the particles, hydrodynamic radius and the monodispersity or polydispersity of the particle. DLS works based on the Brownian motion principle, in which particles' random movement submerged in a liquid is used to calculate hydrodynamic radii. The velocity of particles or the rate of Brownian motion is called the translational diffusion coefficient (D), which can be converted to particle size using the Stokes-Einstein equation:

$$D = \frac{k_B T}{6\pi\eta R_H} \quad (3.1)$$

where D = translational diffusion coefficient (speed of particles)

k_B = Boltzmann constant ($m^2kg/K s^2$),

T = solution temperature (K)

η = viscosity (Pa.s)

R_H = Hydrodynamic radius (m)

Figure 3-2 illustrates the fundamental setup of a Dynamic Light Scattering (DLS) machine. The setup involves illuminating a laser beam toward the sample placed within the cuvette. A laser beam interacts with the particles present in the sample the particles then scatter the light in various directions, while a detector captures the snapshots of the intensity fluctuations scattered from the sample undergoing Brownian motions. The

angle at which the light is scattered is converted to a signal utilized to calculate the diffusion coefficient. The correlator takes rapid snapshots of the fluctuating intensities and compares the lagged signal with the original signal based on the autocorrelation phenomenon. Larger particles show slower diffusion and longer correlation, whereas, smaller particles show rapid diffusion and shorter to no correlation with the passage of time.

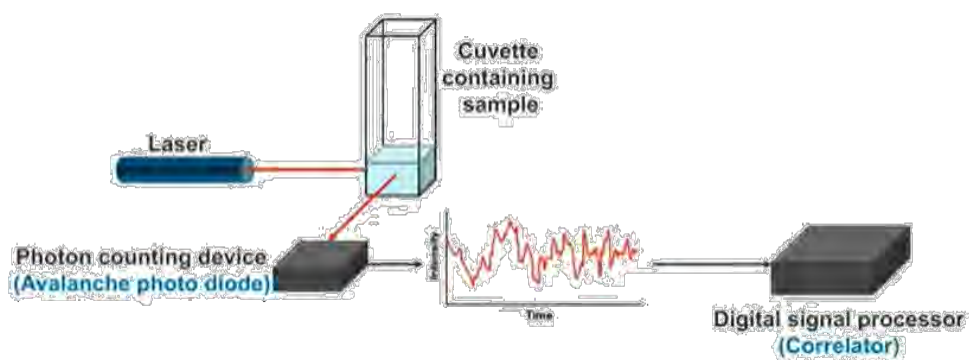


Figure 3-2 Dynamic Light Scattering machine set up

The hydrodynamic radii of the liposomes were determined following the appropriate dilution of the liposomal samples in phosphate-buffered saline (PBS) at room temperature. The test sample is created by diluting 15 μL of liposomes in 1 mL of PBS solution. Subsequently, the sample was transferred to a cuvette, readings were recorded to measure the liposome's hydrodynamic radii and polydispersity index.

3.2.7 Quantification of Lipid content of the prepared liposomal formulations using Stewart Assay

The phospholipid content of the liposomes is estimated using the Stewart assay. This technique is essential and relies on the ability of phospholipids to interact with ammonium ferrothiocyanate (FTC) and form a complex. One notable advantage of this assay is its ability to avoid interference from inorganic phosphate. Unlike other assays, the presence of inorganic phosphate does not affect the actual measurement of the phospholipids [97].

The initial step of this assay involves preparing a calibration curve by dissolving DPPC in chloroform at various concentrations and measuring the absorbance at 485 nm. Following this, prepared liposomes (100 μL) are transferred into a (250 mL) round-bottomed flask and subjected to a rotary evaporator to break the liposomes under

vacuum for 15 minutes. Subsequently, 1 mL of chloroform is added to the flask and sonicated for 10 minutes, until existing particles are no longer visible. Furthermore, samples are prepared using varying volumes of liposomes, chloroform, and FTC according to the quantities shown in Table 3-1 with a total volume of 4 ml and added into centrifuge tubes. In total 8 sample tubes were prepared including two blank samples (without liposomes) to establish a baseline. FTC is a red inorganic compound that is insoluble in chloroform; however, when the solution is vigorously vortexed for 20 seconds, it initiates a reaction between the liposomes and FTC.

Table 3-1 The sample preparation of the Stewart Assay

Control Liposomes	Targeted Liposomes	Liposomes (μL)	Chloroform (μL)	FTC (μL)
1	4	75	1925	2000
1A	4A	75	1925	2000
2	5	125	1875	2000
2A	5A	125	1875	2000
3	6	200	1800	2000
3A	6A	200	1800	2000
Blank 1		-	2000	2000
Blank 2		-	2000	2000

The sample tubes are centrifuged at 1000 rpm for 10 mins, resulting in a biphasic distribution, with a top dark layer and a bottom clear layer. The top layer is discarded; however, the bottom chloroform phase is pipetted using a Pasteur pipette and added to a quartz cuvette. The optical density of the chloroform phase is measured using the Evolution™ 60S ultraviolet-visible (UV-Vis) spectroscopy (ThermoFisher Scientific, Madison, WI, USA) along with the VISIONlite software at a max absorbance peak of

485 nm against pure chloroform with an optical density of zero (used as a reference) [98]. The procedure is repeated for Herceptin-conjugated liposomes.

Following these steps, a calibration curve can be constructed and the absorbance measurements obtained from the liposomal samples can be accurately compared and analyzed. The preparations and blank samples ensure precise and reliable results for the analysis.

3.2.8 Quantification of antibody conjugation using bicinchoninic acid (BCA) assay

The BCA assay is the most popular method for colorimetric detection used for the measurement of the concentration of proteins in a sample. It uses a bicinchoninic acid reagent, giving the assay its name is a highly sensitive chelating agent. This assay relies on the ability of proteins to reduce cupric ions Cu^{+2} to cuprous ions Cu^{+1} in an alkaline medium, also known as the biuret reaction. Secondly, the chelation of two bicinchoninic acid molecules with one cuprous ion then reacts with the to form a purple-colored complex, whose intensity is directly proportional to the concentration of protein in the sample. The intense purple complex has a peak absorbance of 562 nm and can be measured spectrophotometrically[99].

The bicinchoninic acid reagent was prepared as follows: 4.5 mL of QuantiPro™ buffer QA was mixed with 4.5 mL of QuantiPro™ buffer QB, and 180 μL of CuSO_4 solution using the QuantiPro™ BCA kit purchased from Sigma-Aldrich Chemie GmbH (supplied through LABCO LLC., Dubai, UAE) was added. Buffer QA consists of sodium carbonate, sodium bicarbonate, bicinchoninic acid and sodium tartrate in 0.1 M sodium hydroxide, whereas Buffer QB consists of 4% cupric sulfate. Eight microfuge tubes were prepared using varying volumes of liposomes, PBS, and BCA reagent to achieve a final volume of 2 mL. The quantities are specified in the provided Table 3-2. In addition, two blank samples containing only PBS and BCA agents were prepared to specifically establish a baseline for comparison.

The microfuge tubes containing the prepared samples were incubated in a water bath set at 60°C for 60 minutes. Following the incubation period, samples were carefully removed from the bath and allowed to cool down to room temperature. Subsequently,

the cooled samples were transferred into cuvettes for the measurement of absorbance at a wavelength of 562 nm using Evolution™ 60S ultraviolet-visible (UV-Vis) spectroscopy (ThermoFisher Scientific, Madison, WI, USA) along with the VISIONlite software.

Table 3-2 BCA assay sample preparation

Samples	Liposomes (μL)	PBS (μL)	BCA reagent (μL)
Blank 1	-	1000	1000
Blank 2	-	1000	1000
C1	800	200	1000
C2	400	600	1000
C3	200	800	1000
H1	800	200	1000
H2	400	600	1000
H3	200	800	1000

3.2.9 Cryogenic transmission electron microscopy (Cryo-TEM)

Cryo-Electron microscopy was used to visualize the structural properties of eLiposomes at ultra-low temperatures. Cryo-TEM use aimed to confirm the encapsulation of nanoemulsions within the liposomes. The samples were instantly frozen to preserve the structural integrity using liquid nitrogen, to achieve temperature below -150°C. This prevented the formation of ice crystals in the nanostructured samples that may distort their structure or introduce artifacts and allow imaging in their near-native state. The frozen samples are analyzed using an electron microscope, maintaining the true structures at cryogenic temperatures.

3.2.10 Low-frequency ultrasound release of calcein

Calcein is a fluorescent molecule with an excitation wavelength of 495 nm and an emission wavelength of 515 nm. To initiate the release of calcein from liposomes and eLiposomes, low-frequency ultrasound (LFUS) at a 20-kHz was applied using an ultrasonic probe (model VCX750, Sonics & Materials Inc., Newtown, CT, USA) and the changes in fluorescence were monitored using a QuantaMaster QM 30 Phosphorescence Spectrofluorometer (Photon Technology International, Edison NJ, USA). Figure 3-3 shows the setup employed to monitor drug release from liposomes.



Figure 3-3 Low-frequency ultrasound probe and phosphorescence spectrofluorometer setup for drug release

The sample was prepared by diluting 75 μl of liposomes in 3 ml PBS in a fluorescence cuvette. The four slits of the sample compartment of the spectrofluorometer were set to 1.25 mm. The cuvette was placed inside the spectrofluorometer chamber, and a 20-kHz ultrasonic probe was inserted approximately 2 mm into the cuvette through the specified opening. The experiment started by establishing and recording the baseline or initial fluorescence intensity for 50 seconds without sonication. Subsequently, pulsed US was initiated with cycles of 20 seconds of sonication followed by 20 seconds of rest for seven minutes. Calcein released was observed at three machine power settings: 20%, 25% and 30%, corresponding to power densities of 6.2, 9, and 10 mW/cm^2 , respectively (as measured by the hydrophone). The sonication cycles were repeated until a plateau was reached, and at this point, 50 μL of Triton X-100 (Tx100) was added to the cuvette to lyse the liposomes, in order to release all encapsulated calcein.

Recorded fluorescent intensities were substituted in the below equation to measure the percentage release:

$$\% \text{ encapsulated drug release} = \frac{F_{US} - F_i}{F_{tot} - F_i} * 100 \quad (3.2)$$

Where F_i is the baseline intensity, F_{US} is the intensity at the time of application of US (20 kHz), and F_{tot} is the maximum fluorescence obtained by lysing the eLiposomes.

3.2.11 Statistical analysis

In order to compare the disparities between the results obtained, statistical analysis was conducted using a two-tailed t-test with unequal variances. A P-value of 0.05 was used as an indicator, and a p-value of less than or equal to 0.05 indicated that the differences were statistically significant, whereas p-values above 0.05 indicated that the results were insignificant.

3.2.12 Kinetic modeling of drug release

In drug delivery systems, mathematical models are employed to monitor and comprehend the kinetics of drug release, assess its efficacy and optimize the drug delivery systems. Controlled release of the encapsulated drug is a crucial factor that helps achieve desirable therapeutic efficacy. Mathematical models aid in quantifying physical parameters associated with the release, such as the diffusion coefficient of the drug that provides quantitative data about the drug's ability to disperse within the system. In this thesis, two different mathematical models are used to predict the acoustic release kinetics of calcein associated with the release process.

3.2.12.1 *The zero-order model*

In drug delivery systems, zero-order model drug release kinetics follows a constant rate of change in the amount of drug diffused per unit time. The drug in a solution at any given time can be represented as C_t and according to the hypothesis, the drug concentration in the solution behaves as:

$$\frac{dC_t}{dt} = k_0 \quad (3.3)$$

Where k_0 is the arbitrary constant representing the rate at which drug is released, regardless of the concentration. Integrating the above differential equation by parts

within the time bounds of 0 to a given time t , gives us the solution for the drug concentration [100], [101].

$$C_t - C_0 = k_0(t - 0) \quad (3.4)$$

Where C_t represents the amount of drug released at a specific time, t , C_0 represents the initial amount of drug in the solution, and usually negligible or zero and k_0 is the zero-order release constant.

Cumulative Fraction Released (CFR) is a measure used to quantify the amount of drug released over a period of time. It is given by the following equation:

$$CFR = \frac{C_t - C_0}{C_T} = \frac{\text{Drug released at any time, } t - \text{initial drug concentration}}{\text{Total concentration of the drug}} \quad (3.5)$$

Dividing the above equation by total drug concentration i.e., C_T , we obtain:

$$CFR = \frac{k_0 t}{C_T} \quad (3.6)$$

Where, $K_0 = \frac{k_0}{C_T}$ is the new release constant and the equation for the zero-order kinetics can be expressed as follows:

$$CFR = K_0 t \quad (3.7)$$

It is important to point out that CFR takes into consideration the initial concentration of the drug that can be zero, and thus, the CFR plot is expected to exhibit a linear pattern passing through the origin (0,0) with the slope representing the rate constant K_0 specific to the release. In the case of calcein, the initial baseline C_0 measured using a fluorometer, refers to the initial level of fluorescence and serves as a baseline for measurements.

3.2.12.2 The first-order model

In the year 1967, Gibaldi and Feldman introduced the Noyes-Whitney equation that enabled an understanding of the process of drug dissolution in a liquid medium. The release rate of the drug, at any time t , is proportional to the concentration of the drug remaining in the system and, thus, decreases exponentially over time.

It can be expressed as:

$$\frac{dC(t)}{d(t)} = -kC(t) \quad (3.8)$$

Where, $C(t)$ is the amount of the drug in solution at any given time t , and k is the first-order release percent constant corresponding rate at which the drug is release, with units of per unit time. Integrating the above differential equation using integration by parts within the time limits of 0 and a given time t , yields the solution for the drug concentration.

$$\ln \frac{C(t)}{C_0} = -k(t - 0) \quad (3.9)$$

Taking the exponential on both sides of the above equation, gives:

$$\frac{C_t}{C_0} = e^{-kt} \quad (3.10)$$

Equating the above equation to CFR gives us the following;

$$CFR = \frac{C_t - C_0}{C_T} = \frac{C_0}{C_t} (e^{-kt} - 1) \quad (3.11)$$

$$\ln(CFR + \frac{C_t - C_0}{C_T}) = \ln(\frac{C_0}{C_t}) - kt \quad (3.12)$$

First-order release kinetics model plots $\ln(CFR + \frac{C_t - C_0}{C_T})$ versus time as a straight line with $-k$ as the slope and $\ln(\frac{C_0}{C_t})$ as the y-intercept.

Chapter 4 Results and Analysis

In this chapter, we present a detailed overview of the physical and chemical properties of the liposomal and eliposomal formulations to gain a thorough understanding of their characteristics. Furthermore, we extensively evaluate their drug release performance by studying the release kinetics of the encapsulated drug. These results and analysis helped us gain insights into liposomal drug formulations' size, morphology, stability, and overall quality.

4.1 Estimation of size using Dynamic Light Scattering (DLS)

The sizes of the three batches for each control liposome, emulsions and eLiposomes, and targeted liposomes and eLiposomes, each were assessed using dynamic light scattering (DLS). As mentioned earlier, measuring the radii ensured the liposomal formulations were within the 200-nm diameter to ensure enhanced permeability (EPR) effect, as mentioned earlier. Additionally, the polydispersity index was also measured to ensure the uniformity of the liposome size within each sample. A polydispersity index of 20% is acceptable for drug delivery applications. The average diameters and percent polydispersity index (%Pd) value for each batch of liposomes are summarized in Table 4-1, whereas, for eLiposomes and their respective emulsions are presented in Table 4-2.

Table 4-1 DLS results for control and HER-conjugated liposomes

Batches	Control Liposomes		HER Liposomes	
	Radius (nm)	PDI (%Pd)	Radius (nm)	PDI (%Pd)
Batch 1	89.70	10.40	91.50	11.20
Batch 2	87.90	13.60	86.80	14.20
Batch 3	87.20	12.00	90.50	16.20
Average	88.27 ± 1.29	12 ± 1.60	89.60 ± 2.48	13.87 ± 2.52

Statistical analysis was conducted on different liposomal formulations, and examinations disclosed that Herceptin conjugated liposomes demonstrated a slightly larger size than the control liposomes, and the difference was statistically significant (p-value = 0.022). This can be attributed to the conjugation of Herceptin to the

liposomal surface. Herceptin has a molecular weight of 100 kDa, and is estimated to increase the liposome size by 2.5 nm.

Table 4-2 DLS results for emulsions, eLiposomes and HER-conjugated eLiposomes

	Emulsions		eLiposomes		HER eLiposomes	
Batches	Radius (nm)	PDI (%Pd)	Radius (nm)	PDI (%Pd)	Radius (nm)	PDI (%Pd)
Batch 1	50.60	16.00	99.00	20.60	104.20	29.10
Batch 2	49.90	12.50	95.40	16.40	102.70	26.10
Batch 3	49.30	9.20	91.80	14.50	101.80	24.40
Average	49.93 ± 0.65	12.57 ± 3.40	95.40 ± 3.60	17.17 ± 3.12	102.90 ±1.21	28.20 ± 1.82

The size of eLiposomes was slightly larger compared to both control and HER liposomes. A statistically significant difference was observed between eLiposomes and control liposomes (p-value = 0.0339), whereas, the difference between eLiposomes and HER liposomes was statistically insignificant (p-value = 0.119). This discrepancy could be attributed to 50-nm emulsions encapsulated with the liposomes. eLiposomes demonstrated slightly larger size compared to both control and HER liposomes; however, the difference between eLiposomes and control liposomes was found to be statistically significant (p-value = 0.0339), whereas, the difference between the HER liposomes and eLiposomes was statistically insignificant (p-value = 0.119). This may be due to 50 nm emulsions encapsulated within the liposomes. However, it is worth noting that the eLiposomes lacked heavy molecular weight moiety on their surface. Figure 4-1 provides a size distribution for all the liposomes.

Based on the aforementioned observation, Herceptin-conjugated eLiposomes demonstrated the largest size compared to all the liposomal formulations. This can be attributed to the presence of encapsulated emulsions, in addition to the Herceptin on its surface. However, it is worth noting that all the liposomal formulations showed radii within 200 nm that can be used to exploit to enhanced permeability and retention effect (EPR effect).

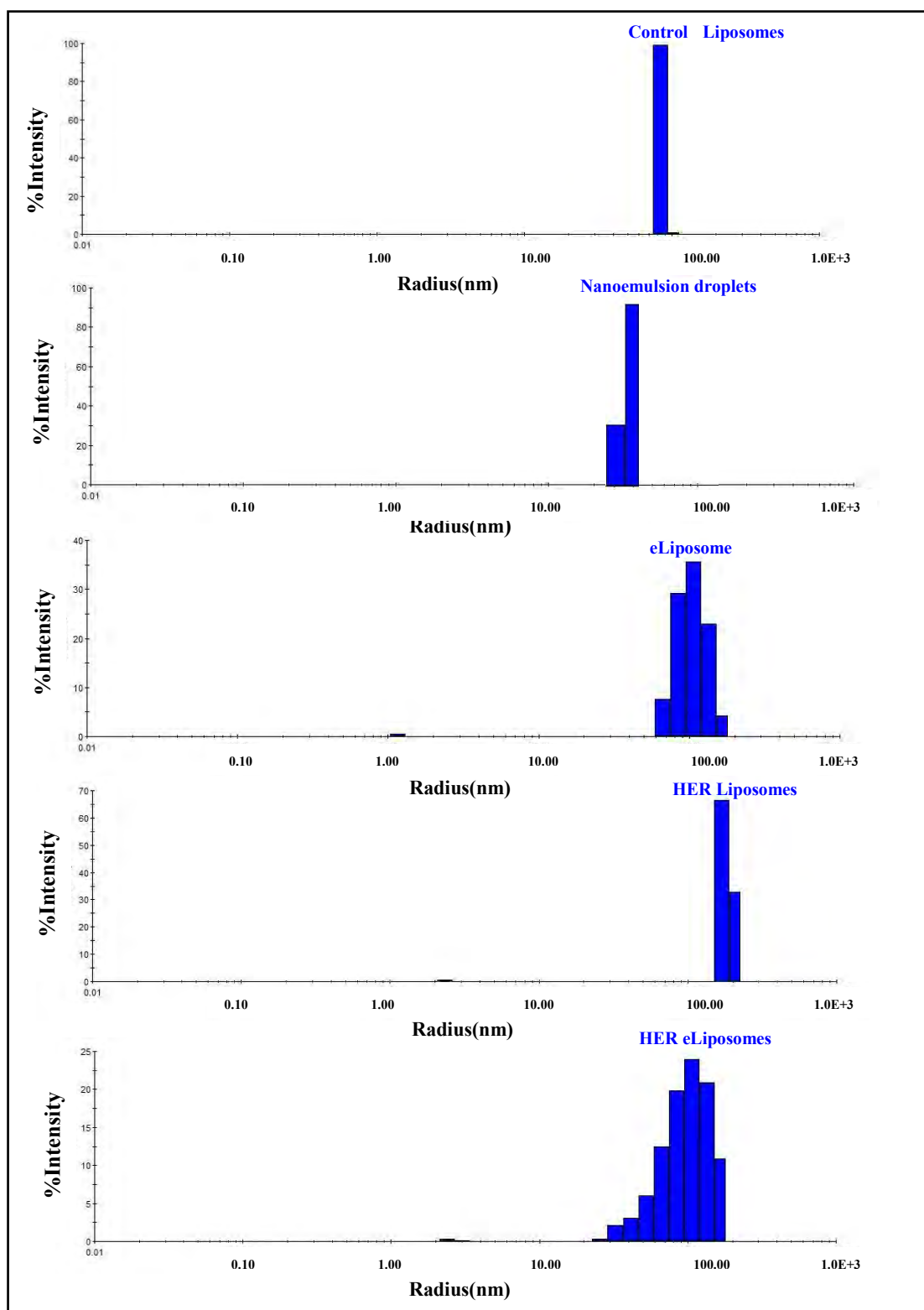


Figure 4-1 Size distribution of control liposomes, emulsions, eLiposomes, HER-conjugated liposomes and HER-conjugated eLiposomes

4.2 Quantification of total lipid concentration using the Stewart Assay

In this study, all liposomal formulations, including emulsions, were prepared using DPPC as the primary lipid component and it absorbs light at a specific wavelength of 485 nm. The preceding chapter provided a comprehensive detail of the procedure employed in the Stewart assay to determine the phospholipid content within the liposomes. To ascertain precise lipid content, a calibration curve was generated using known DPPC concentrations in mg/mL against the absorbed wavelength.

Table 4-3 Stewart Assay results for control liposomes and HER-conjugated liposomes

Batches	Control Liposomes (mg/mL)	HER Liposomes (mg/mL)	Control-to-HER liposome ratio (mg/mL)
Batch 1	14.97	6.13	2.44
Batch 2	14.66	6.74	2.17
Batch 3	10.12	6.05	1.67
Average	13.25 ± 2.71	6.31 ± 0.38	

Table 4-3 observations reveal a significant contrast in the lipid content between the control and HER-conjugated liposomes. The lipid content in control liposomes is nearly twice as high as that in the HER-conjugated liposomes. This trend can be anticipated due to the additional column purification process employed by the targeted liposomes after the HER-conjugation process. The purification process aims to enhance the quality of HER-conjugated liposomes, meanwhile, inadvertently introducing entrapment of lipids within the porous structure of the column beads, thus leading to a decreased final lipid concentration.

4.3 Estimation of protein content through BCA assay

In this study, we employed the BCA assay to assess the protein content in both control and HER-conjugated liposomes, with a comprehensive procedure outlined in section 3.2.8. The color intensity difference between the control liposomes and HER-conjugated liposomes is shown in Figure 4-2. Similar to the Stewart assay, linear

calibration plot was constructed and employed to measure the UV absorbance at 562 nm using a spectrophotometer.

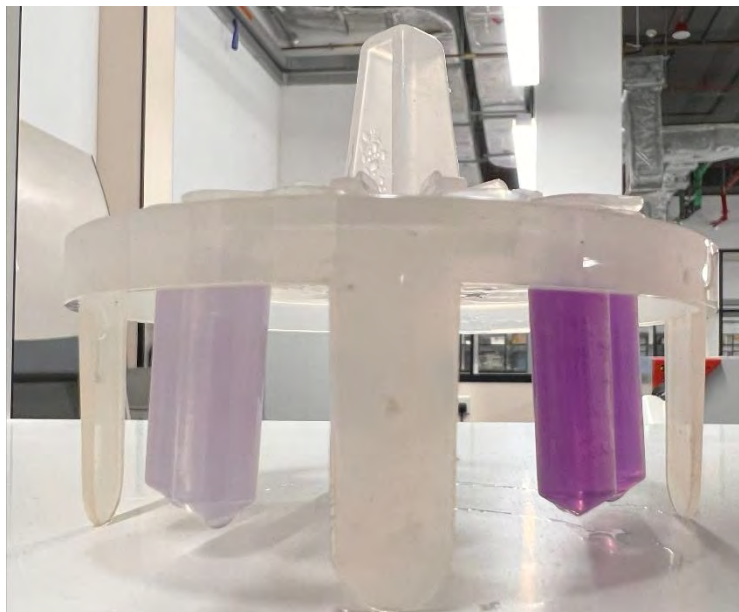


Figure 4-2 The difference in color intensity observed between control liposomes (left) and Herceptin-conjugated liposomes (right)

Table 4-4 provides a comparative analysis of the protein content in control and HER-conjugated liposomes.

Table 4-4 BCA assay results for control liposomes and HER-conjugated liposomes

Batch	Protein concentration ($\mu\text{g/mL}$)		
	Control Liposomes	HER Liposomes	Her-to-control liposome ratio
Batch 1	46.84	81.03	1.73
Batch 2	24.42	50.08	2.05
Batch 3	46.84	95.11	2.03

Analysis of Table 4-4 indicates that the protein concentration in HER-conjugated liposomes is approximately twofold than that in the control liposomes across all synthesized batches. This observation aligns with the anticipated pattern, as Herceptin is an additional protein conjugated to the liposomal surfaces in the targeted liposomes. However, there is no statistically significant difference between the two liposomes ($p\text{-value} = 0.077$).

4.4 Cryogenic electron microscopy (Cryo-TEM) images:

In order to confirm the encapsulation of nanoemulsions inside the core of liposomes, cryo-TEM images were obtained. Figure 4-3 is a high-resolution image revealing the visual evidence of successfully internalized nanoemulsions within the liposomal structure. These findings align with the previous studies that have demonstrated the successful encapsulation of nanoemulsions within liposomes [61]. The absence of any physical deformation and preservation of the individual liposomal and emulsion structures within the eLiposomes, confirms the suitability and stability of eLiposomes as nanocarriers. Furthermore, it validates the compatibility of liposomes and nanoemulsions, thus maintaining the drug delivery properties and maximizing therapeutic efficacy.

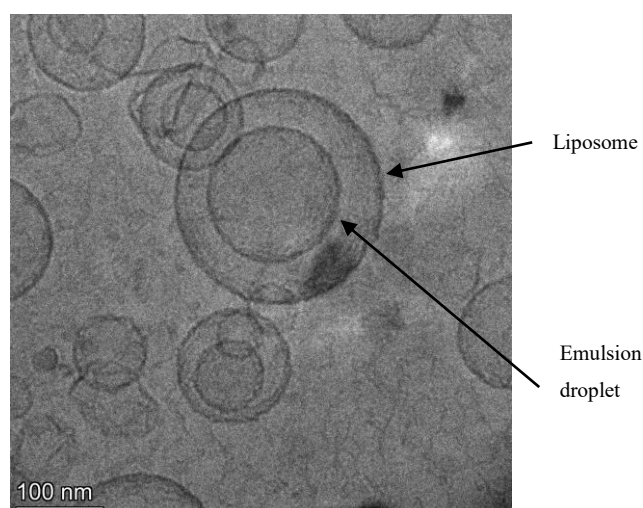


Figure 4-3 Cryo-TEM images for liposomes encapsulated with nanoemulsions

4.5 Stimulation of drug release from liposomal formulations using low-frequency ultrasound (LFUS):

In this study, low-frequency US release was conducted on three batches of control liposomes, HER - conjugated liposomes, emulsion liposomes and, HER-conjugated eLiposomes (with three replicates per batch). Each liposomal formulation was loaded with calcein as a model drug. To trigger controlled drug release, low-frequency ultrasound (LFUS) was employed, with varying power densities as discussed in section 3.2.10.

Three independent trials for each liposomal formulation were conducted at different pulses. The findings related to the release profiles depicting the cumulative fraction release of the encapsulated model drug, calcein, over time and the impact of LFUS-mediated drug release from control, targeted and eLiposome formulations are illustrated in Figures 4-4, 4-5, and 4-6.

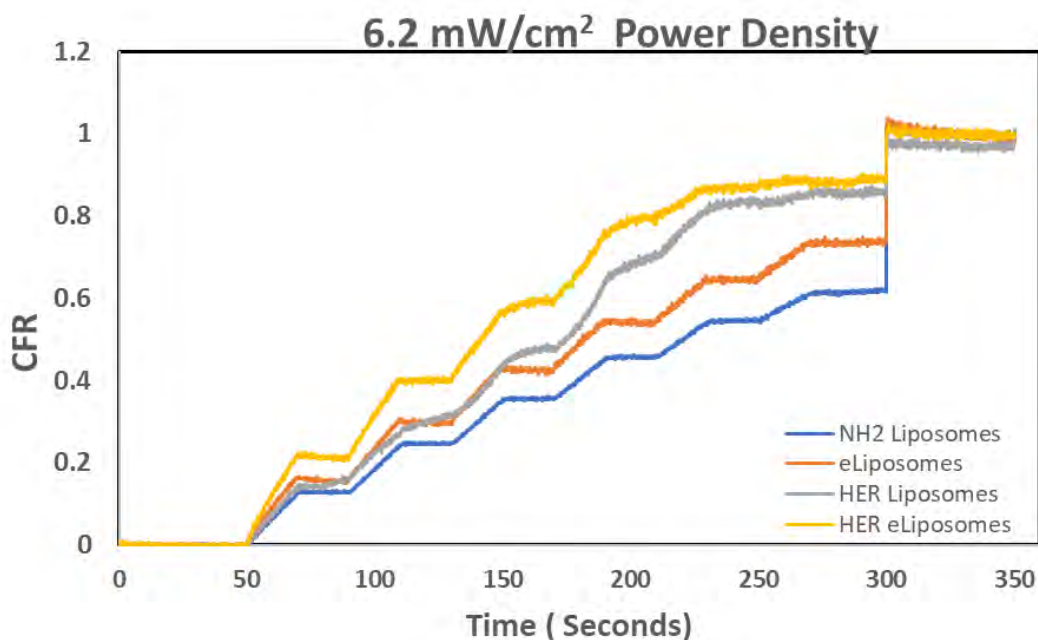


Figure 4-4 Comparison of Cumulative Fractional Release from control liposomes, eLiposomes, HER-conjugated liposomes and HER-conjugated eLiposomes at 6.2mW/cm² power density

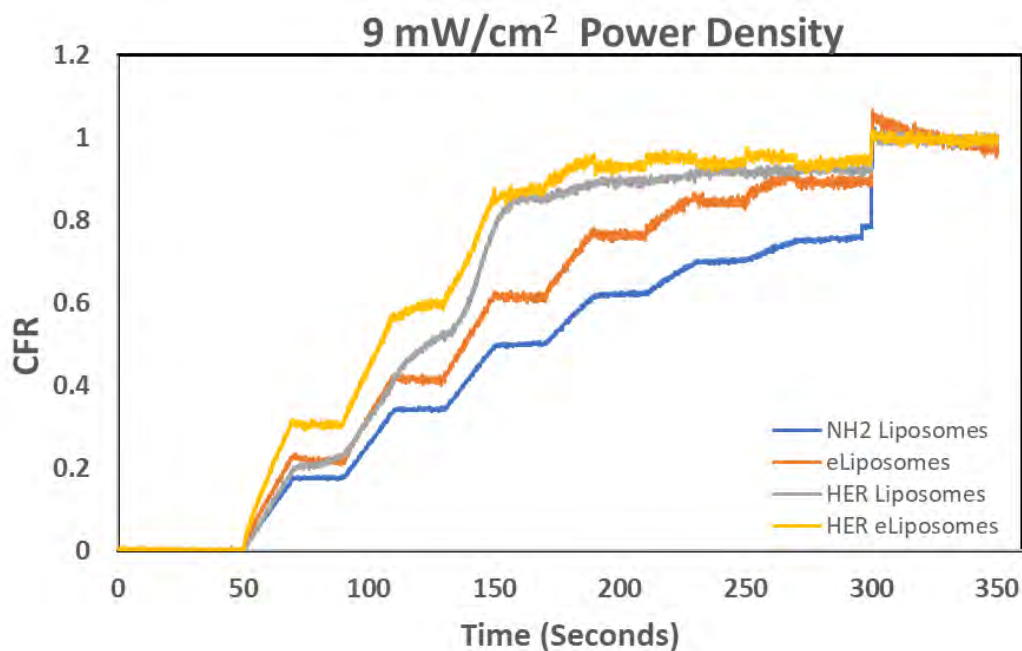


Figure 4-5 Comparison of Cumulative Fractional Release from control liposomes, eLiposomes, HER-conjugated liposomes and HER-conjugated eLiposomes at 9mW/cm² power density

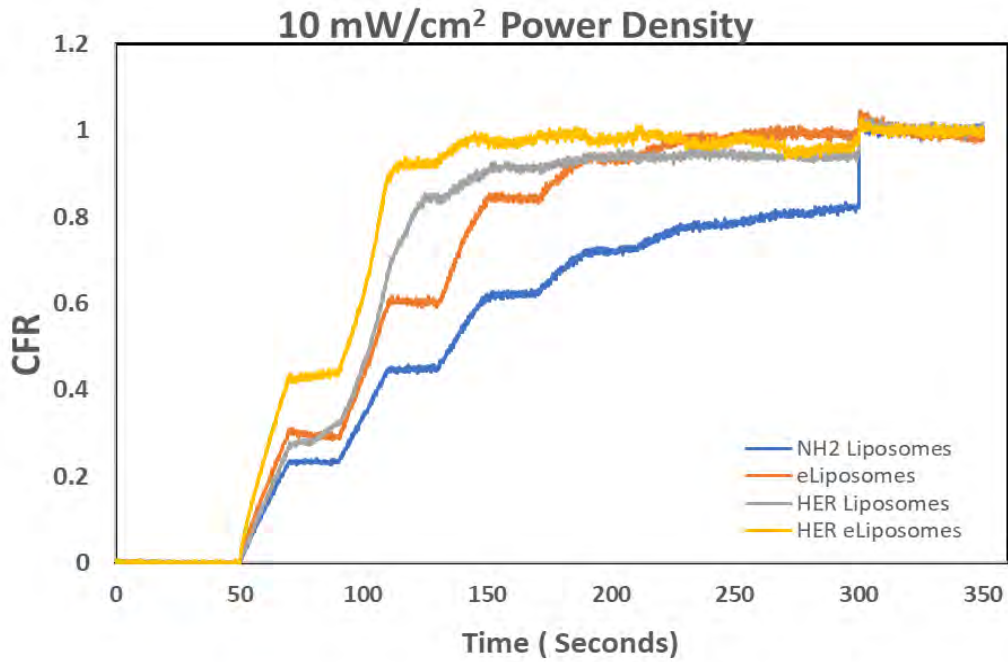


Figure 4-6 Comparison of Cumulative Fractional Release from control liposomes, eLiposomes, HER-conjugated liposomes and HER-conjugated eLiposomes at power density 10mW/cm². Initially, a fluorescence baseline I_0 was established before sonication for 50 seconds, ensuring no premature drug release occurred during this preliminary phase. Subsequently, precise sonication pulses were applied by employing a 20-kHz transducer to induce localized agitation within the liposomes at 20-second intervals. This notably increases the fluorescence intensity due to calcein release and this change is measured over time and denoted at I_t . As time progressed, LFUS-mediated drug release from liposomes commonly reached a plateau, generally observed around 300 seconds mark (5 minutes). At this point, Triton X-100, a surfactant known for its lytic property, was introduced to lyse the liposomes and achieve a maximum encapsulated drug release and is denoted by I_{100} . The entire process was repeated for three distinct power density settings: 6.2, 9, and 10 mW/cm² to calculate the cumulative fraction release (CFR) using the provided equation:

$$CFR = \frac{I_t - I_0}{I_{100} - I_0} \quad (3.13)$$

Figures 4-4, 4-5, and 4-6 comprehensively depict the drug release from different liposomal formulations when subjected to ultrasound pulses. It can be observed from the graphs that there is a progressive increase in drug release upon sonication (pulse-on), and minimum release during OFF pulses, thus demonstrating a positive correlation between ultrasound power density and drug release percentage (%Release).

Furthermore, adding triton-X at 300 seconds achieves the maximum release of the encapsulated drug i.e., 100%. Moreover, the graphs provide insights into the influence of power density on the percent release at a given time. The release of the encapsulated drug is significantly influenced by increasing the power density, where the highest power density resulted in the highest percent release of the encapsulated drug. At 6.2 mW/cm², all liposomal formulations do not reach their full potential and their CFR values are significantly below the maximum drug release (Triton-X). HER-conjugated eLiposomes show the highest release followed by HER-conjugated liposomes, eLiposomes and control liposomes.

In addition to the aforementioned observations, the graphs demonstrate that both eLiposomes and HER eLiposomes consistently show significantly faster release compared to the rest of the liposomal formulations. This can be attributed to the presence of emulsions within the liposomes that causes the liposomes to burst open and release most of the encapsulated drug during the first two ultrasound pulses. HER eLiposomes show the maximum release after the 4th, 3rd and 2nd pulses at 6.2, 9, and 10mW/cm² power densities, respectively. It can be concluded that a higher %Release can be obtained in a shorter time by increasing the power density.

Figures 4-7, 4-8, 4-9, and 4-10 provide comprehensive overview of the cumulative fraction released for different liposomal formulations in a bar chart format at different power densities. The error bars represent the slight variations in the drug released for each power density. Upon closer examination, it becomes apparent that after the first 20-second pulse, both eLiposomes and HER-conjugated eLiposomes show significantly more pronounced drug release than control liposomes and HER-conjugated liposomes. The plausible explanation for the observed increase in the CFR can be the presence of emulsions within liposomes that destabilize the structure, thus, resulting in a faster release. Furthermore, it can be observed that after the second pulse, HER-conjugated liposomes and HER-conjugated eLiposomes show a pronounced increase in drug release, which can be attributed to the presence of the heavy Herceptin moiety onto the surface of the liposomes.

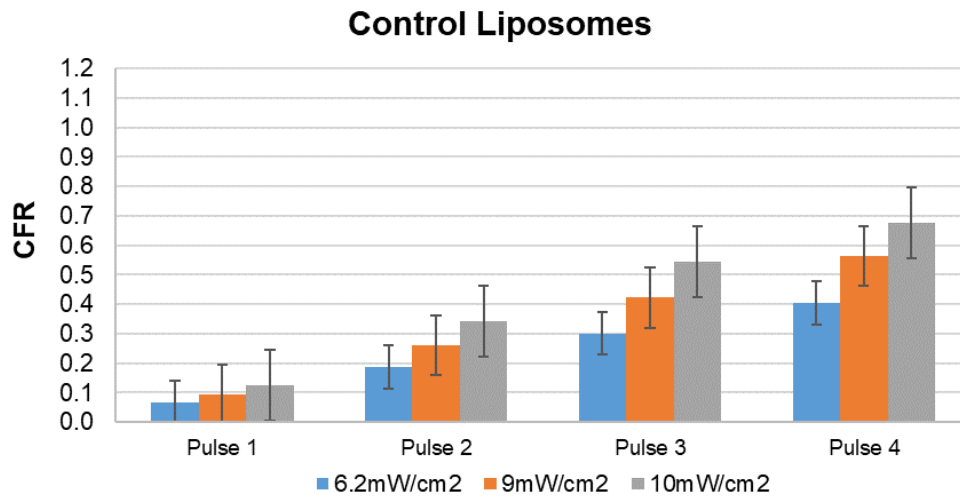


Figure 4-7 Comparison of cumulative fractional release from control liposomes after four pulses at different power densities

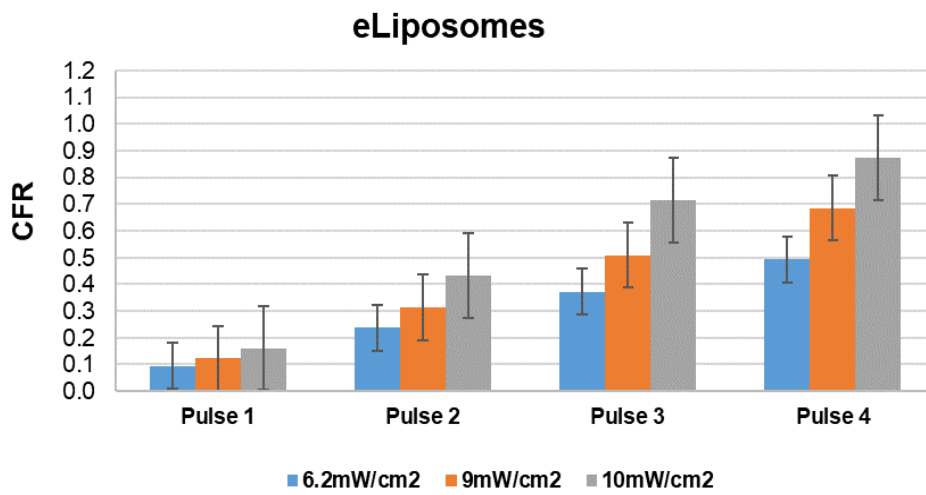


Figure 4-8 Comparison of cumulative fractional release from eLiposomes after four pulses at different power densities

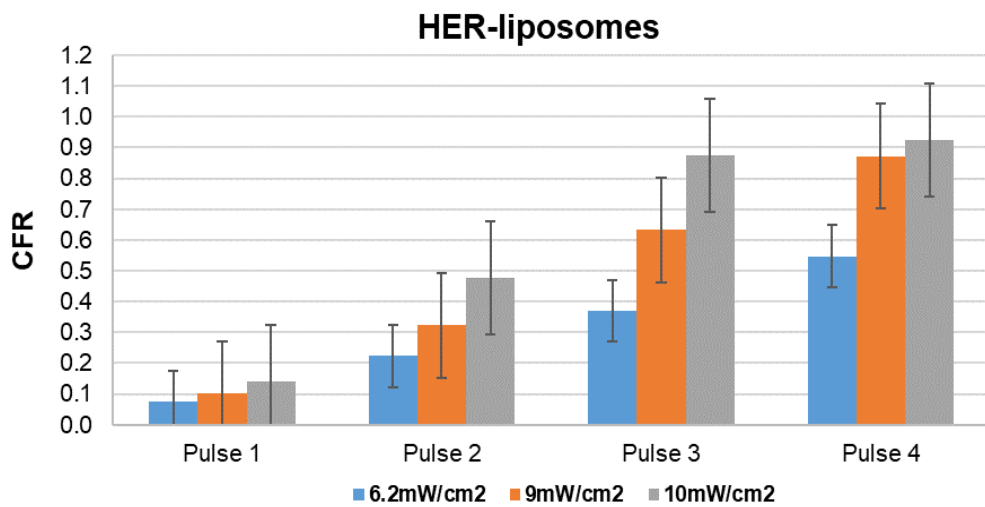


Figure 4-9 Comparison of cumulative fractional release from HER-Liposomes after four pulses at different power densities

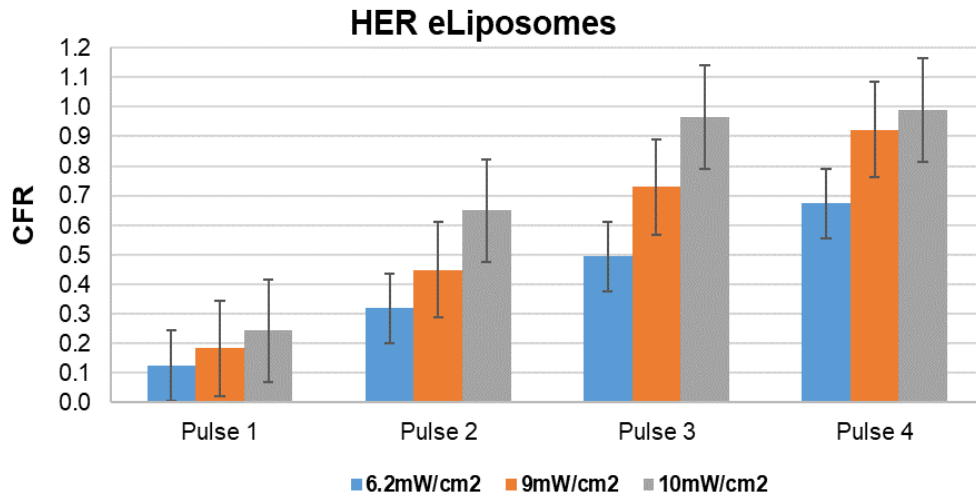


Figure 4-10 Comparison of cumulative fractional release from HER-eLiposomes after four pulses at different power densities

In summary, the above CFR profiles provide a detailed perspective on the disparities in the CFR among different liposomal formulations at different power densities, with higher power densities contributing to enhanced drug release from one pulse to the next. Data reveals that HER-conjugated eLiposomes show a significantly higher release than all the liposomal formulations, where the release reaches almost 100% by the third and 4th pulse 10 mW/cm². These findings suggest that both encapsulation of emulsions within liposomes and a heavy receptor target conjugated to the surface of liposomes play a crucial role in modulating the drug release behavior.

Tables 4-5 and 4-6 present a comprehensive analysis of the release behavior of four different liposomal formulations compared to the control liposomes through a p-values heat map. P-values offer insights into the statistical significance of the release profile differences, with low p-values indicating a high degree of statistical significance. The level of significance is differentiated by different color shades, allowing quick interpretation of results. A higher p-value corresponds to a lesser degree of statistical significance and can be attributed to random chance. The information presented in Table 4-5 during the first pulse reveals that the differences between the eLiposomes and HER-conjugated eLiposomes show the highest level of statistical significance in comparison with control liposomes at a specific power density, whereas HER-conjugated liposomes reveal a relatively lower level of statistical significance compared to the control liposomes at a specific power density. As stated earlier, this statistically significant behaviour observed in the liposomal formulations can be attributed to the

encapsulated emulsions that instantly destabilize the liposomes at the start of sonication.

Table 4-5 Statistical comparison of cumulative fractional release values at different power densities after the first pulse

1 st Pulse		Control Liposomes				
		7.46	9.85	17.31		
Control Liposomes	7.46	1	8.81E-05	4.07E-12		
	9.85	8.81172E-05	1	1.63E-05		
	17.31	4.06926E-12	1.63E-05	1		
eLiposomes	7.46	2.07429E-07	0.808959	8.9E-08		
	9.85	2.72468E-07	0.001668	0.773305		
	17.31	1.13594E-09	7.79E-07	0.000267		
HER liposomes	7.46	0.019617085	0.007856	9.98E-10		
	9.85	1.76436E-05	0.191123	0.003036		
	17.31	1.77852E-08	3.44E-05	0.050067		
HER eLiposomes	7.46	1.20773E-05	0.007513	0.965705		
	9.85	3.58198E-10	6.78E-08	5.2E-06		
	17.31	3.35092E-12	1.51E-10	1.48E-09		
p ≥ 0.05		0.04 ≤ p < 0.05	0.03 ≤ p < 0.04	0.02 ≤ p < 0.03	0.01 ≤ p < 0.02	p < 0.01

The analysis of the data presented in Table 4-6 suggests that the release behavior after the second pulse demonstrates a substantial statistical significance from all liposomal formulations at different power densities. In summary, Table 4-5 and 4-6 display valuable information about the efficacy and effectiveness of the synthesized nanocarriers in drug delivery.

Tables 4-7 and 4-8 present a comprehensive overview of the average release obtained from corresponding liposomal formulations during the first two pulses to assess drug release speed. This table offers insight into the efficacy and effectiveness of the formulated nanocarriers at different power densities. It can be observed that after the first pulse ultrasound is applied at various power densities, eLiposomal formulations reveal a higher %Release compared to liposomes without encapsulated emulsions. Furthermore, a noteworthy observation can be made about the %Release from the HER-conjugated eLiposomes after the first pulse at a lower power density of 6.2 mW/cm² is

comparable to that achieved by the rest of the liposomal formulations at the highest density 10 mW/cm².

Table 4-6 Statistical comparison of cumulative fractional release values at different power densities after the second pulse

2 nd Pulse		Control Liposomes				
		7.46	9.85	17.31		
Control Liposomes	7.46	1	2.3118E-08	1.93165E-13		
	9.85	2.3118E-08	1	3.97176E-10		
	17.31	1.93165E-13	3.97176E-10	1		
eLiposomes	7.46	0.000660406	7.40962E-05	1.27252E-11		
	9.85	6.84367E-07	0.017966395	0.003364306		
	17.31	1.06295E-12	1.5222E-10	1.58644E-06		
HER liposomes	7.46	0.000286361	0.001000845	1.37845E-10		
	9.85	7.42792E-11	2.70375E-07	0.82911042		
	17.31	1.24183E-14	3.03986E-13	6.01494E-11		
HER eLiposomes	7.46	8.41836E-08	0.003687145	0.003099004		
	9.85	1.64885E-10	3.16281E-08	0.000202196		
	17.31	6.4268E-10	7.91494E-09	2.15948E-07		
p ≥ 0.05		0.04 ≤ p < 0.05	0.03 ≤ p < 0.04	0.02 ≤ p < 0.03	0.01 ≤ p < 0.02	p < 0.01

Table 4-7 Comparison of the average fractional release values at different power densities after first pulse

First Pulse	Power densities (mW/cm ²)		
	6.2	9	10
Control Liposomes	0.066161	0.094551	0.133539
eLiposomes	0.094509	0.124826	0.162627
HER liposomes	0.078818	0.106052	0.14163
HER eLiposomes	0.124917	0.186794	0.245954

Furthermore, a comparative analysis of the release after the second pulse indicates that HER-conjugated liposomes demonstrated the most rapid drug release and released a substantial portion within a short duration. HER-conjugated liposomes consistently achieve the fastest drug release and as much release at the lowest power density as the

rest of the liposomal formulations at the high-power density after both the first and second pulses. This is essential in cancer drug delivery applications where rapid and efficient drug release is prioritized.

Table 4-8 Comparison of the average fractional release values at different power densities after first pulse

Second Pulse	Power densities (mW/cm ²)		
	6.2	9	10
Control Liposomes	0.130132	0.184568	0.240605
eLiposomes	0.158005	0.21504	0.323139
HER liposomes	0.165155	0.245884	0.388257
HER eLiposomes	0.221983	0.326383	0.538842

4.6 Kinetic Modeling:

4.6.1 Control liposomes release modeling

The release data from all the batches of control liposomes is collected and thoroughly analyzed by conducting release kinetics modeling. Two distinct mathematical models are employed to characterize the release profile: zero-order and first-order release kinetics. The goodness of fit for both models is evaluated by the R² value. The model exhibiting the highest R² value, post linearization of mathematical expressions, is the best fit for the release behavior. Thus, accurately predicting the release kinetics of the encapsulated drug. Table 4-9 presents the R² values for the two models analyzed while fitting the calcein release profile.

Table 4-9 R² values for calcein release from control liposomes

Power density	Model	R ² value			Average
		Batch1	Batch2	Batch3	
6.2 mW/cm ²	Zero-order	0.9929	0.9962	0.9951	0.9947
	First-order	0.7456	0.8258	0.7989	0.7901
9 mW/cm ²	Zero-order	0.9965	0.9928	0.7614	0.9169
	First-order	0.7456	0.7739	0.7614	0.7603
10 mW/cm ²	Zero-order	0.9917	0.976	0.998	0.9886
	First-order	0.6941	0.7276	0.7554	0.7257

The control liposomes best fit the zero-order release kinetics model (R^2 values of 0.9947, 0.9169, and 0.9886 at 6.2, 9, and 10 mW/cm², respectively). This agrees with the visual representation of the two models across all three batches at different power densities illustrated through a series of graphs in Appendix A.

4.6.2 eLiposomes release modeling

The experimental data obtained from the eLiposomal release pattern is analyzed by kinetic release modeling, and R^2 values for the zero-order and first-order models after fitting the eLiposomal release pattern are presented in Table 4-10

Table 4-10 R^2 values for calcein release from eLiposomes

Power density	Model	R^2 value			Average
		Batch1	Batch2	Batch3	
6.2 mW/cm ²	Zero-order	0.9963	0.9943	0.9856	0.9921
	First-order	0.7456	0.7663	0.7514	0.7544
9 mW/cm ²	Zero-order	0.9905	0.9905	0.9951	0.9920
	First-order	0.734	0.7456	0.751	0.7435
10 mW/cm ²	Zero-order	0.9986	0.9723	0.9636	0.9782
	First-order	0.7003	0.7003	0.675	0.6919

The results show that the eLiposomes best fit the zero-order release kinetics model (R^2 values of 0.9921, 0.9920, and 0.9782 at power densities of 6.2, 9, and 10 mW/cm², respectively). This agrees with the visual representation of the two models across all three batches at different power densities illustrated through a series of graphs in Appendix B.

4.6.3 HER-conjugated liposomes release modeling

Table 4-11 presents the R^2 values for the zero-order and first-order models obtained after fitting the HER-conjugated liposomes release data of calcein release.

The R^2 values show that the HER-conjugated liposomes best fit the zero-order release kinetics model (R^2 values of 0.9904, 0.9920, and 0.9962 at power densities of 6.2, 9, 10 mW/cm², respectively). This agrees with the visual representation of the two models across all three batches at different power densities illustrated through a series of graphs in Appendix C.

Table 4-11 R² values for calcein release from HER-conjugated liposomes

Power density	Model	R ² value			Average
		Batch1	Batch2	Batch3	
6.2 mW/cm ²	Zero-order	0.9811	0.9943	0.9959	0.9904
	First-order	0.7456	0.7663	0.7514	0.7544
9 mW/cm ²	Zero-order	0.9905	0.9905	0.9951	0.9920
	First-order	0.7340	0.7456	0.7510	0.7435
10 mW/cm ²	Zero-order	0.9982	0.9915	0.9988	0.9962
	First-order	0.7003	0.7003	0.6750	0.6919

4.6.4 HER-conjugated eLiposomes release modeling

Table 4-12 presents the R² values for the zero-order and first-order models obtained after fitting the release data of calcein release.

Table 4-12 R² values for calcein release from HER-conjugated eLiposomes

Power density	Model	R ² value			Average
		Batch1	Batch2	Batch3	
6.2 mW/cm ²	Zero-order	0.9974	0.9924	0.9947	0.9948
	First-order	0.7456	0.8138	0.7999	0.7864
9 mW/cm ²	Zero-order	0.9978	0.9979	0.9976	0.9978
	First-order	0.7292	0.7456	0.7451	0.7400
10 mW/cm ²	Zero-order	0.9976	0.998	0.9978	0.9978
	First-order	0.4598	0.468	0.5144	0.4807

The results show that the HER-conjugated eLiposomes best fit the zero-order release kinetics model (R² values of 0.9948, 0.9978, and 0.9978 at power densities of 6.2, 9, 10 mW/cm², respectively). This agrees with the visual representation of the two models across all three batches at different power densities illustrated through a series of graphs in Appendix D. In summary, the R² values provide a quantitative assessment of the best fit for the four liposomal formulations prepared in this thesis and helped understand the factors influencing the release of model drug calcein from these formulations.

All liposomal formulations prepared in this thesis fit the zero-order release kinetics profile, HER-conjugated eLiposomes demonstrated R^2 values of almost 1.

Figures 4-11, 4-12, 4-13, and 4-14 demonstrate distinct release characteristics for all the liposomes with the consistent release rate of calcein after each ultrasonic pulse. It can be observed that the behavior of all liposomal formulations, when subjected to ultrasonic triggers at different power densities, caused the drug to be released at a nearly constant rate over time, regardless of the concentration during each pulse individually.

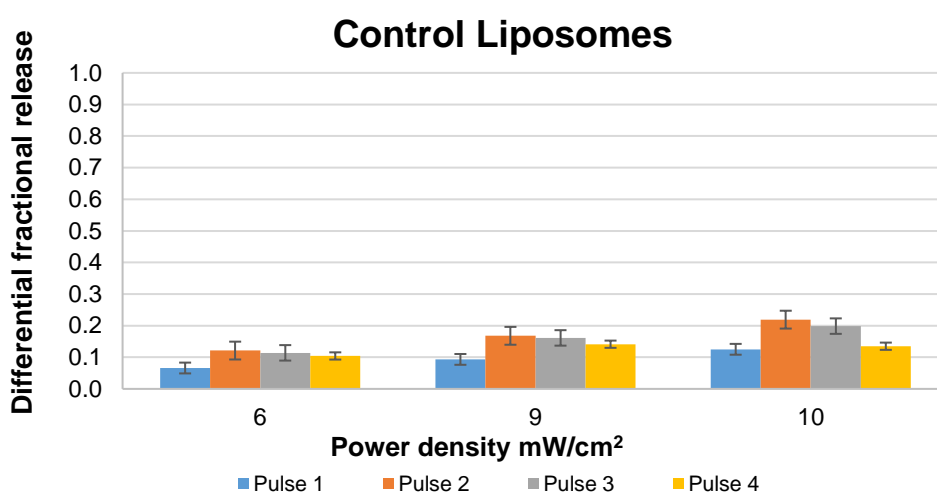


Figure 4-11 Comparison of differential fractional release from control liposomes after individual pulses at different power densities

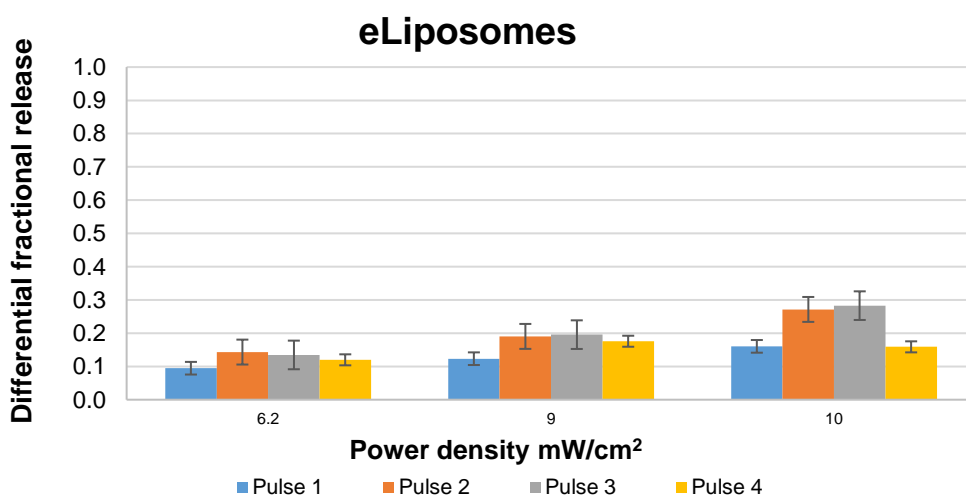


Figure 4-12 Comparison of differential fractional release from e-Liposomes after individual pulses at different power densities

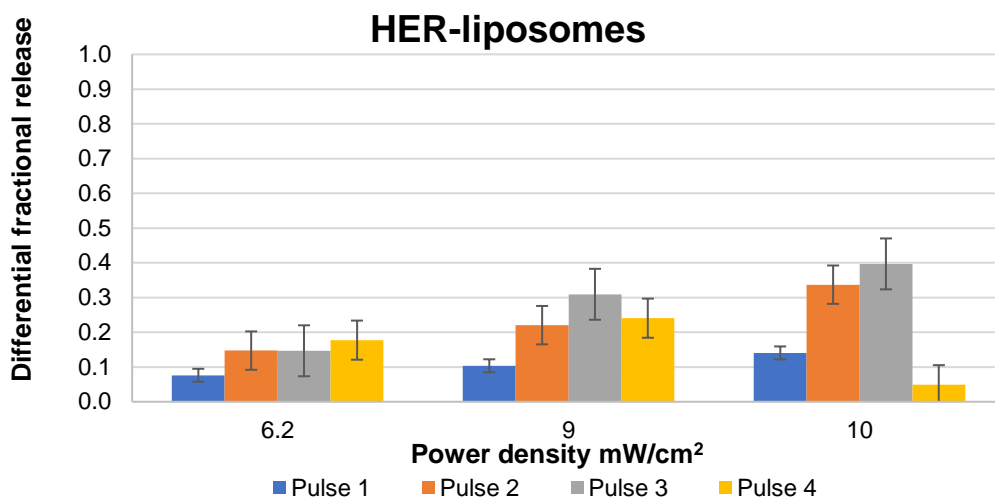


Figure 4-13 Comparison of differential fractional release from HER-liposomes after individual pulses at different power densities

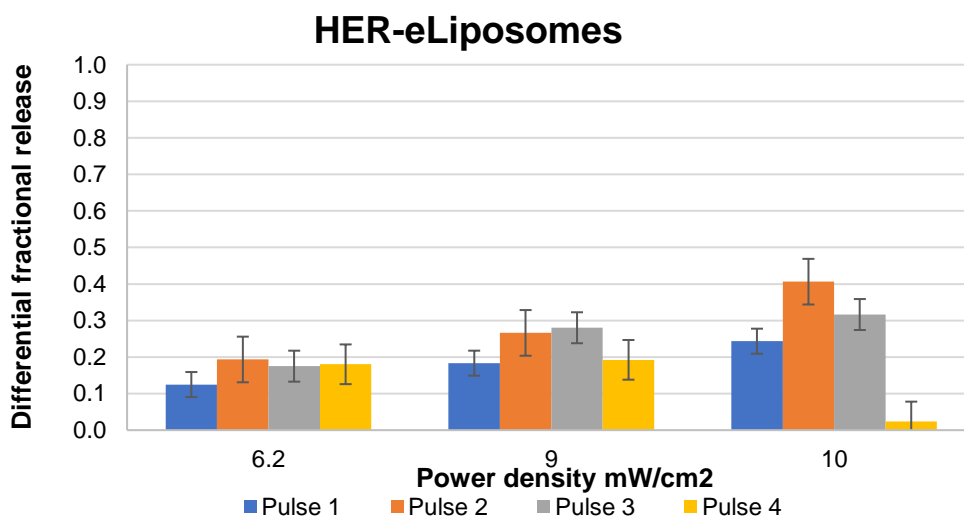


Figure 4-14 Comparison of differential fractional release from HER-eLiposomes after individual pulses at different power densities

Furthermore, similarities can be observed from the control liposomes release profile at 10 mW/cm² and HER-conjugated eLiposomes at 6.2 mW/cm². As discussed earlier, the release behavior of control liposomes at high power density is similar to that of HER-conjugated liposomes at low power density. Using lower power intensity for cancer-targeted treatment helps reduce heat induction or tissue damage caused by high power intensities, thus, providing controlled drug release in space and time and increasing the efficacy and treatment effectiveness.

Chapter 5. Conclusion and Future Work

In this thesis, a thorough investigation was conducted on twelve batches of different liposomal formulations: control liposomes, eLiposomes, HER-conjugated liposomes, and HER-conjugated eLiposomes. Three independent batches of each of the aforementioned liposomal formulations were thoroughly explored by comparing their physical and chemical properties, including size, morphology, composition, and release kinetics, using Dynamic Light Scattering (DLS), Cryogenic – Transmission Electron Microscope (Cryo-TEM). Primarily, characterization tests and assays were conducted throughout the thesis to characterize and evaluate the properties of different liposomal formulations. The size was assessed using the DLS technique. All liposomal formulations exhibited a size within/up to 200 nm diameter, thus enabling them to exploit the enhanced permeability and retention effect (EPR), rendering them promising and efficient nanocarriers in cancer drug delivery applications. The lipid content within different liposomal formulations was quantified using the Stewart assay. Furthermore, the protein concentration in Herceptin-conjugated liposomes was twofold higher in the control liposomes across all synthesized batches. Low-frequency ultrasound was used to release calcein and to assess the %release using 20-second on/off sonication pulses. All the liposomal formulations demonstrated that ultrasound was the driving force that triggered the formulations to release during on pulses and no significant release during the off pulses. Additionally, all liposomal formulations demonstrated statistically significant results in this thesis. Notably, liposomes encapsulated with emulsions showed rapid drug release rates, whereas conjugation of Herceptin the destabilization of the liposomal envelope during the escape. A noteworthy observation about the %release from the HER-conjugated eLiposomes at the lowest power density achieved as much drug release as the control liposomes at the highest power density used in this study. The release of calcein from liposomes was fit to zero-order and first-order kinetic models, and this drug delivery system was found to follow zero-order kinetics. The results obtained from this study highlight the potential of nanoemulsions along with targeting moieties and low-frequency ultrasound (LFUS) to trigger, control, and enhance the release of therapeutic drugs from liposomes. These findings provide valuable information for further the research and development of future *in-vitro* and *in-vivo* studies that aim to exploit the overexpression of Herceptin

and rapidly release the drug upon sonication. In conclusion, this research is promising in improving the prognosis of cancer patients and rendering chemotherapy more humane by minimizing the side effects associated with conventional chemotherapy, ultimately enhancing patient well-being and quality of life.

As future work, conducting *in-vitro* and *in-vivo* studies on targeted eLiposomes will provide more insights into this innovative drug delivery system. Rigorous evaluation of various aspects of eLiposomal behavior, including toxicity, pharmacokinetics, biodistribution, and immunogenicity, need to be explored to ensure adherence to the standards required for clinical application. Additionally, we plan on performing cryo-TEM on eLiposomal samples, to ensure the rupturing of the liposomal coat upon exposure to ultrasound.

References

- [1] L. Kumar, A. Upadhyay and A. S. Jayaraj, "Chemotherapy and immune check point inhibitors in the management of cervical cancer," *Current Problems in Cancer*, vol. 46, (6), 2022.
- [2] D. Mukhopadhyay *et al*, "Ultrasound-Triggered Immunotherapy for Cancer Treatment: An Update," *Current Protein & Peptide Science*, vol. 22, (6), pp. 493-504, 2021.
- [3] H. O. Al-Shamsi, A. M. Abyad and S. Rafii, "A Proposal for a National Cancer Control Plan for the UAE: 2022–2026," *Clinics and Practice*, vol. 12, (1), pp. 118, 2022.
- [4] J. Durland Justin, "Genetics, Mutagenesis", *StatPearls [Internet]*, 19 September 2022.
- [5] *The Genetics of Cancer*. CancerNet Editorial Board, 2012 Available: <https://www.cancer.net/navigating-cancer-care/cancer-basics/genetics/genetics-cancer>. (Online), (accessed 23 June 2023)
- [6] J. Wang, K. Lei and F. Han, "Tumor microenvironment: recent advances in various cancer treatments," *European Review for Medical and Pharmacological Sciences*, vol. 22, (12), pp. 3855, 2018.
- [7] *How cancer starts*. CancerResearchUK, 2014. Available: <https://www.cancerresearchuk.org/about-cancer/what-is-cancer/how-cancer-starts>. (Online), (accessed 2 January 2023)
- [8] J. A. Harry and M. L. Ormiston, "Novel Pathways for Targeting Tumor Angiogenesis in Metastatic Breast Cancer," *Front Oncol*, vol. 11, 2021.
- [9] T. Koltai, "The pH paradigm in cancer chapter 2," in *pH Paradigm in Cancer ResearchGate*, 2018.
- [10] L. Eldridge. *Cancer Cells vs. Normal Cells: How Are They Different?* Available: <https://www.verywellhealth.com/cancer-cells-vs-normal-cells-2248794>. (Online), (accessed 4 May 2023)
- [11] T. W. Mudd, M. Khalid and A. K. Guddati, "Cardiotoxicity of chemotherapy and targeted agents," *Am J Cancer Res*, vol. 11, (4), pp. 1132-1147, 2021.
- [12] T. D. Wagner and G. Y. Yang, "The Role of Chemotherapy and Radiation in the Treatment of Locally Advanced Non-Small Cell Lung Cancer (NSCLC)," *Current Drug Targets*, vol. 11, (1), pp. 67-73, 2010.
- [13] L. Nekhlyudov *et al*, "Cancer-related impairments and functional limitations among long-term cancer survivors: Gaps and opportunities for clinical practice," *Cancer*, vol. 128, (2), pp. 222-229, 2022.

- [14] What is cancer, *National Cancer Institute*. Available: <https://www.cancer.gov/about-cancer/understanding/what-is-cancer> (Online), (accessed October 11 2021).
- [15] X. Ning *et al*, "The prospect of immunotherapy combined with chemotherapy in patients with advanced non-small cell lung cancer: a narrative review," *Ann Transl Med*, vol. 9, (22), 2021.
- [16] M. Vanneman and G. Dranoff, "Combining Immunotherapy and Targeted Therapies in Cancer Treatment," *Nat Rev Cancer*, vol. 12, (4), pp. 237-251, 2012.
- [17] S. Zhou *et al*, "Cytoreductive Surgery and Hyperthermic Intraperitoneal Chemotherapy in Young Patients With Peritoneal Metastasis of Colorectal Cancer—An Asian Experience," *Journal of Surgical Research*, vol. 281, pp. 97-103, 2023.
- [18] K. Gupta, R. Walton and S. P. Kataria, "Chemotherapy-Induced Nausea and Vomiting: Pathogenesis, Recommendations, and New Trends," *Cancer Treatment and Research Communications*, vol. 26, pp. 100278, 2021.
- [19] T. J. Brown, R. Sedhom and A. Gupta, "Chemotherapy-Induced Peripheral Neuropathy," *JAMA Oncol*, vol. 5, (5), pp. 750-750, 2019.
- [20] *Chemotherapy Side Effects*. CancerCare. Available: <http://www.cancer.org/chemo-side-effects>. (Online), (accessed 23 April 2023).
- [21] M. FLORESCU, M. CINTEZA and D. VINEREANU, "Chemotherapy-induced Cardiotoxicity," *Maedica (Bucur)*, vol. 8, (1), pp. 59-67, 2013.
- [22] J. Gillet and M. M. Gottesman, "Mechanisms of multidrug resistance in cancer," *Methods Mol Biol*, vol. 596, pp. 47-76, 2010.
- [23] M. Chamundeeswari, J. Jeslin and M. L. Verma, "Nanocarriers for drug delivery applications," *Environ Chem Lett*, vol. 17, (2), pp. 849-865, 2019.
- [24] Z. Su *et al*, "Novel nanomedicines to overcome cancer multidrug resistance," *Drug Resistance Updates*, vol. 58, pp. 100777, 2021.
- [25] L. R. Avula and P. Grodzinski, "Nanotechnology-aided advancement in the combating of cancer metastasis," *Cancer Metastasis Rev*, pp. 1-22, 2022.
- [26] S. Chakraborty and T. Rahman, "The difficulties in cancer treatment," *Ecancermedicalscience*, vol. 6, 2012.
- [27] *Understanding Targeted Therapy*. Cancer.Net Editorial Board. Available: <https://www.cancer.net/navigating-cancer-care/how-cancer-treated/personalized-and-targeted-therapies/understanding-targeted-therapy>. (Online), (accessed 23 June 2023).
- [28] J. Patel, "Liposomal doxorubicin: Doxil®," *J Oncol Pharm Pract*, vol. 2, (4), pp. 201-210, 1996.

- [29] A. Ayub and S. Wettig, "An Overview of Nanotechnologies for Drug Delivery to the Brain," *Pharmaceutics*, vol. 14, (2), 2022.
- [30] S. E. Ahmed *et al*, "Improving the Efficacy of Anticancer Drugs via Encapsulation and Acoustic Release," *Current Topics in Medicinal Chemistry*, vol. 18, (10), pp. 857-880, 2018.
- [31] S. Biswas *et al*, "Recent advances in polymeric micelles for anti-cancer drug delivery," *European Journal of Pharmaceutical Sciences*, vol. 83, pp. 184-202, 2016.
- [32] L. Zhao *et al*, "Curcumin loaded mixed micelles composed of Pluronic P123 and F68: Preparation, optimization and in vitro characterization," *Colloids and Surfaces, B, Biointerfaces*, vol. 97, pp. 101-108, 2012.
- [33] F. Abedi-Gaballu *et al*, "PAMAM dendrimers as efficient drug and gene delivery nanosystems for cancer therapy," *Applied Materials Today*, vol. 12, pp. 177-190, 2018.
- [34] S. G. Antimisiaris *et al*, "Overcoming barriers by local drug delivery with liposomes," *Advanced Drug Delivery Reviews*, vol. 174, pp. 53-86, 2021.
- [35] A. Akbarzadeh *et al*, "Liposome: classification, preparation, and applications," *Nanoscale Res Lett*, vol. 8, (1), pp. 1-9, 2013.
- [36] D. E. Large *et al*, "Liposome composition in drug delivery design, synthesis, characterization, and clinical application," *Advanced Drug Delivery Reviews*, vol. 176, pp. 113851, 2021.
- [37] G. Bozzuto and A. Molinari, "Liposomes as nanomedical devices," *International Journal of Nanomedicine*, vol. 10, pp. 975-999, 2015.
- [38] P. Liu, G. Chen and J. Zhang, "A Review of Liposomes as a Drug Delivery System: Current Status of Approved Products, Regulatory Environments, and Future Perspectives," *Molecules (Basel, Switzerland)*, vol. 27, (4), pp. 1372, 2022.
- [39] R. Nisini *et al*, "The Multirole of Liposomes in Therapy and Prevention of Infectious Diseases," *Front. Immunol.*, vol. 9, 2018.
- [40] E. Kim and H. Jeong, "Liposomes: Biomedical Applications," *Chonnam Med J*, vol. 57, (1), pp. 27-35, 2021.
- [41] K. M. Aguilar-Pérez *et al*, "Insight Into Nanoliposomes as Smart Nanocarriers for Greening the Twenty-First Century Biomedical Settings," *Front. Bioeng. Biotechnol.*, vol. 0, 2020.
- [42] E. Nogueira *et al*, "Design of liposomal formulations for cell targeting," *Colloids and Surfaces B: Biointerfaces*, vol. 136, pp. 514-526, 2015.
- [43] H. Kanda, T. Katsube and M. Goto, "Preparation of Liposomes from Soy Lecithin Using Liquefied Dimethyl Ether," *Foods*, vol. 10, (8), 2021.

- [44] D. Calle *et al*, "Magnetoliposomes Loaded with Poly-Unsaturated Fatty Acids as Novel Theranostic Anti-Inflammatory Formulations," *Theranostics*, vol. 5, (5), pp. 489, 2017.
- [45] J. Zhou, *Multi-Drug Resistance in Cancer*. (1st ed.) Humana Totowa, NJ, 2012.
- [46] A. Prieu *et al*, "Determination of Critical Micelle Concentration of Lipopolymers and Other Amphiphiles: Comparison of Sound Velocity and Fluorescent Measurements," *Langmuir*, vol. 18, (3), pp. 612-617, 2002.
- [47] D. Guimarães, A. Cavaco-Paulo and E. Nogueira, "Design of liposomes as drug delivery system for therapeutic applications," *International Journal of Pharmaceutics*, vol. 601, pp. 120571, 2021.
- [48] V. Weissig, "Liposomes came first: The early history of liposomology," in *Liposomes*, 2016.
- [49] M. A. Elkhodiry *et al*, "Synergistic Nanomedicine: Passive, Active, and Ultrasound-Triggered Drug Delivery in Cancer Treatment," *J Nanosci Nanotechnol*, vol. 16, (1), pp. 1-18, 2016.
- [50] Y. Lu *et al*, "Characterization and Anticancer Effects of Folate Targeted Inotodiol Liposome From Inonotus Obliquus (Chaga Mushroom)," 2021.
- [51] S. M. Haftcheshmeh *et al*, "Liposomal doxorubicin targeting mitochondria: A novel formulation to enhance anti-tumor effects of Doxil® in vitro and in vivo," *Journal of Drug Delivery Science and Technology*, vol. 62, pp. 102351, 2021.
- [52] A. A. Lohade *et al*, "A Novel Folate-Targeted Nanoliposomal System of Doxorubicin for Cancer Targeting," *AAPS PharmSciTech*, vol. 17, (6), pp. 1298-1311, 2015.
- [53] M. Morales and X. Xue, "Targeting iron metabolism in cancer therapy," *Theranostics*, vol. 11, (17), pp. 8412-8429, 2021.
- [54] A. Jhaveri *et al*, "Transferrin-targeted, resveratrol-loaded liposomes for the treatment of glioblastoma," *Journal of Controlled Release*, vol. 277, pp. 89-101, 2018.
- [55] N. M. AlSawaftah *et al*, "Transferrin-modified liposomes triggered with ultrasound to treat HeLa cells," *Sci Rep*, vol. 11, 2021.
- [56] Elamir *et al*, "Ultrasound-triggered herceptin liposomes for breast cancer therapy," *Scientific Reports*, vol. 11, (1), pp. 7545, 2021.
- [57] M. J. Bloom *et al*, "Quantifying the Effects of Combination Trastuzumab and Radiation Therapy in Human Epidermal Growth Factor Receptor 2-Positive Breast Cancer," *Cancers*, vol. 14, (17), pp. 4234, 2022.

- [58] J. Lee, D. H. Shin and J. Kim, "Anticancer Effect of Metformin in Herceptin-Conjugated Liposome for Breast Cancer," *Pharmaceutics*, vol. 12, (1), pp. 11, 2019.
- [59] J. Wang, J. Gong and Z. Wei, "Strategies for Liposome Drug Delivery Systems to Improve Tumor Treatment Efficacy," *AAPS PharmSciTech*, vol. 23, (1), pp. 27, 2021.
- [60] M. Javadi *et al*, "Encapsulating Nanoemulsions Inside eLiposomes for Ultrasonic Drug Delivery," *Langmuir*, vol. 28, (41), pp. 14720-14729, 2012.
- [61] M. N. Zafar, W. H. Abuwatfa and G. A. Hussein, "Acoustically-Activated Liposomal Nanocarriers to Mitigate the Side Effects of Conventional Chemotherapy with a Focus on Emulsion-Liposomes," *Pharmaceutics*, vol. 15, (2), pp. 421, 2023.
- [62] E. Pérez-Herrero and A. Fernández-Medarde, "Advanced targeted therapies in cancer: Drug nanocarriers, the future of chemotherapy," *Eur J Pharm Biopharm*, vol. 93, pp. 52-79, 2015.
- [63] C. Liu *et al*, "MRI-FI-guided superimposed stimulus-responsive co-assembled liposomes for optimizing transmembrane drug delivery pathways and improving cancer efficacy," *Applied Materials Today*, vol. 26, pp. 101368, 2022.
- [64] P. Liu, G. Chen and J. Zhang, "A Review of Liposomes as a Drug Delivery System: Current Status of Approved Products, Regulatory Environments, and Future Perspectives," *Molecules*, vol. 27, (4), 2022.
- [65] R. Taléns-Visconti *et al*, "Nanoliposomes in Cancer Therapy: Marketed Products and Current Clinical Trials," *Ijms*, vol. 23, (8), 2022.
- [66] M. P. Nikolova, E. M. Kumar and M. S. Chavali, "Updates on Responsive Drug Delivery Based on Liposome Vehicles for Cancer Treatment," *Pharmaceutics*, vol. 14, (10), 2022.
- [67] L. Ye *et al*, "Antitumor effect and toxicity of Lipusu in rat ovarian cancer xenografts," *Food and Chemical Toxicology*, vol. 52, pp. 200-206, 2013.
- [68] N. Minocha and V. Kumar, "Nanostructure system: Liposome – A bioactive carrier in drug delivery systems," *Materials Today: Proceedings*, 2022.
- [69] D. E. Large *et al*, "Liposome composition in drug delivery design, synthesis, characterization, and clinical application," *Advanced Drug Delivery Reviews*, vol. 176, pp. 113851, 2021.
- [70] F. Danhier, O. Feron and V. Préat, "To exploit the tumor microenvironment: Passive and active tumor targeting of nanocarriers for anti-cancer drug delivery," *Journal of Controlled Release*, vol. 148, (2), pp. 135-146, 2010.
- [71] L. Arthur, S. Christine, M. Lawrence, J. Andrew, "Fixed Drug Ratios For Treatment Of Hematopoietic Cancers And Proliferative Disorders", US20070901772P 20070216, 06/14/2019.

- [72] P. Singh *et al*, "Particle size analyses of polydisperse liposome formulations with a novel multispectral advanced nanoparticle tracking technology," *International Journal of Pharmaceutics*, vol. 566, pp. 680-686, 2019.
- [73] E. Beltrán-Gracia *et al*, "Nanomedicine review: clinical developments in liposomal applications," *Cancer Nano*, vol. 10, (1), pp. 1-40, 2019.
- [74] K. Entzian and A. Aigner, "Drug Delivery by Ultrasound-Responsive Nanocarriers for Cancer Treatment," *Pharmaceutics*, vol. 13, (8), 2021.
- [75] A. Carovac, F. Smajlovic and D. Junuzovic, "Application of Ultrasound in Medicine," *Acta Inform Med*, vol. 19, (3), pp. 168-171, 2011.
- [76] D. V. B. Batchelor *et al*, "Nested Nanobubbles for Ultrasound-Triggered Drug Release," *ACS Appl. Mater. Interfaces*, 2020.
- [77] S. E. Ahmed, A. M. Martins and G. A. Hussein, "The use of ultrasound to release chemotherapeutic drugs from micelles and liposomes," *J. Drug Target.*, vol. 23, (1), pp. 16-42, 2015.
- [78] T. Boissenot *et al*, "Ultrasound-triggered drug delivery for cancer treatment using drug delivery systems: From theoretical considerations to practical applications," *Journal of Controlled Release*, vol. 241, pp. 144-163, 2016.
- [79] N. Ingram *et al*, "Ultrasound-triggered therapeutic microbubbles enhance the efficacy of cytotoxic drugs by increasing circulation and tumor drug accumulation and limiting bioavailability and toxicity in normal tissues," *Theranostics*, vol. 10, (24), pp. 10973-10992, 2020.
- [80] R. Abou-Saleh *et al*, "The influence of intercalating perfluorohexane into lipid shells on nano and microbubble stability," *Soft Matter*, vol. 12, (34), pp. 7223-7230, 2016.
- [81] M. Olsman *et al*, "Focused Ultrasound and Microbubble Treatment Increases Delivery of Transferrin Receptor-Targeting Liposomes to the Brain," *Ultrasound in Medicine & Biology*, vol. 47, (5), pp. 1343-1355, 2021.
- [82] C. Su *et al*, "Current advances in ultrasound-combined nanobubbles for cancer-targeted therapy: a review of the current status and future perspectives," *RSC Advances*, vol. 11, (21), pp. 12915-12928, 2021.
- [83] R. J. Wilson *et al*, "Nanoemulsions for drug delivery," *Particuology*, vol. 64, pp. 85-97, 2022.
- [84] Y. Zhou, "Application of acoustic droplet vaporization in ultrasound therapy," *J Ther Ultrasound*, vol. 3, 2015.
- [85] C. Lin and W. G. Pitt, "Acoustic Droplet Vaporization in Biology and Medicine," *BioMed Research International*, vol. 2013, pp. e404361, 2013.

- [86] J. R. Lattin *et al*, "Ultrasound-Induced Calcein Release From eLiposomes," *Ultrasound in Medicine & Biology*, vol. 38, (12), pp. 2163-2173, 2012.
- [87] S. E. Ahmed *et al*, "Effect of pH, ultrasound frequency and power density on the release of calcein from stealth liposomes," *European Journal of Nanomedicine*, vol. 8, (1), pp. 31-43, 2016.
- [88] J. R. Lattin and W. G. Pitt, "Factors Affecting Ultrasonic Release from eLiposomes," *Journal of Pharmaceutical Sciences*, vol. 104, (4), pp. 1373-1384, 2015.
- [89] S. M. Graham *et al*, "Inertial cavitation to non-invasively trigger and monitor intratumoral release of drug from intravenously delivered liposomes," *J Control Release*, vol. 178, pp. 101-107, 2014.
- [90] R. Guo *et al*, "Functional ultrasound-triggered phase-shift perfluorocarbon nanodroplets for cancer therapy," *Ultrasound in Medicine and Biology*, vol. 47, (8), pp. 2064-2079, 2021.
- [91] R. Holman *et al*, "Perfluorocarbon Emulsion Contrast Agents: A Mini Review," *Front Chem*, vol. 9, pp. 810029, 2021.
- [92] P. S. Sheeran *et al*, "Contrast-enhanced ultrasound imaging and in vivo circulatory kinetics with low-boiling-point nanoscale phase-change perfluorocarbon agents," *Ultrasound Med Biol*, vol. 41, (3), pp. 814-831, 2015.
- [93] G. A. Hussein, W. G. Pitt and M. Javadi, "Investigating the Stability of eLiposomes at Elevated Temperatures," *Technology in Cancer Research & Treatment*, vol. 14, (4), pp. 379-382, 2015.
- [94] G. Hussein *et al*, "Investigating the Release Mechanism of Calcein from eLiposomes at Higher Temperatures," *Journal of Colloid Science and Biotechnology*, vol. 3, (3), pp. 239-244, 2014.
- [95] W. G. Pitt, "Cytosolic Delivery of Doxorubicin from Liposomes to Multidrug-Resistant Cancer Cells via Vaporization of Perfluorocarbon Droplets," *Journal of Nanomedicine Research*, vol. 5, (4), 2017.
- [96] J. C. M. Stewart, "The Stewart Assay," 21st January, 2009.
- [97] Thermofisher Scientific, "Protein assay technical handbook," Thermofisher Scientific, 2017.
- [98] C. Shen, "Quantification and analysis of proteins," in *Diagnostic Molecular Biology*, 2019.
- [99] C. S. Borowy and J. V. Ashurst, "Physiology, zero and first order kinetics," in *StatPearls*, 2023.

[100] S. Dash *et al*, "Kinetic modeling on drug release from controlled drug delivery systems," *Acta Poloniae Pharmaceutica*, vol. 67, (3), pp. 217-223, 2010.

Appendix A: Control Liposomes Kinetic Modeling

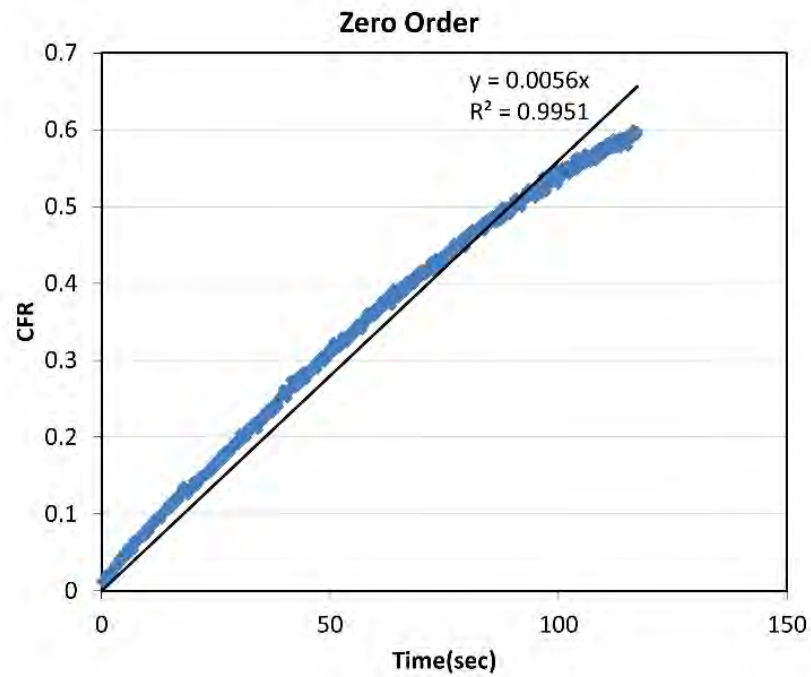


Figure A-1 Calcein release from control liposomes (Batch 1) at 6.2 mW/cm² fitting Zero-order Model

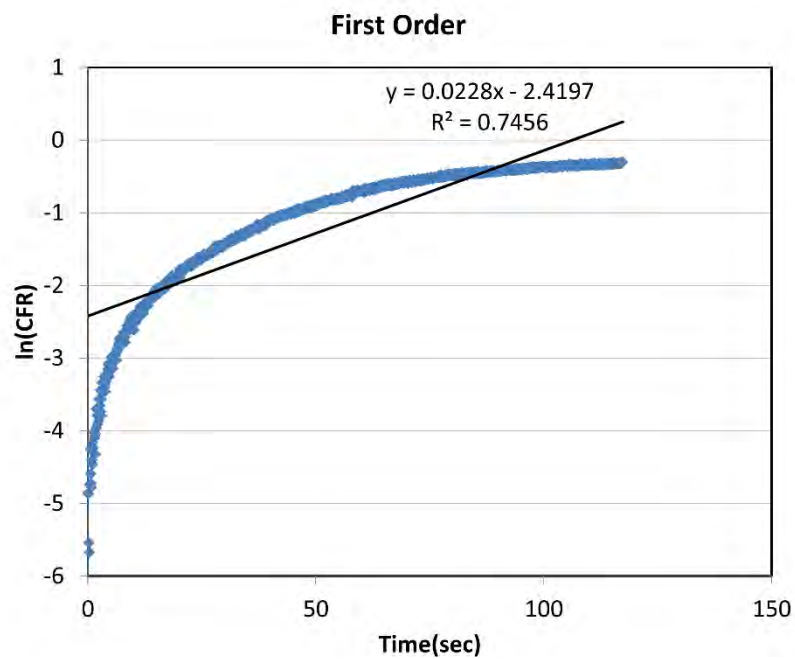


Figure A-2 Calcein release from control liposomes (Batch 1) at 6.2 mW/cm² fitting First-order Model.

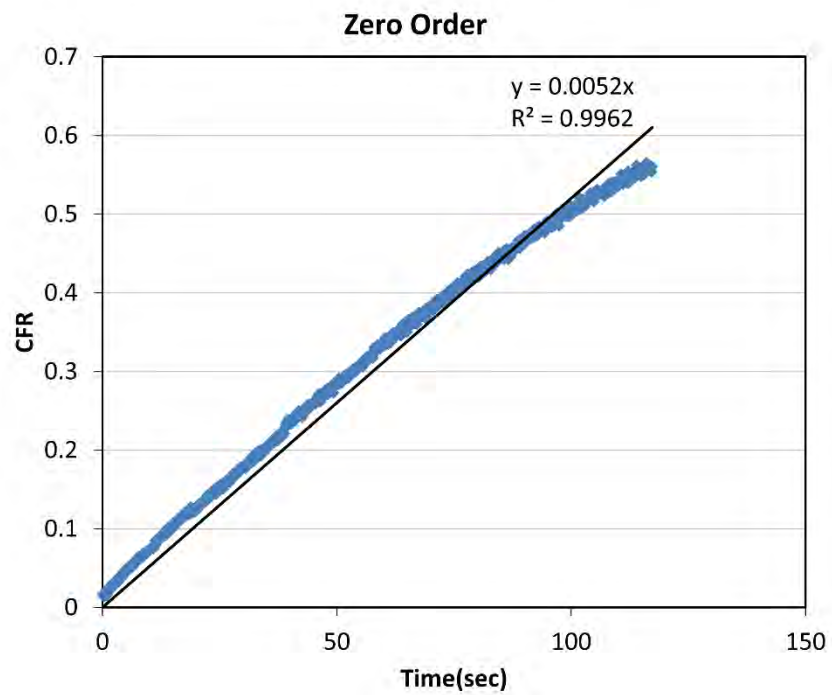


Figure 0A-3 Calcein release from control liposomes (Batch 2) at 6.2 mW/cm² fitting Zero-order Model.

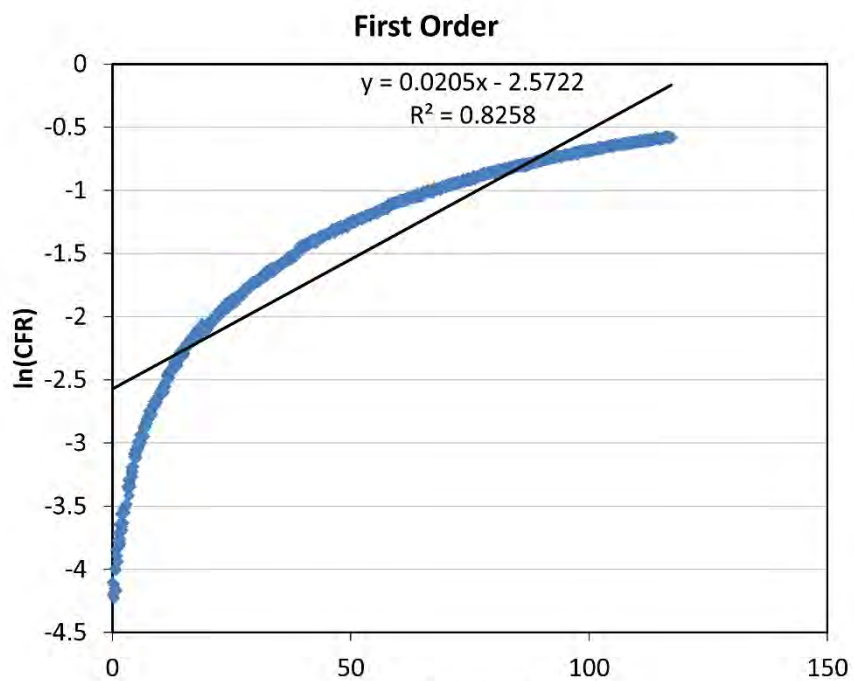


Figure 0 Calcein release from control liposomes (Batch 2) at 6.2 mW/cm² fitting First-order Model.

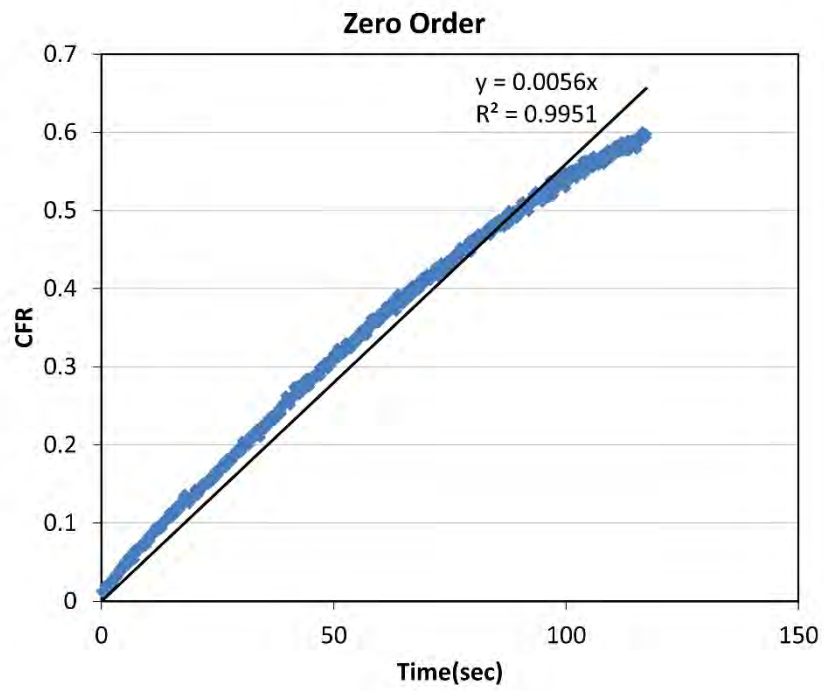


Figure A-5 Calcein release from control liposomes (Batch 3) at 6.2 mW/cm² fitting zero-order Model

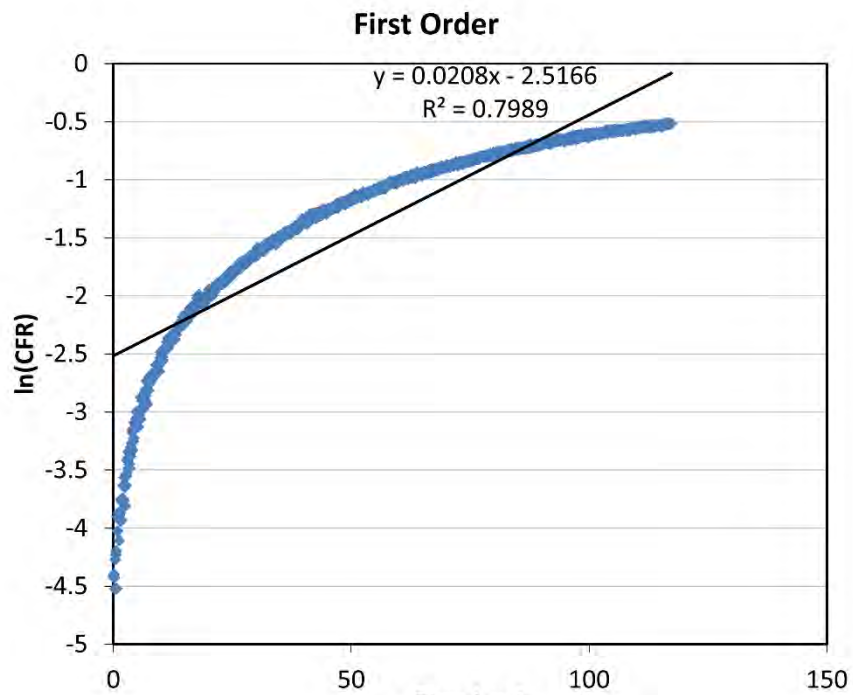


Figure A-6 Calcein release from control liposomes (Batch 3) at 6.2 mW/cm² fitting Zero-order Model

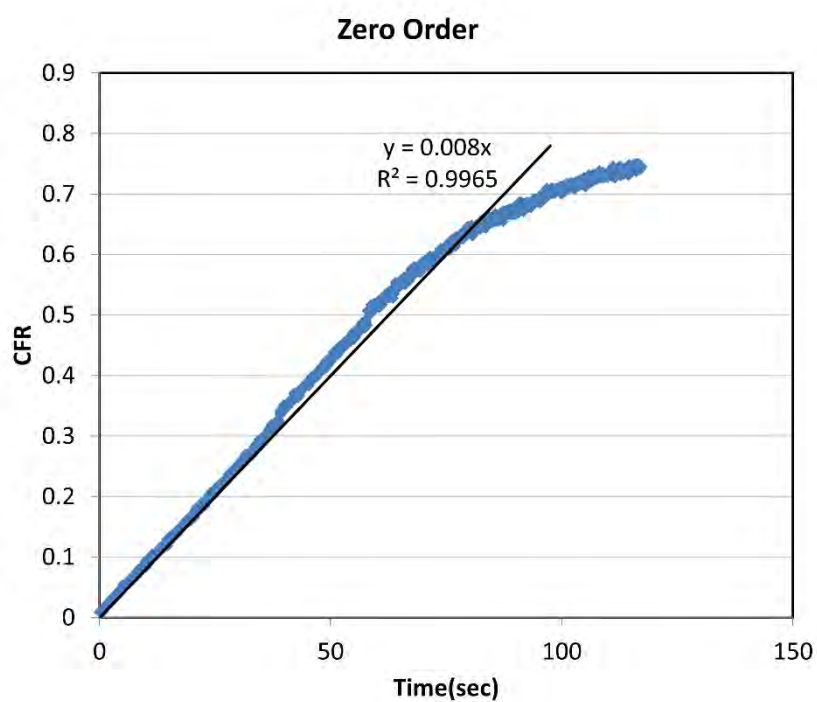


Figure A-7 Calcein release from control liposomes (Batch 1) at 9 mW/cm² fitting Zero-order Model

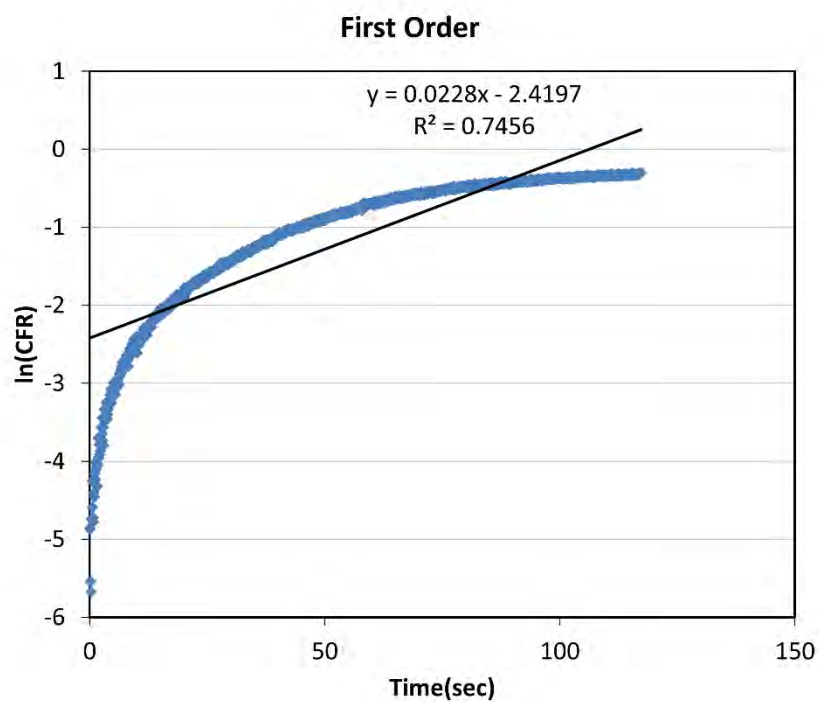


Figure A-8 Calcein release from control liposomes (Batch 1) at 9 mW/cm² fitting First-order Model.

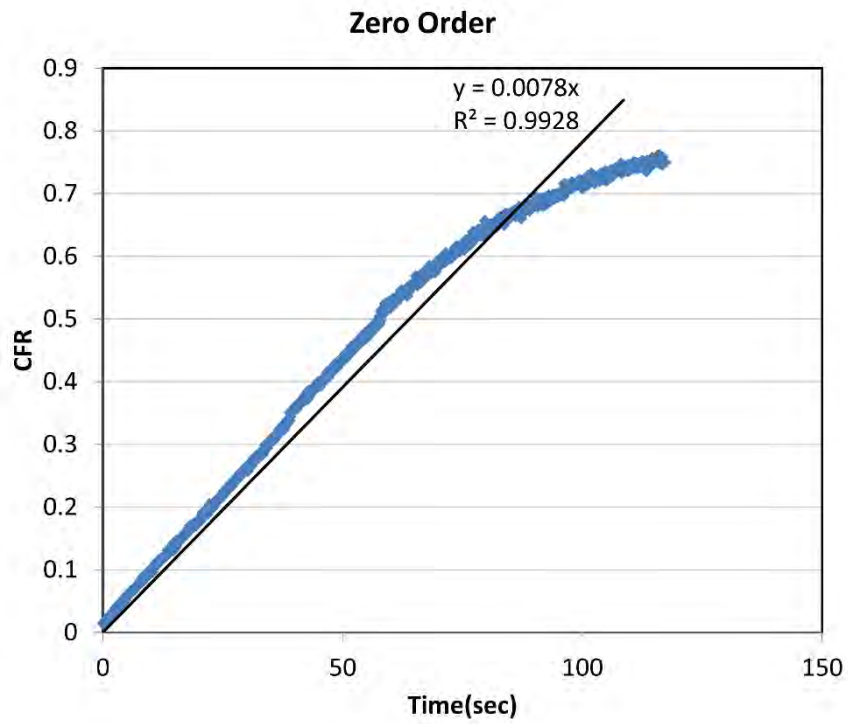


Figure A-9 Calcein release from control liposomes (Batch 2) at 9 mW/cm² fitting Zero-order Model

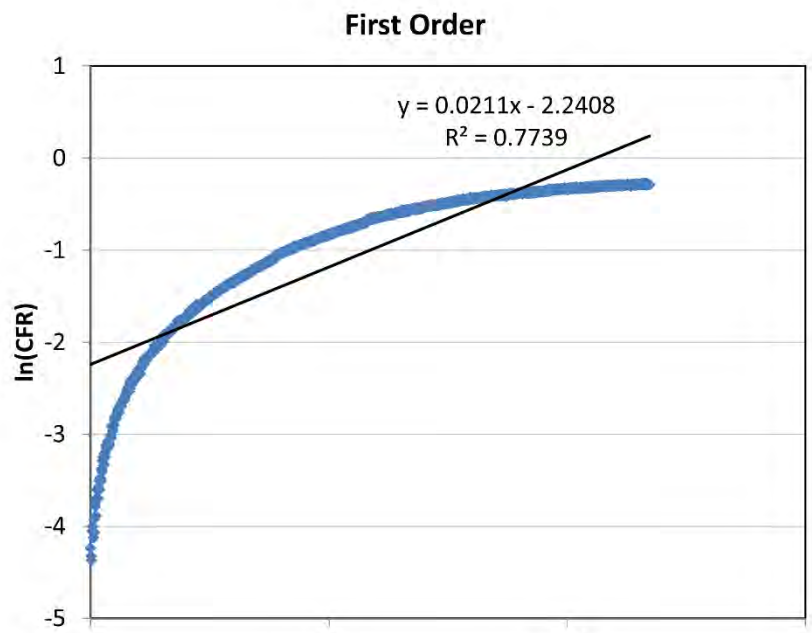


Figure A-10 Calcein release from control liposomes (Batch 2) at 9 mW/cm² fitting First-order Model

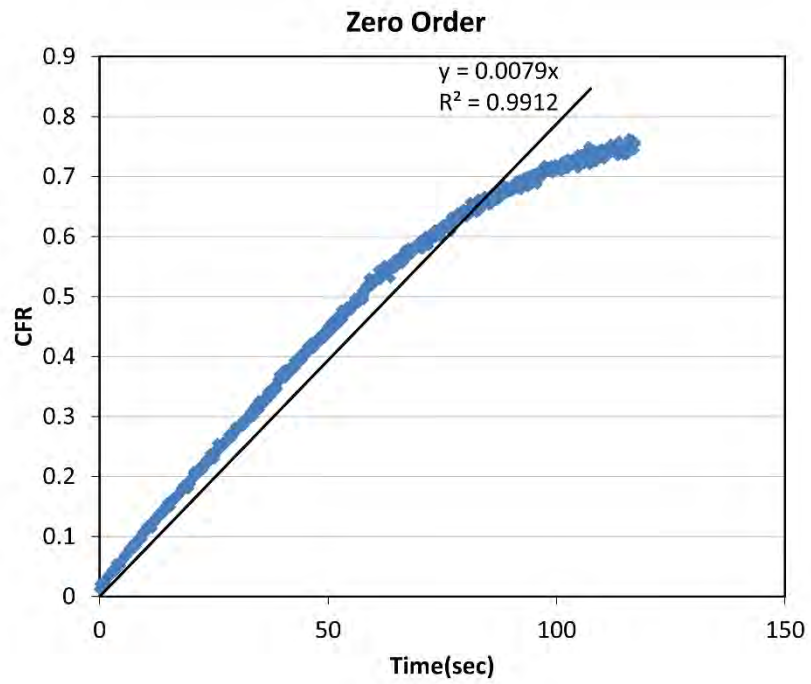


Figure A-11 Calcein release from control liposomes (Batch 3) at 9 mW/cm² fitting Zero-order Model

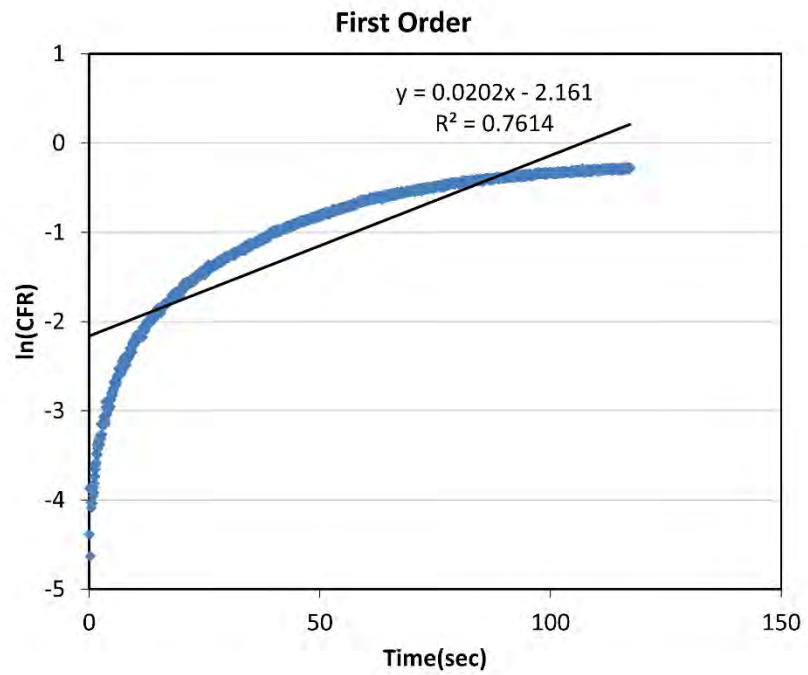


Figure A-12 Calcein release from control liposomes (Batch 3) at 9 mW/cm² fitting First-order Model

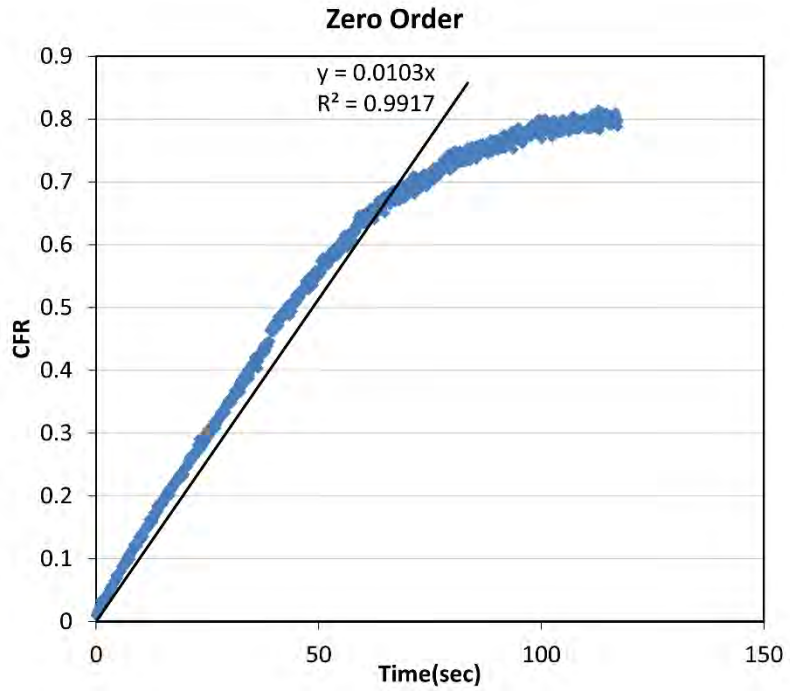


Figure A-13 Calcein release from control liposomes (Batch 1) at 10 mW/cm² fitting Zero-order Model

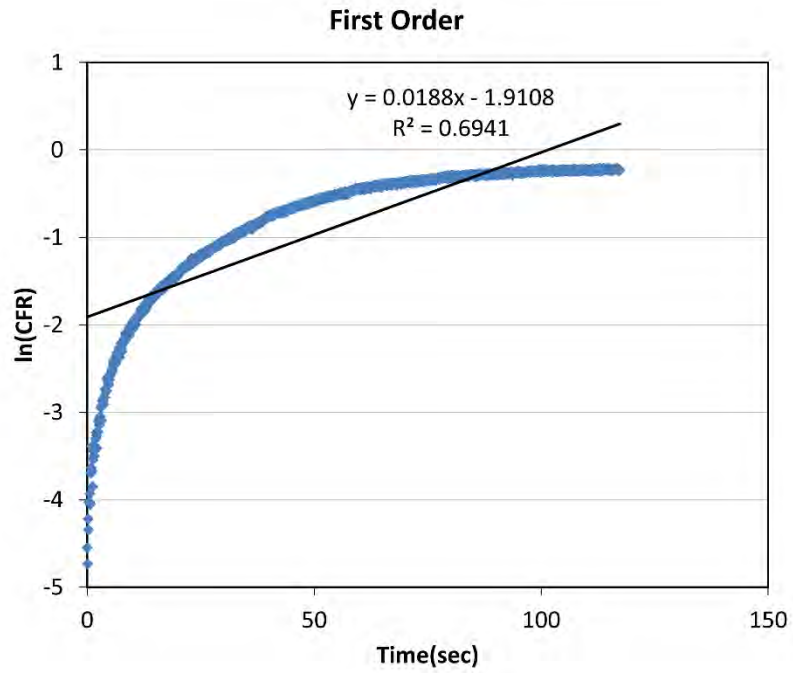


Figure A-14 Calcein release from control liposomes (Batch 1) at 10 mW/cm² fitting First-order Model

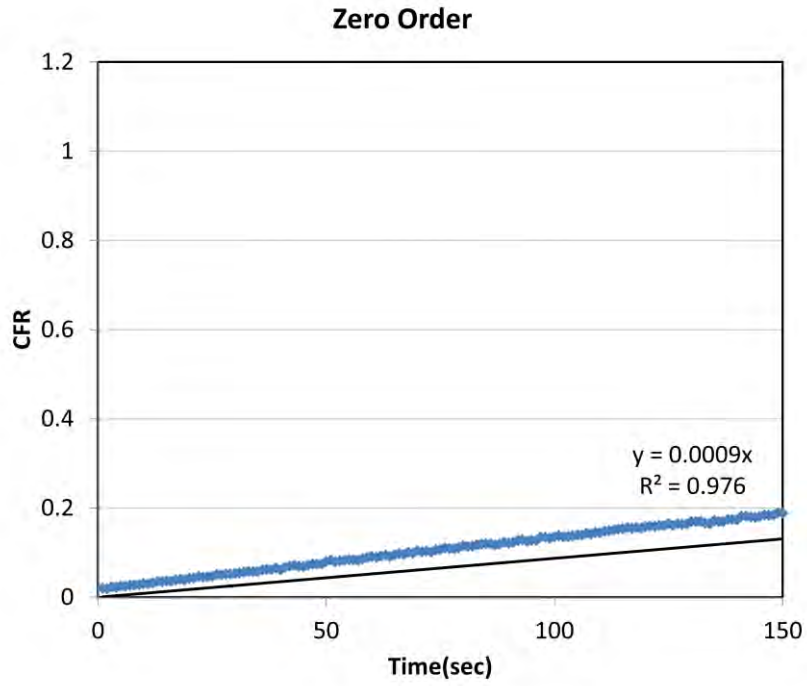


Figure A-15 Calcein release from control liposomes (Batch 2) at 10 mW/cm² fitting Zero-order Model

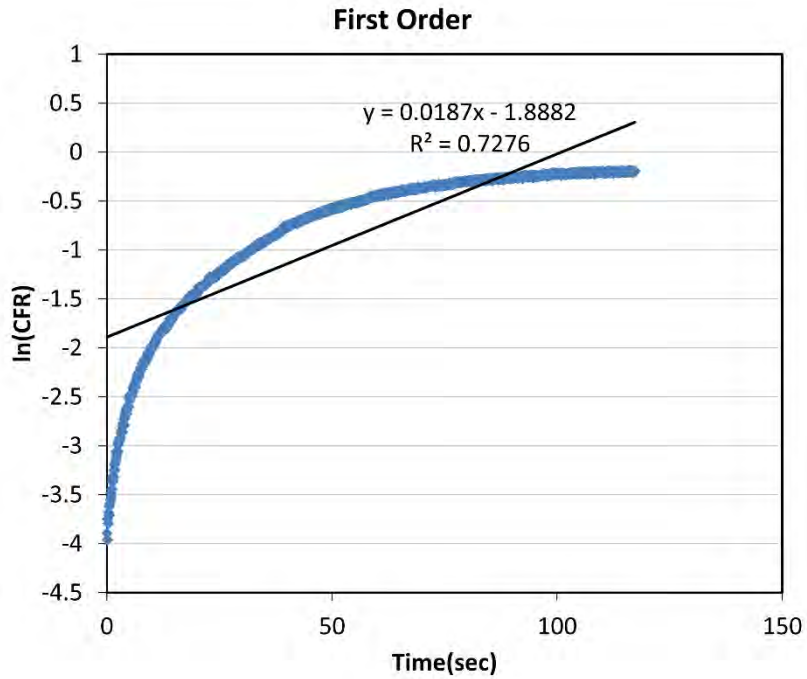


Figure A-16 Calcein release from control liposomes (Batch 2) at 10 mW/cm² fitting First-order Model



Figure A-17 Calcein release from control liposomes (Batch 3) at 10 mW/cm² fitting Zero-order Model



Figure A-18 Calcein release from control liposomes (Batch 3) at 10 mW/cm² fitting First-order Model

Appendix B: eLiposomes kinetic Modeling



Figure B-1 Calcein release from B-2 Calcein release from eLiposomes (Batch 1) at 6.2 mW/cm² fitting Zero-order Model

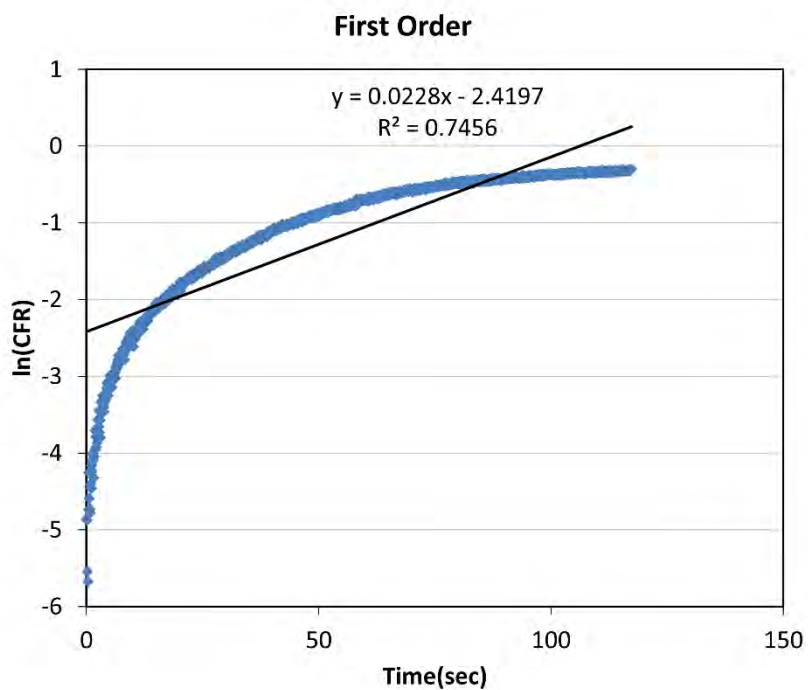


Figure B-2 Calcein release from eLiposomes (Batch 1) at 6.2 mW/cm² fitting First-order Model

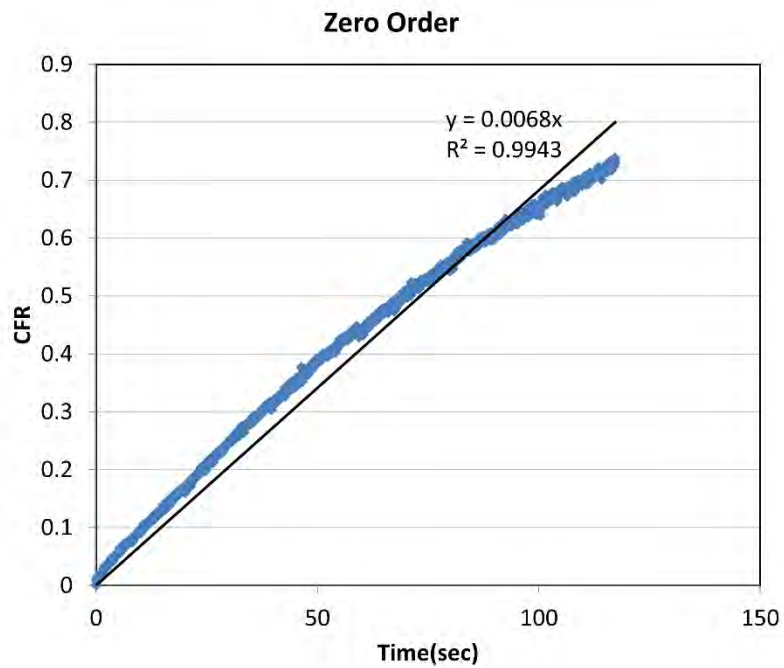


Figure B-3 Calcein release from eLiposomes (Batch 2) at 6.2 mW/cm² fitting Zero-order Model

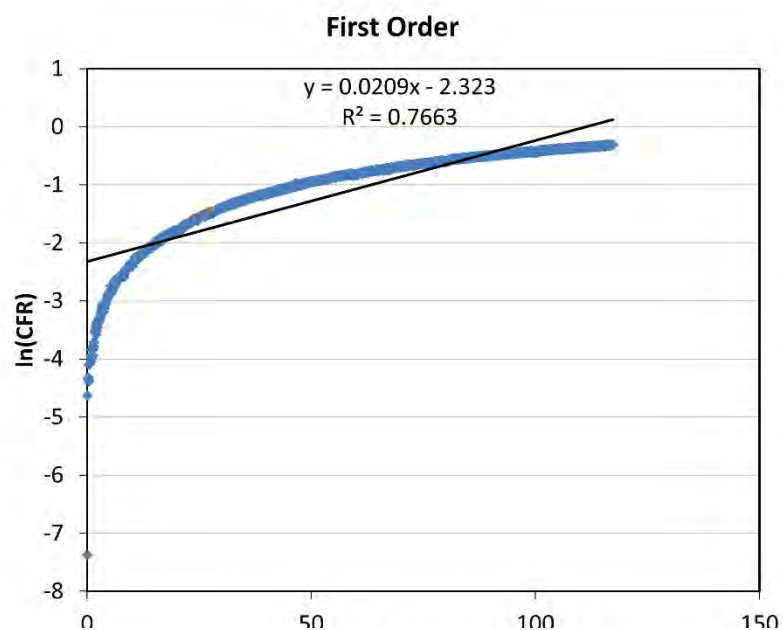


Figure B-4 Calcein release from eLiposomes (Batch 2) at 6.2 mW/cm² fitting First-order Model

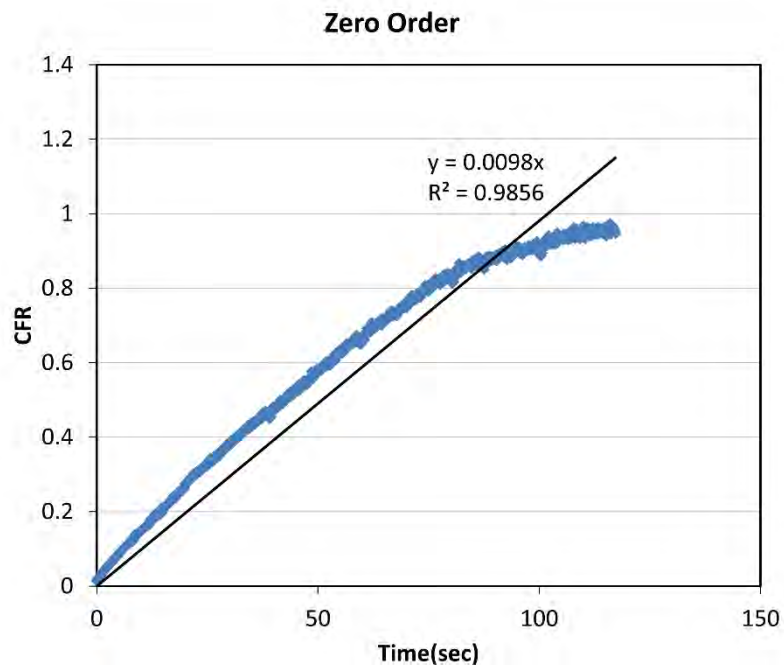


Figure B-5 Calcein release from eLiposomes (Batch 3) at 6.2 mW/cm² fitting Zero-order Model

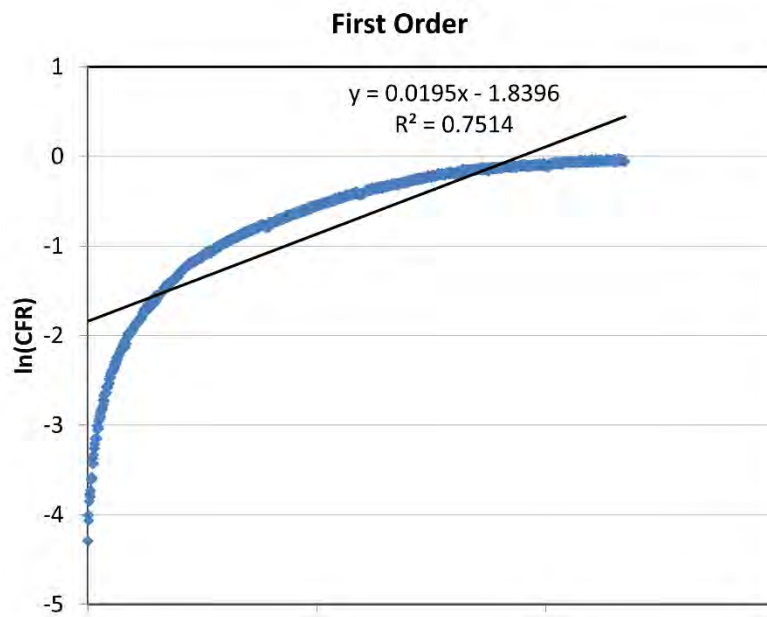
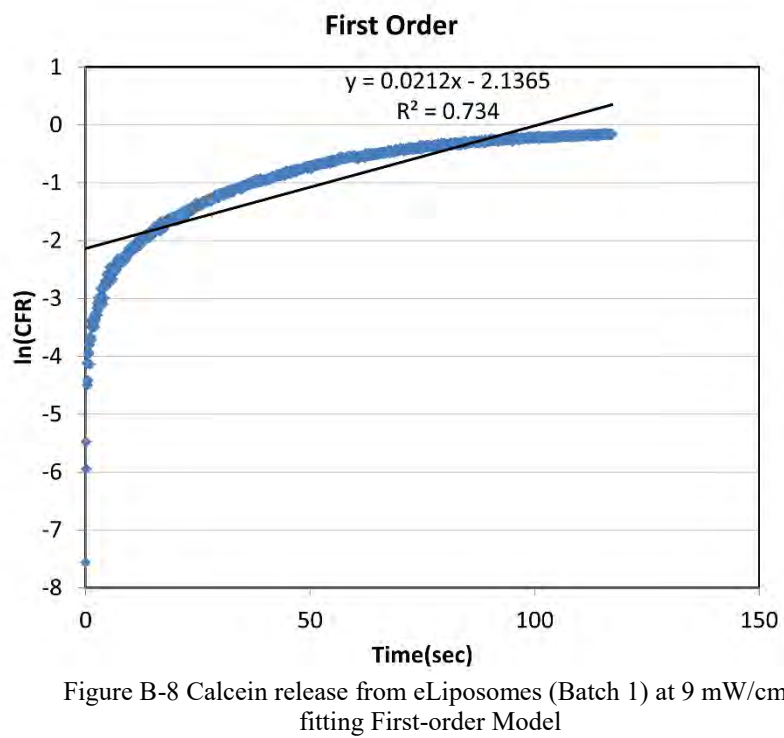
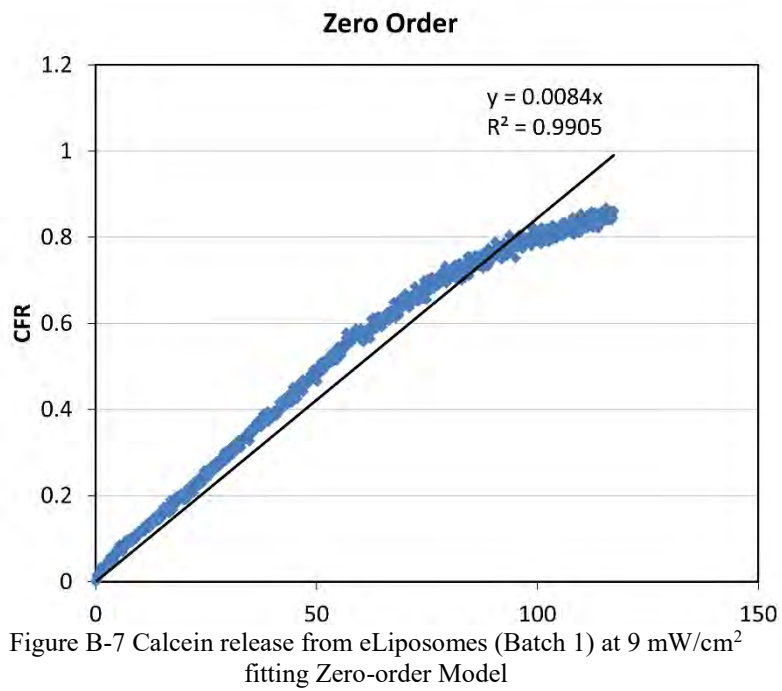


Figure B-6 Calcein release from eLiposomes (Batch 3) at 6.2 mW/cm² fitting First-order Model



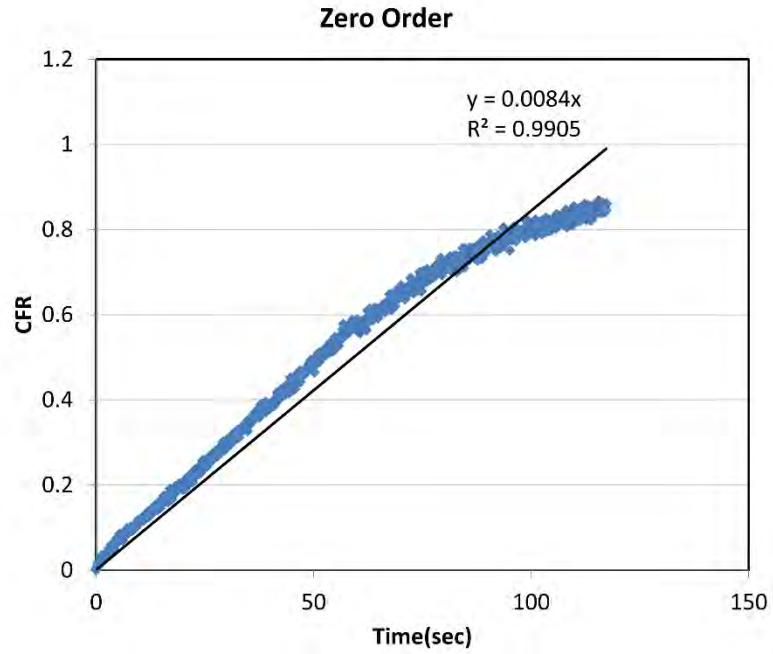


Figure B-9 Calcein release from eLiposomes (Batch 2) at 9 mW/cm² fitting Zero-order Model

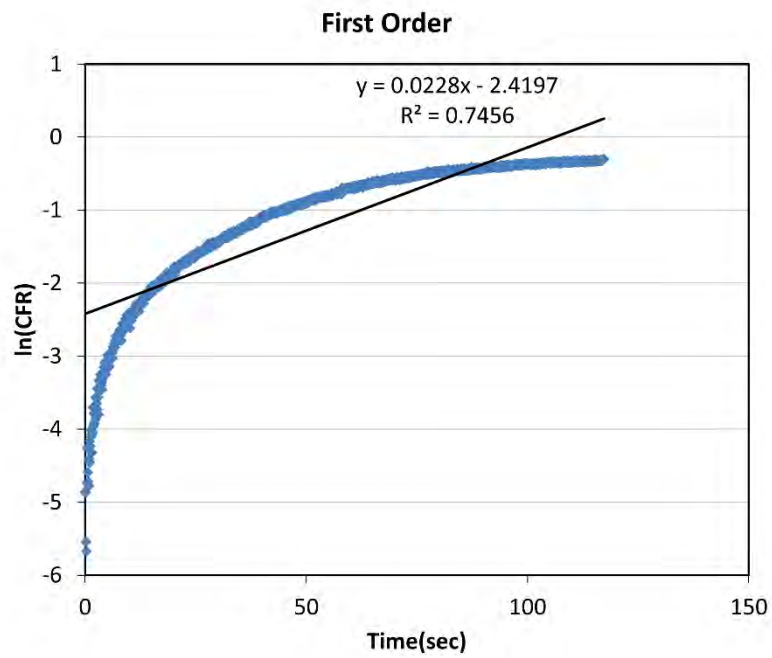


Figure B-10 Calcein release from eLiposomes (Batch 2) at 9 mW/cm² fitting First-order Model

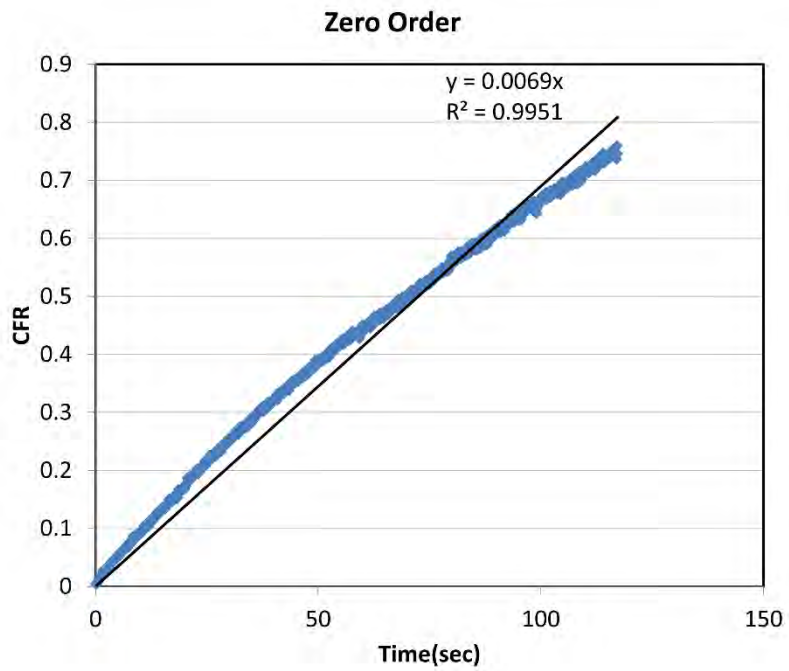


Figure B-11 Calcein release from eLiposomes (Batch 3) at 9 mW/cm² fitting Zero-order Model

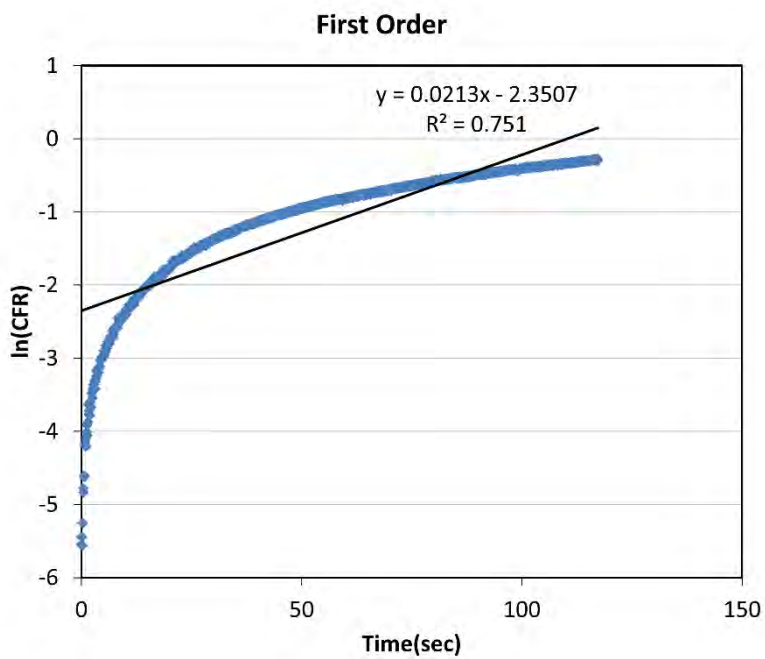


Figure B-12 Calcein release from eLiposomes (Batch 3) at 9 mW/cm² fitting First-order Model

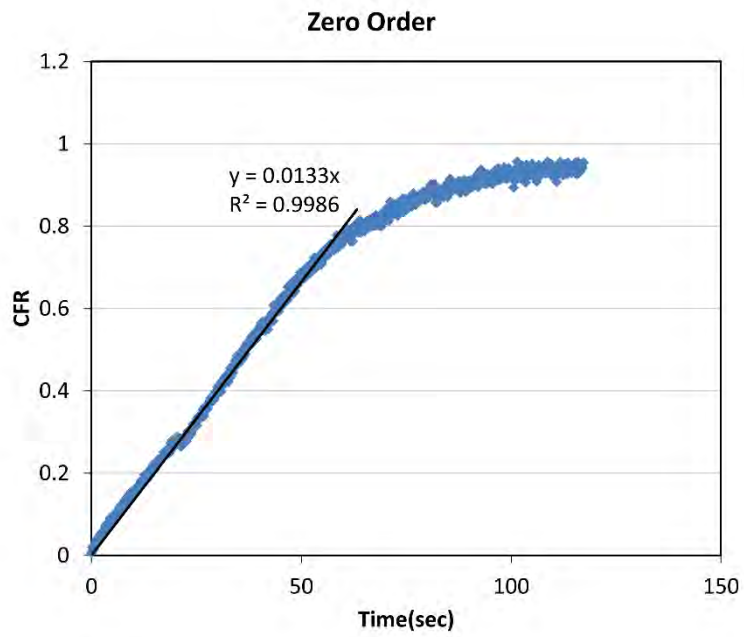


Figure B-13 Calcein release from eLiposomes (Batch 1) at 10 mW/cm² fitting Zero-order Model

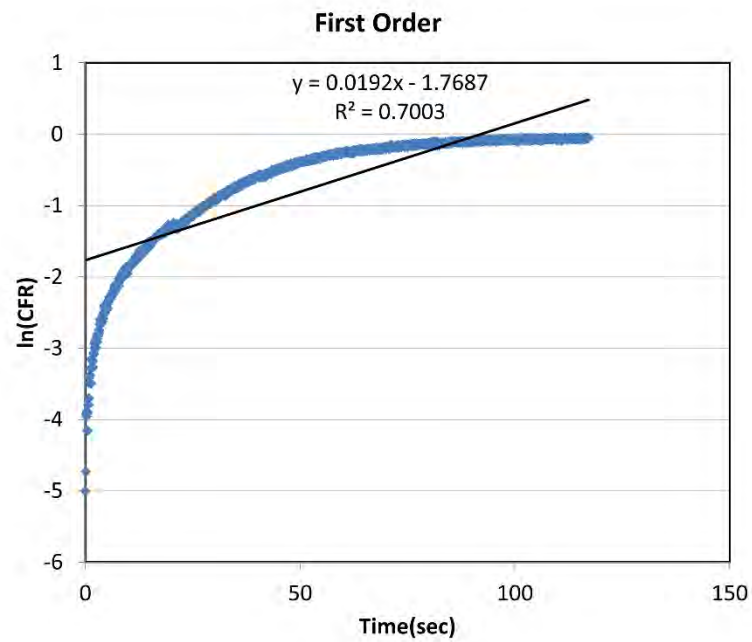


Figure B-14 Calcein release from eLiposomes (Batch 1) at 10 mW/cm² fitting First-order Model

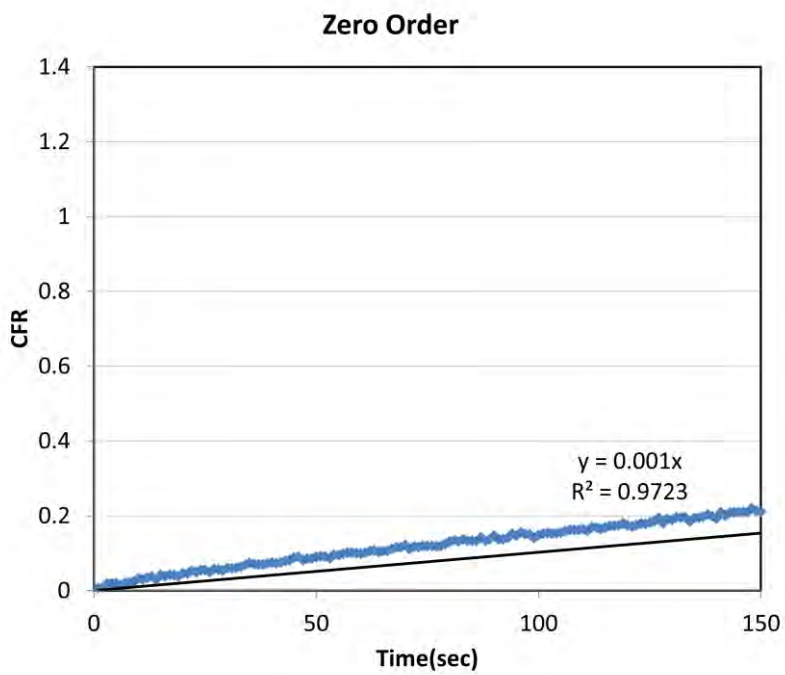


Figure B-15 Calcein release from eLiposomes (Batch 2) at 10 mW/cm² fitting Zero-order Model

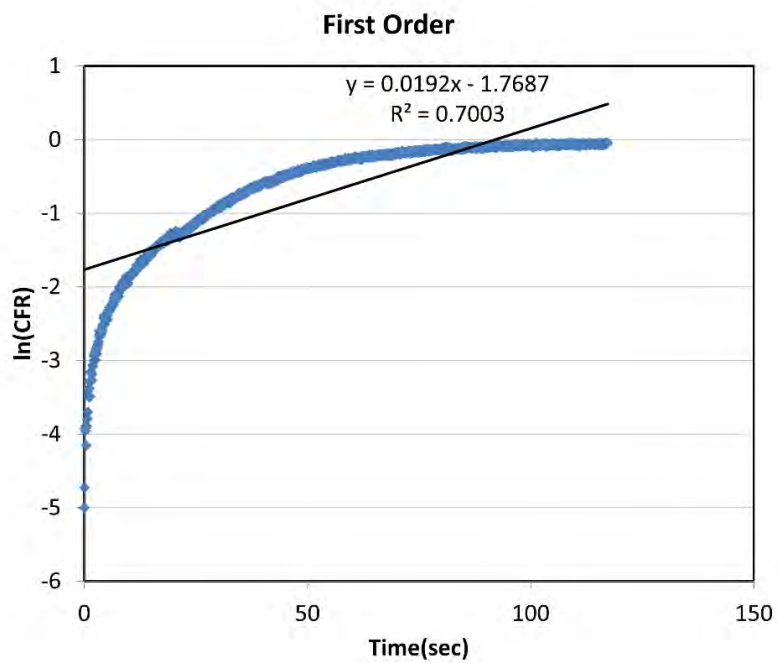


Figure B-16 Calcein release from eLiposomes (Batch 2) at 10 mW/cm² fitting First-order Model

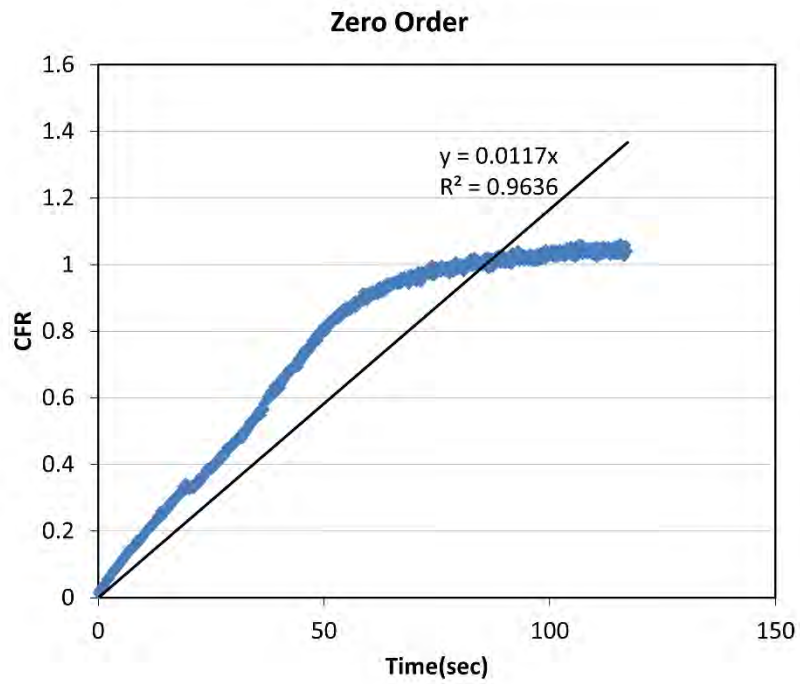


Figure B-17 Calcein release from eLiposomes (Batch 3) at 10 mW/cm² fitting Zero-order Model

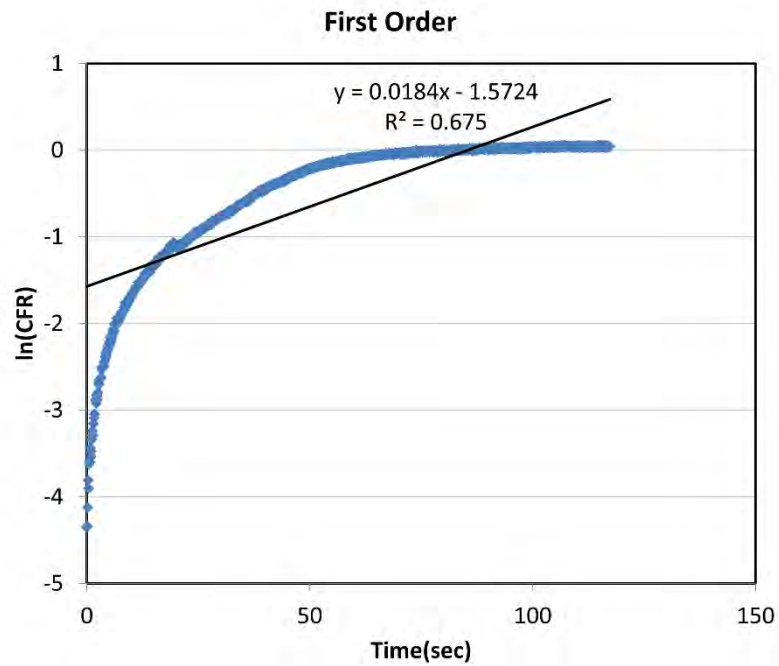
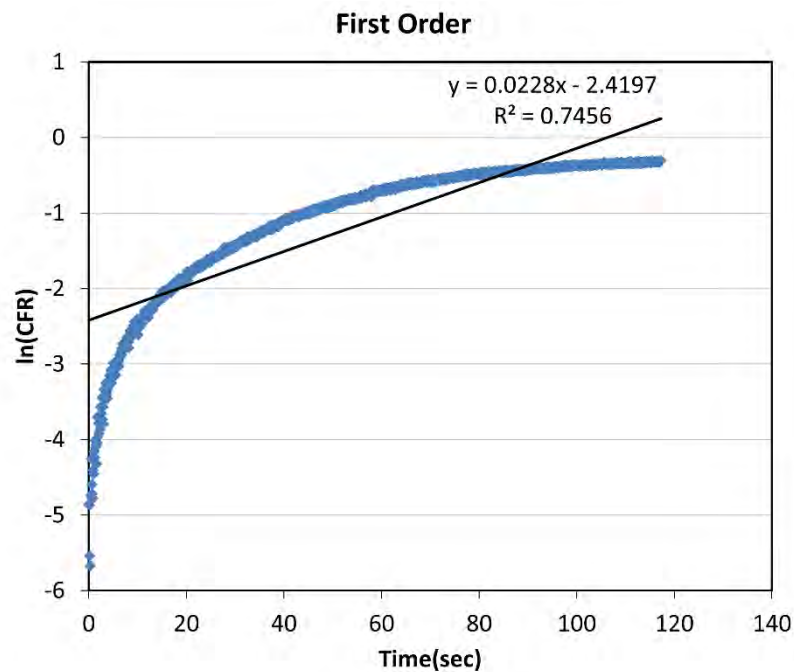


Figure B-18 Calcein release from eLiposomes (Batch 3) at 10 mW/cm² fitting First-order Model

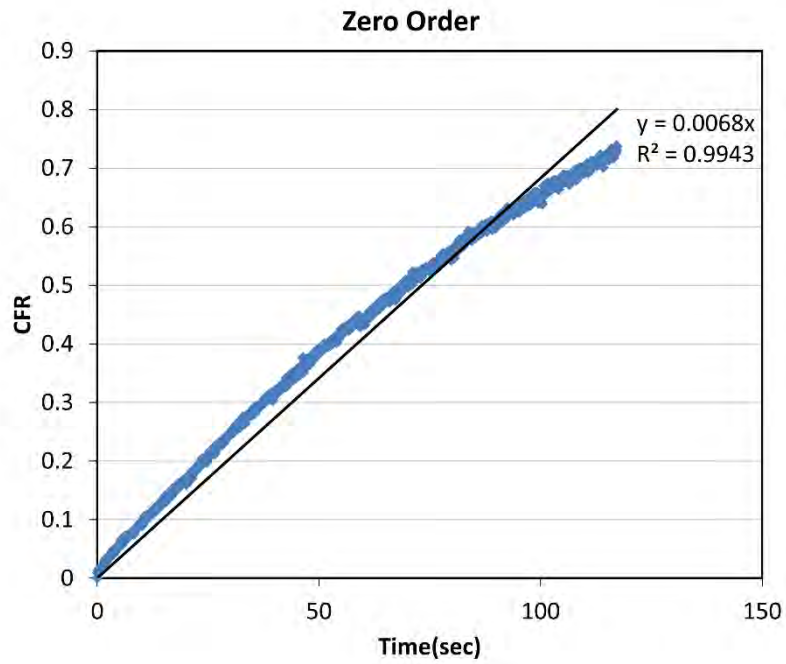
Appendix C: HER-conjugated liposomal kinetic modeling



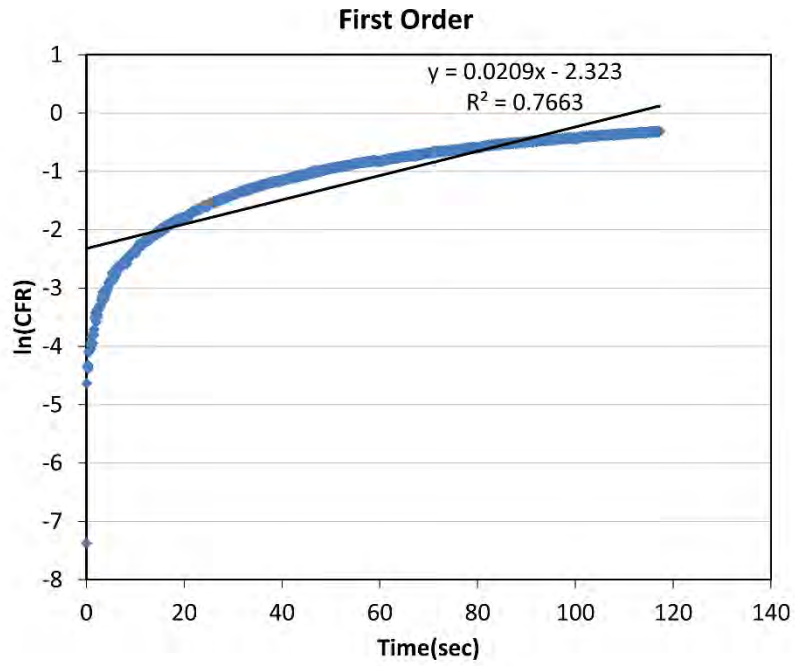
C-1 Calcein release from HER-conjugated Liposomes (Batch 1) at 6.2 mW/cm² fitting Zero-order Model



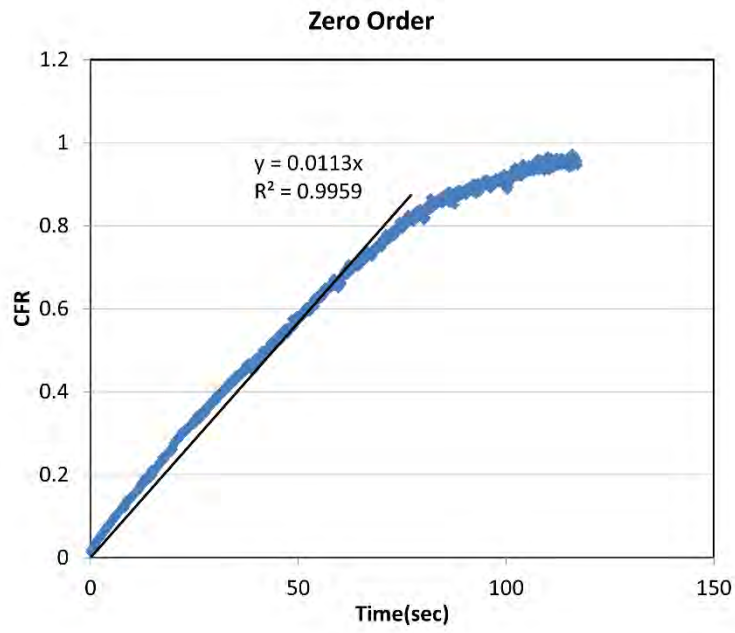
C-2 Calcein release from HER-conjugated Liposomes (Batch 1) at 6.2 mW/cm² fitting First-order Model



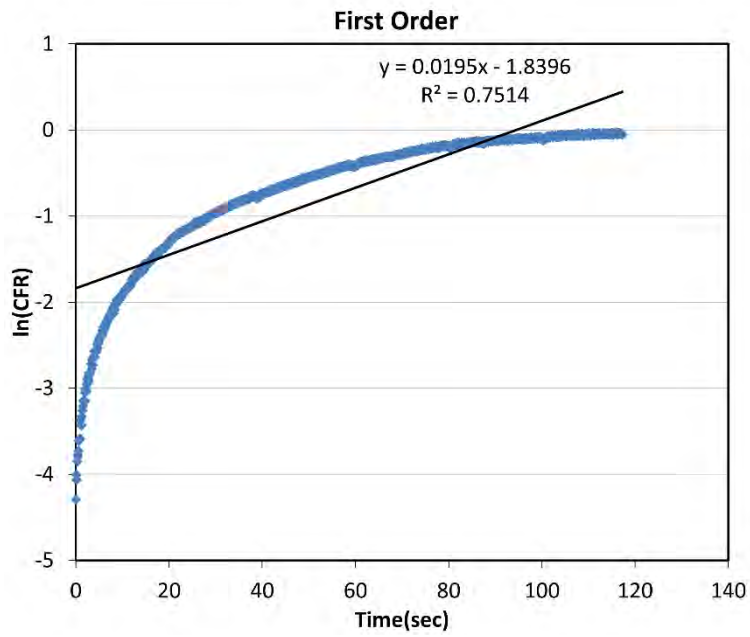
C-3 Calcein release from HER-conjugated Liposomes (Batch 2) at 6.2 mW/cm² fitting Zero-order Model



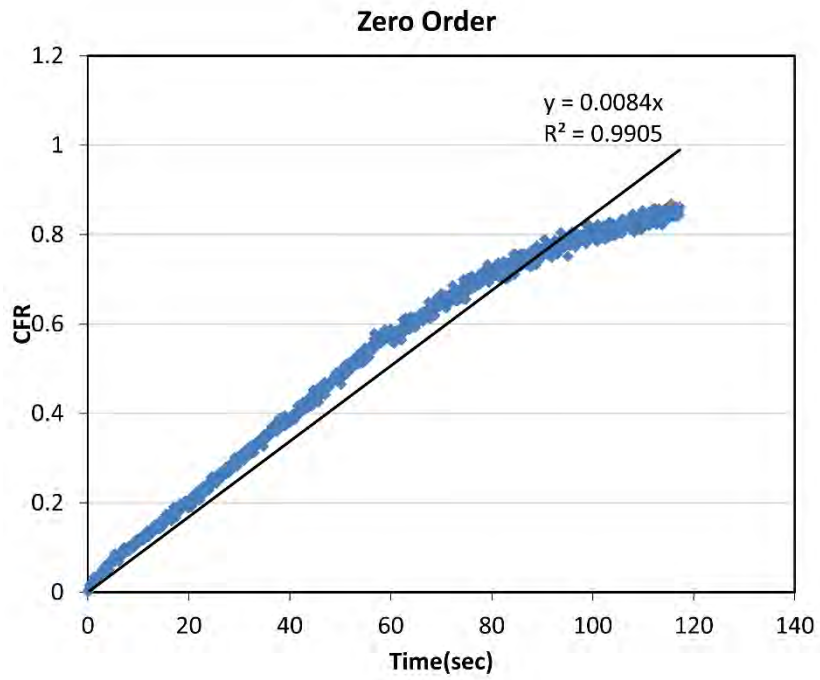
C-4 Calcein release from HER-conjugated Liposomes (Batch 1) at 6.2 mW/cm² fitting First-order Model



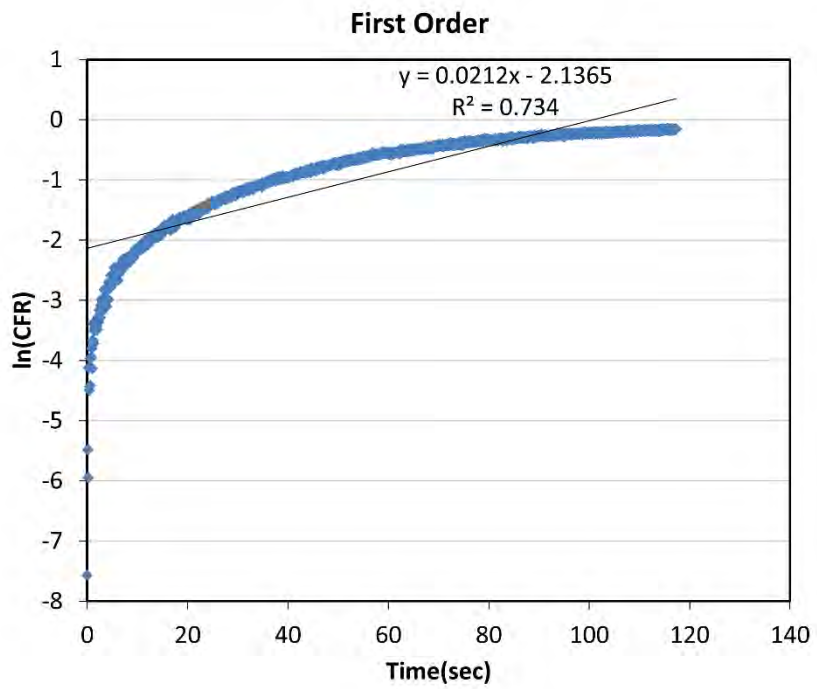
C-5 Calcein release from HER-conjugated Liposomes (Batch 3) at 6.2 mW/cm² fitting Zero-order Model



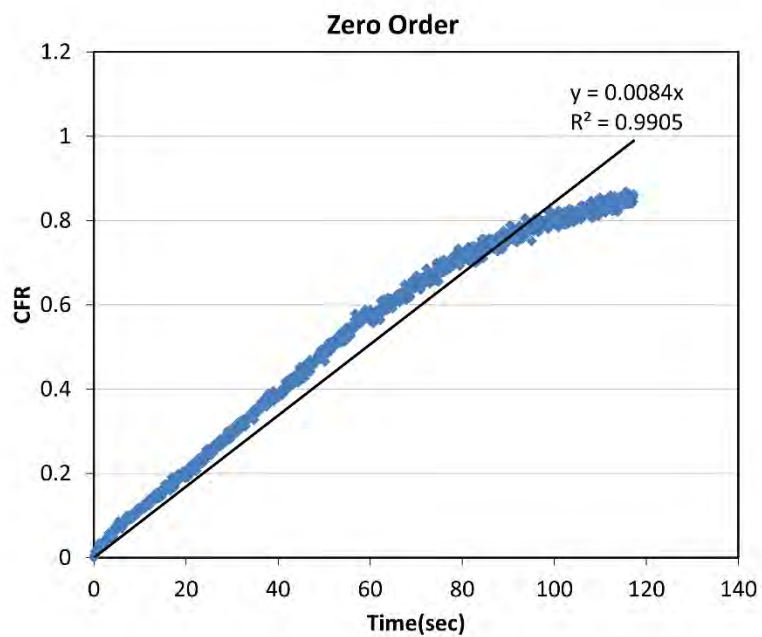
C-6 Calcein release from HER-conjugated Liposomes (Batch 3) at 6.2 mW/cm² fitting First-order Model



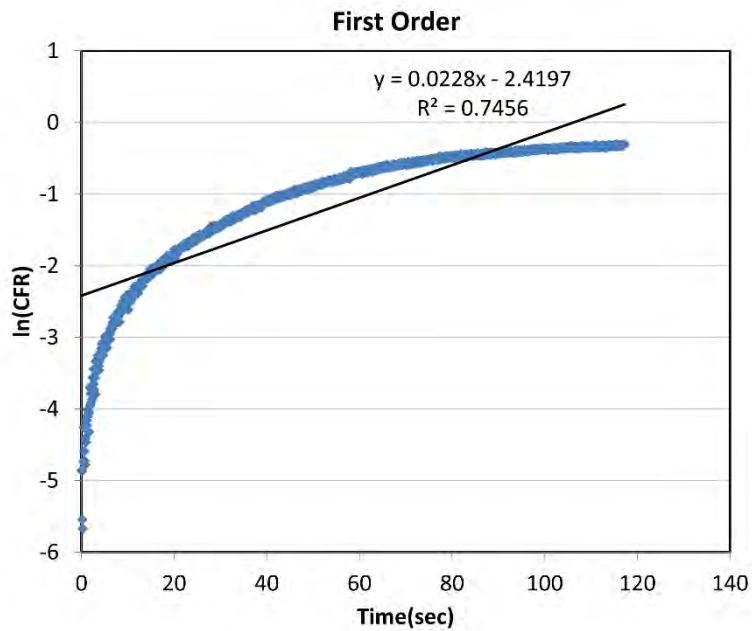
C-7 Calcein release from HER-conjugated Liposomes (Batch 1) at 9 mW/cm² fitting Zero-order Model



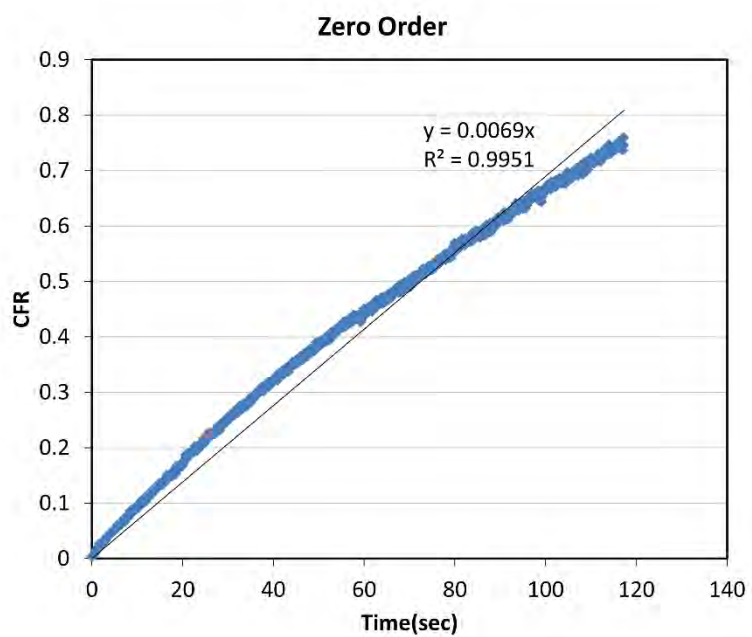
C-8 Calcein release from HER-conjugated Liposomes (Batch 1) at 9mW/cm² fitting First-order Model



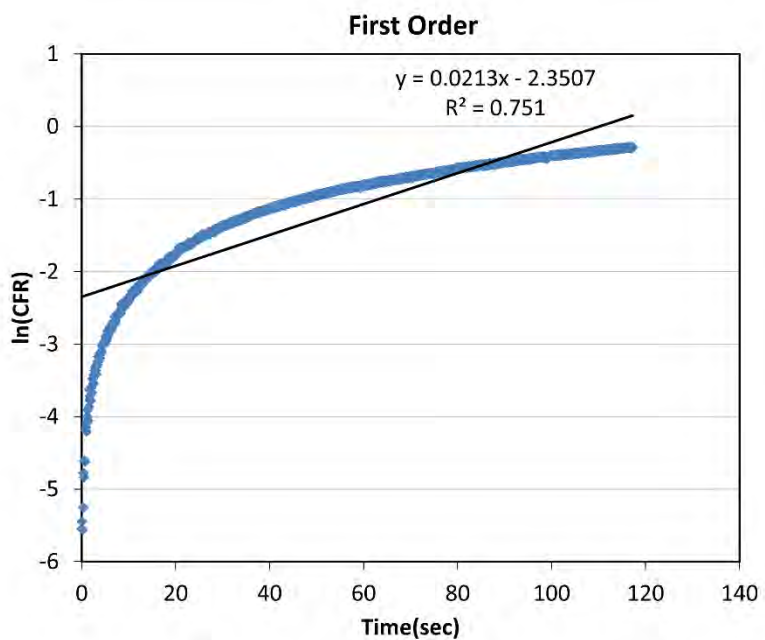
C-9 Calcein release from HER-conjugated Liposomes (Batch 2) at 9 mW/cm² fitting Zero-order



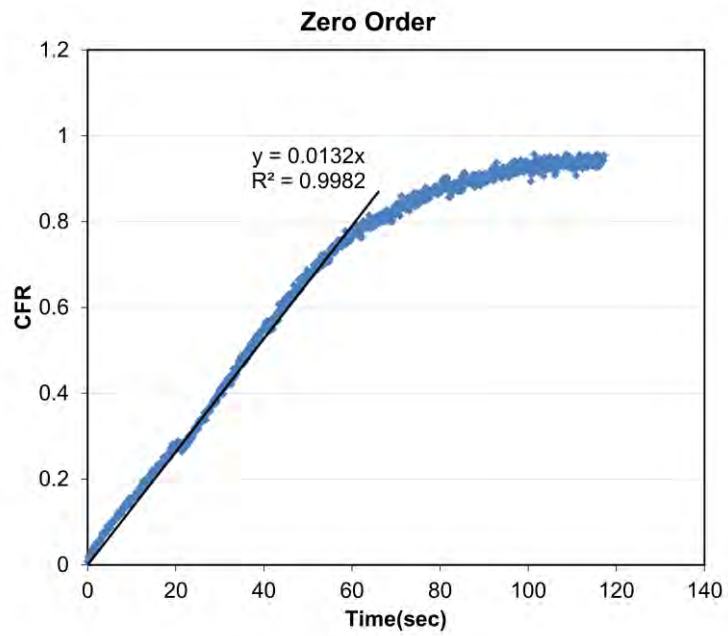
C-10 Calcein release from HER-conjugated Liposomes (Batch 2) at 9 mW/cm² fitting First-order Model



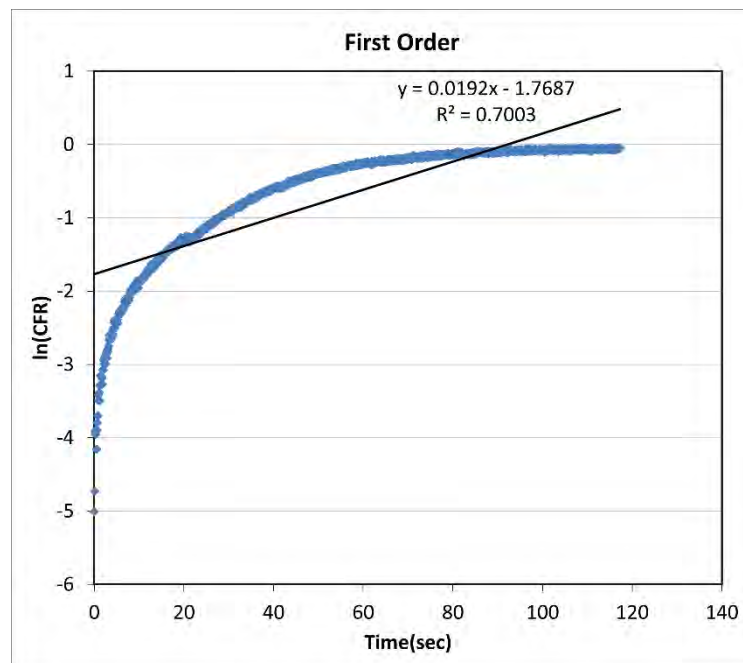
C-11 Calcein release from HER-conjugated Liposomes (Batch 3) at 9 mW/cm² fitting Zero-order Model



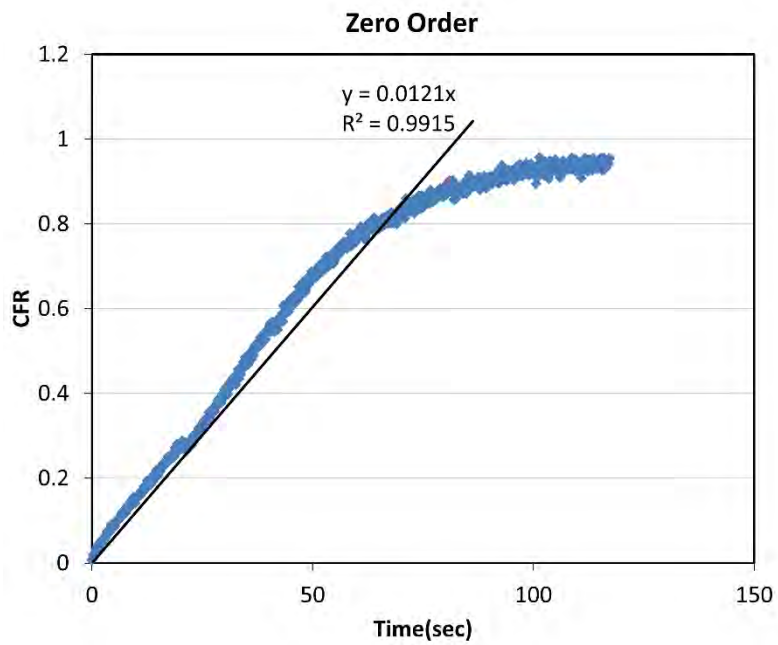
C-12 Calcein release from HER-conjugated Liposomes (Batch 3) at 9 mW/cm² fitting First-order Model



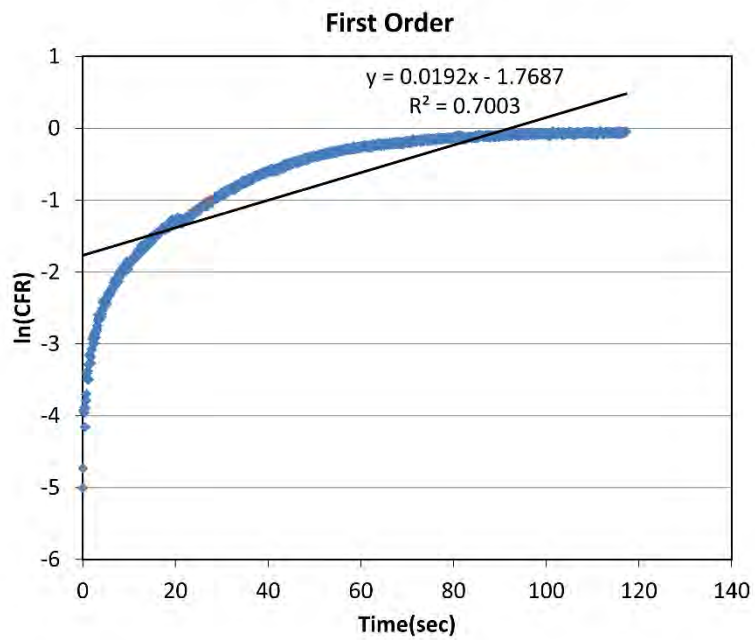
C-13 Calcein release from HER-conjugated Liposomes (Batch 1) at 10 mW/cm² fitting Zero-order Model



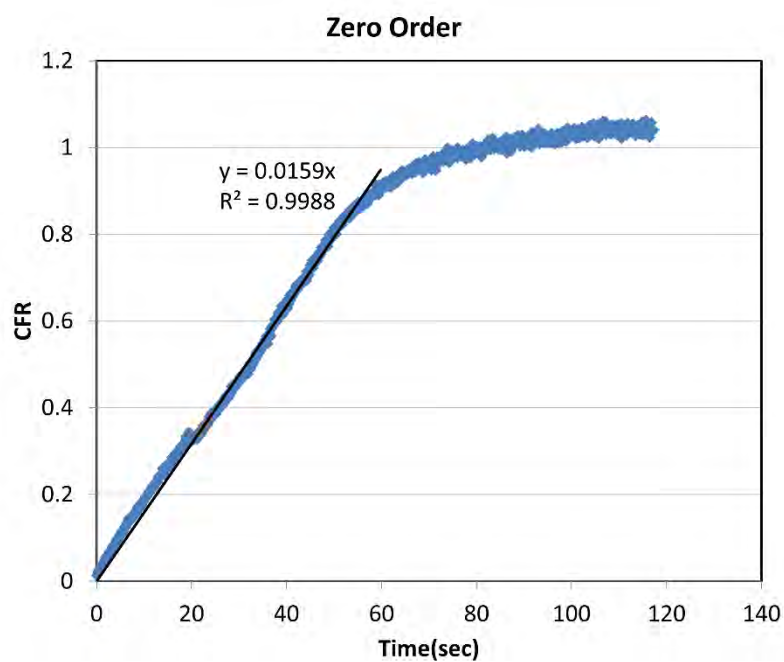
C-14 Calcein release from HER-conjugated Liposomes (Batch 1) at 10 mW/cm² fitting First-order Model



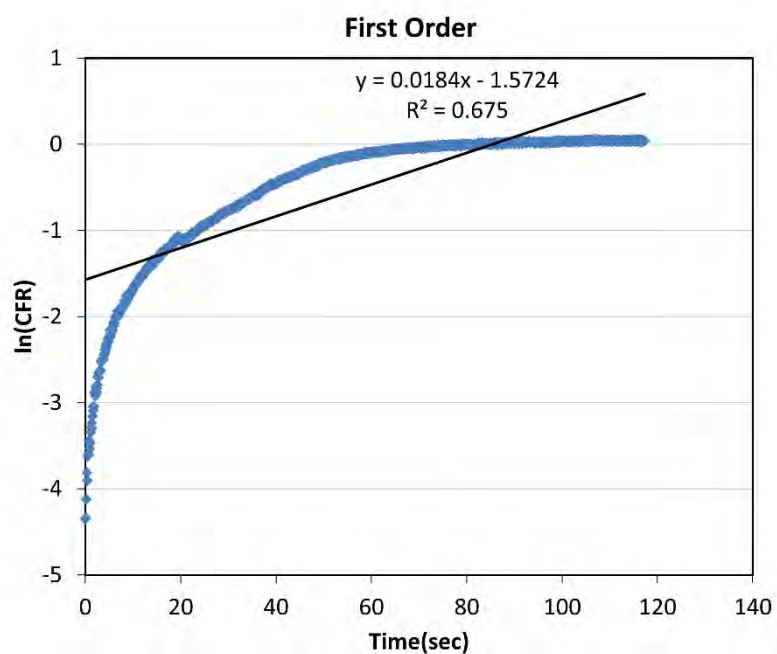
C-15 Calcein release from HER-conjugated Liposomes (Batch 2) at 10 mW/cm² fitting Zero-order Model



C-16 Calcein release from HER-conjugated Liposomes (Batch 2) at 10 mW/cm² fitting First-order Model

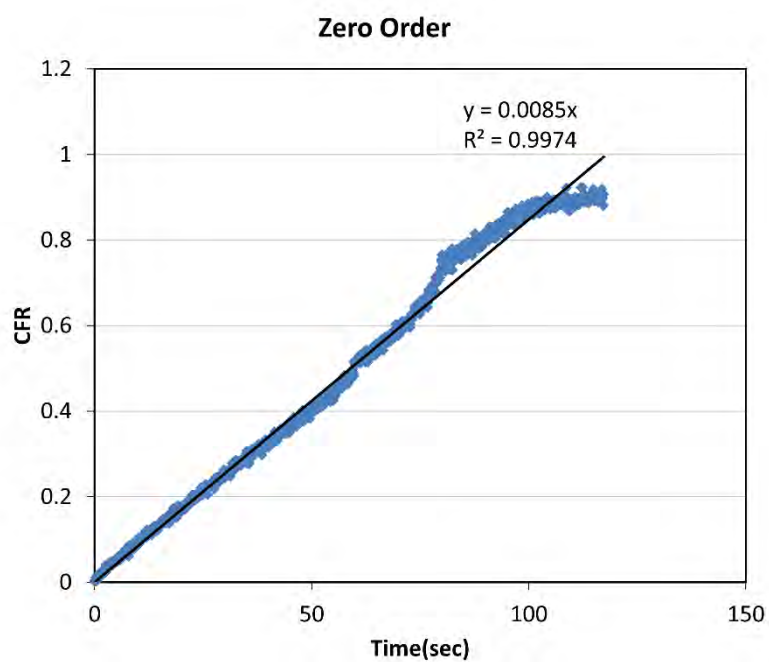


C-17 Calcein release from HER-conjugated Liposomes (Batch 3) at 10 mW/cm² fitting Zero-order Model

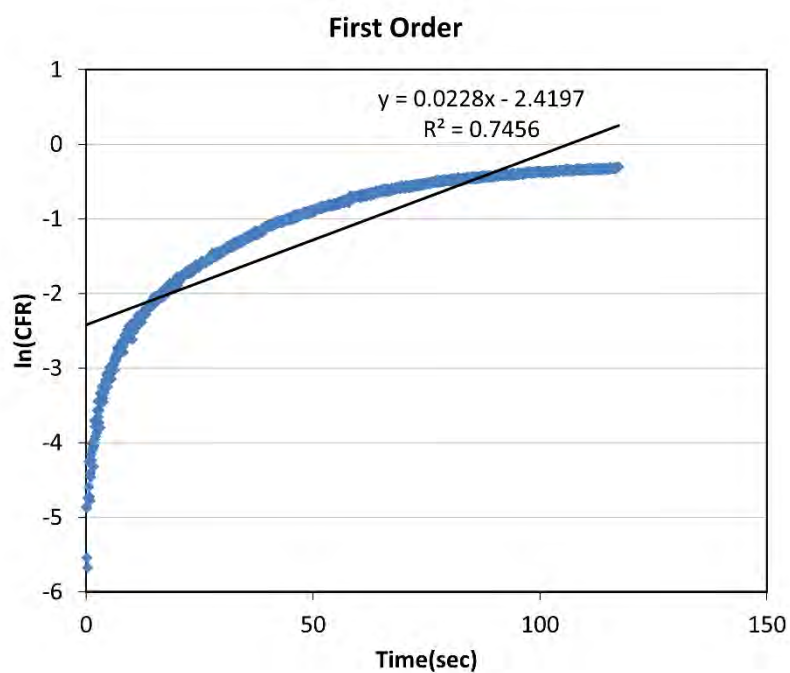


C-18 Calcein release from HER-conjugated Liposomes (Batch 3) at 10 mW/cm² fitting First-order Model

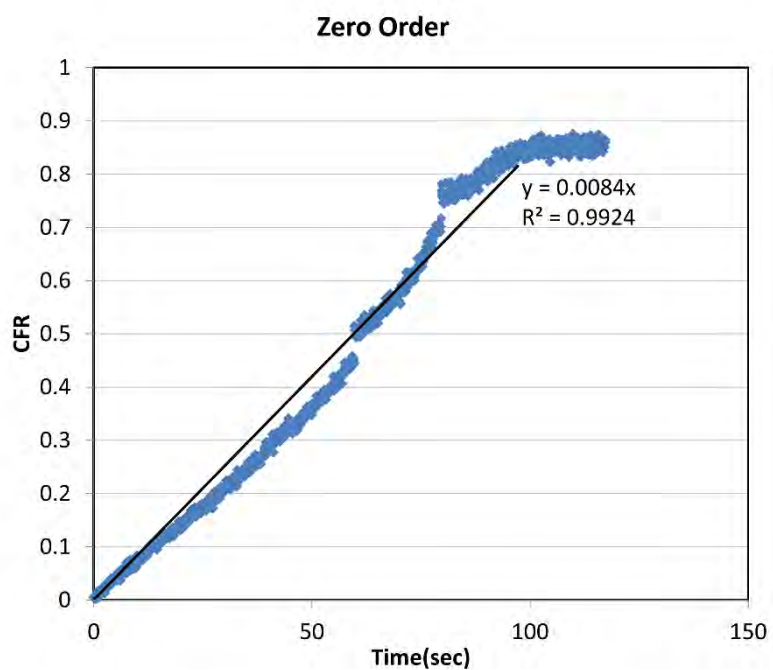
Appendix D: HER-conjugated eLiposomal kinetic modeling



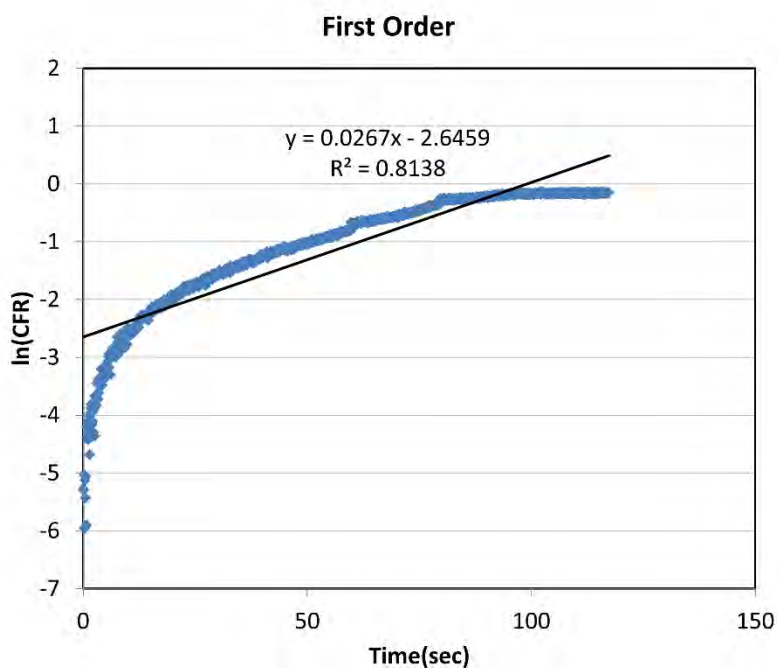
D-1 Calcein release from HER-conjugated eLiposomes (Batch 1) at 6.2 mW/cm² fitting Zero-order Model



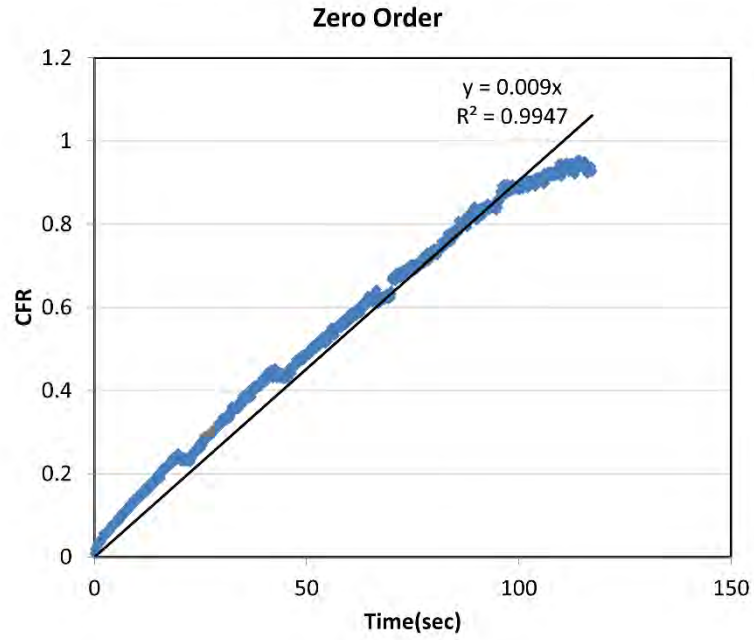
D-2 Calcein release from HER-conjugated eLiposomes (Batch 1) at 6.2 mW/cm² fitting First-order Model



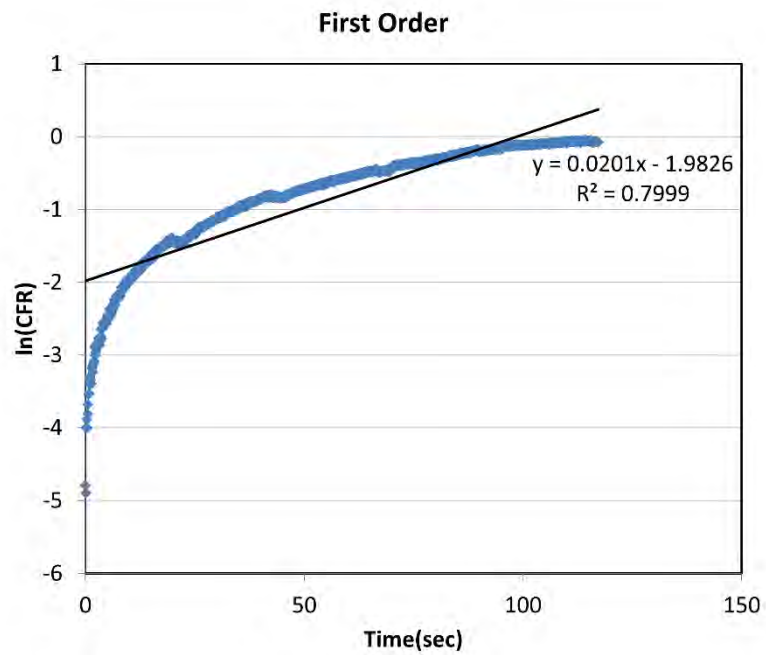
D-3 Calcein release from HER-conjugated eLiposomes (Batch 2) at 6.2 mW/cm² fitting Zero-order Model



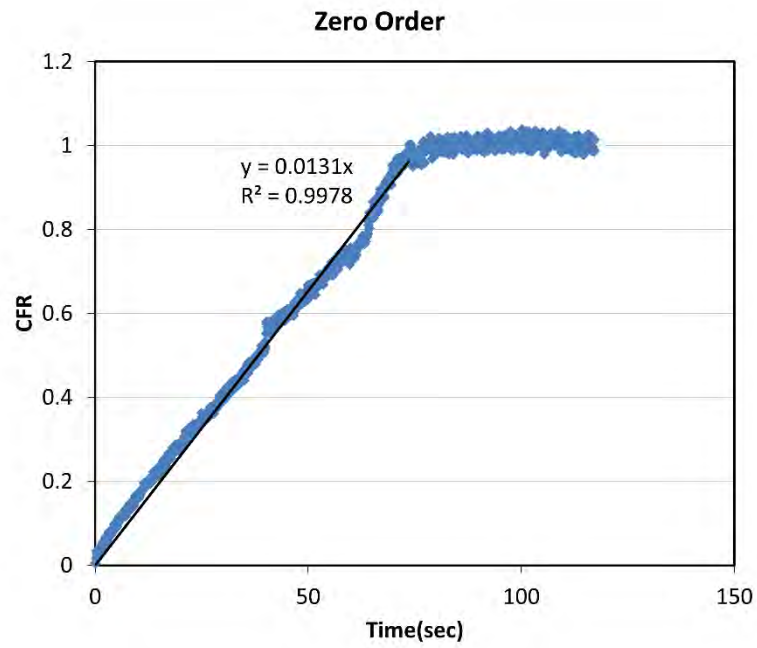
D-4 Calcein release from HER-conjugated eLiposomes (Batch 2) at 6.2 mW/cm² fitting First-order Model



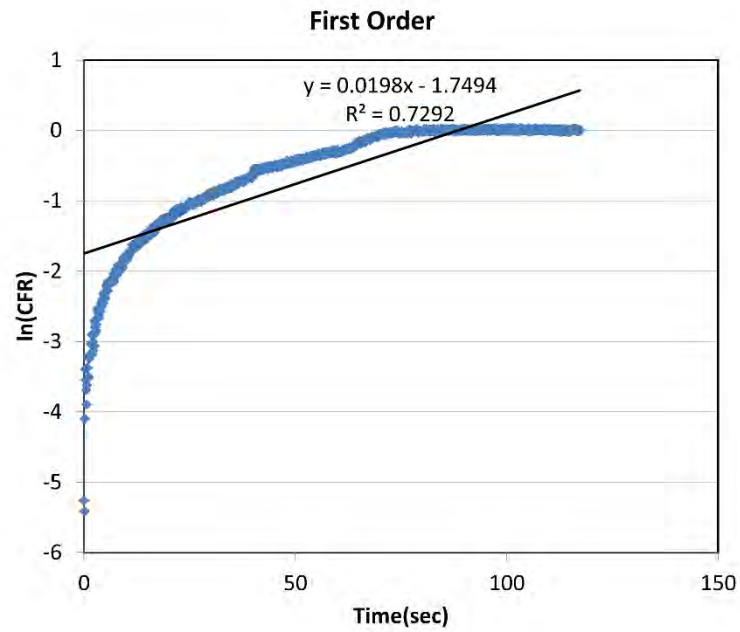
D-5 Calcein release from HER-conjugated eLiposomes (Batch 3) at 6.2 mW/cm² fitting Zero-order Model



D-6 Calcein release from HER-conjugated eLiposomes (Batch 3) at 6.2 mW/cm² fitting First-order Model

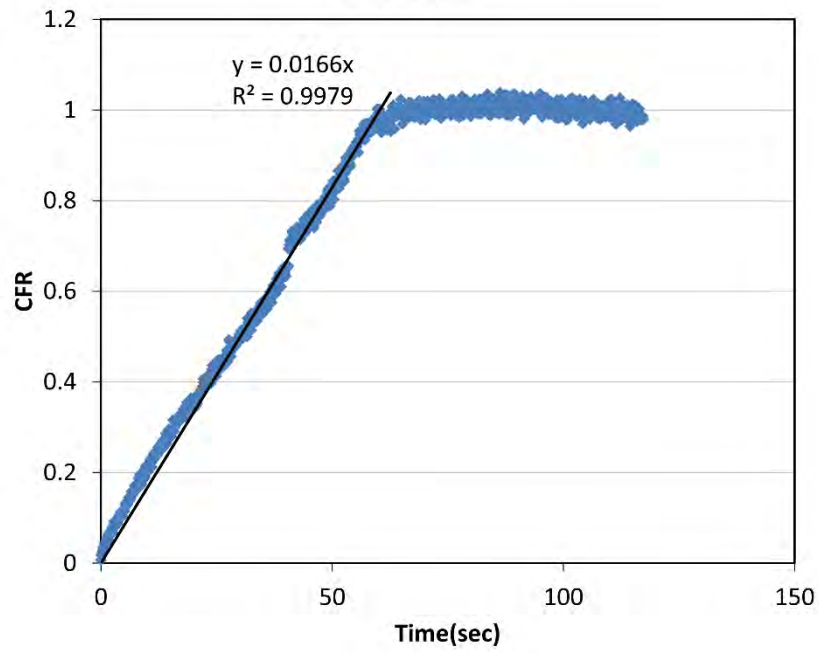


D-7 Calcein release from HER-conjugated eLiposomes (Batch 1) at 9 mW/cm² fitting Zero-order Model



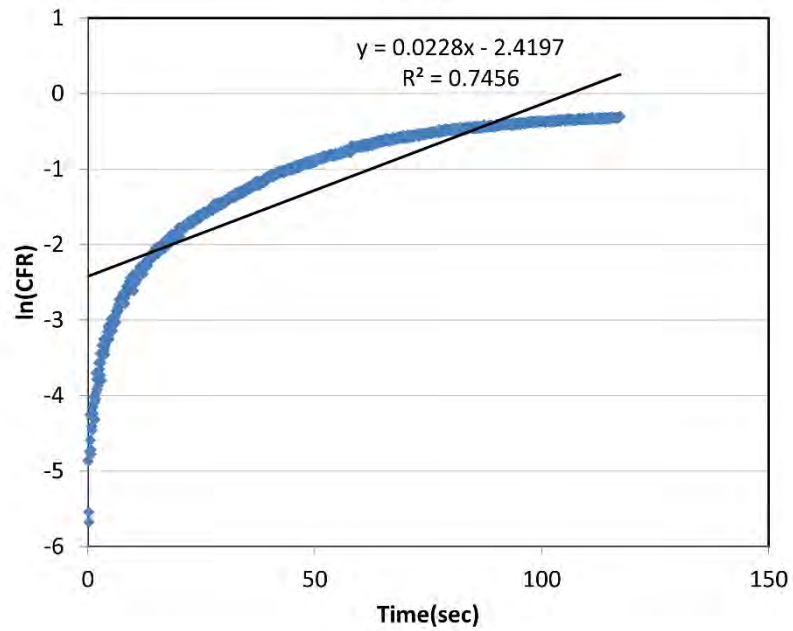
D-8 Calcein release from HER-conjugated eLiposomes (Batch 1) at 9 mW/cm² fitting Zero-order Model

Zero Order

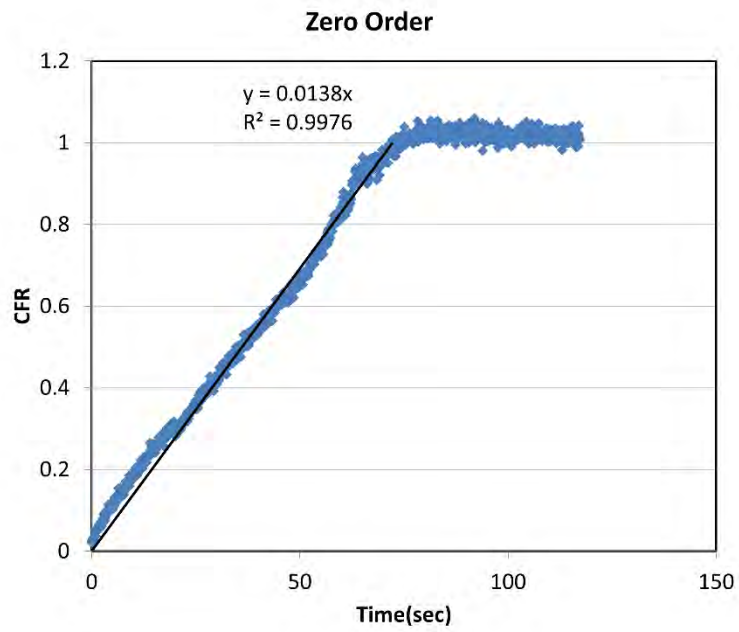


D-9 Calcein release from HER-conjugated eLiposomes (Batch 2) at 9 mW/cm² fitting Zero-order Model

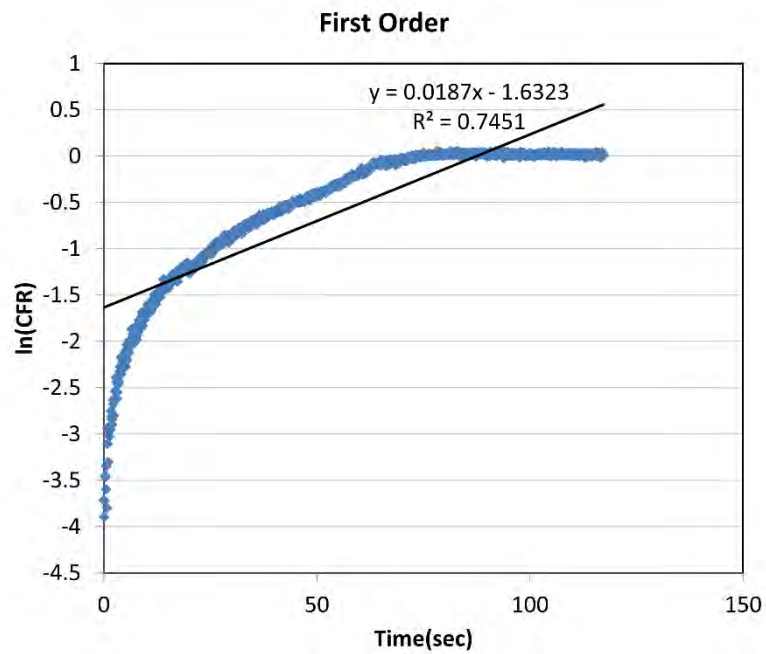
First Order



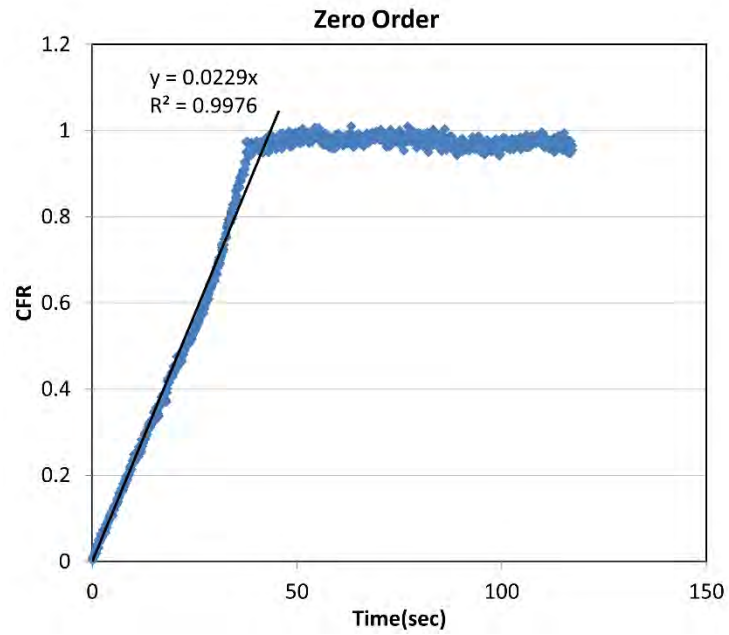
D-10 Calcein release from HER-conjugated eLiposomes (Batch 2) at 9 mW/cm² fitting First-order Model



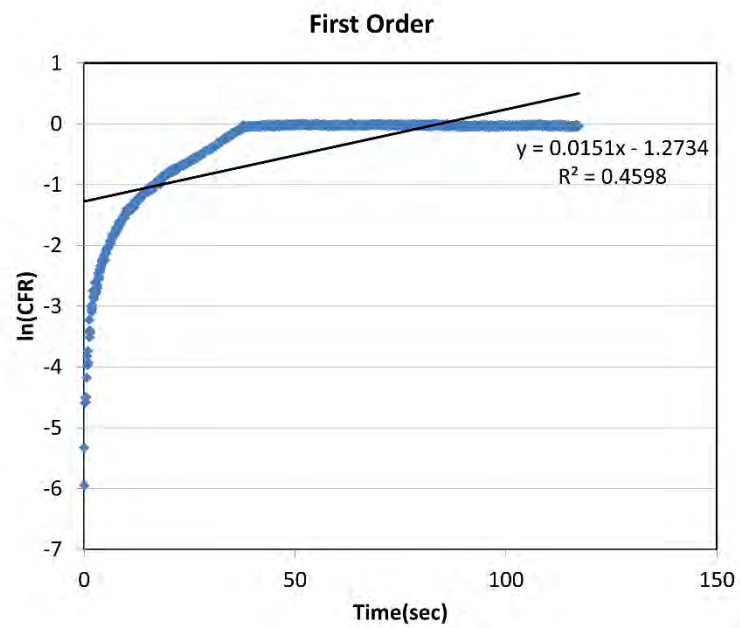
D-11 Calcein release from HER-conjugated eLiposomes (Batch 3) at 9 mW/cm² fitting Zero-order Model



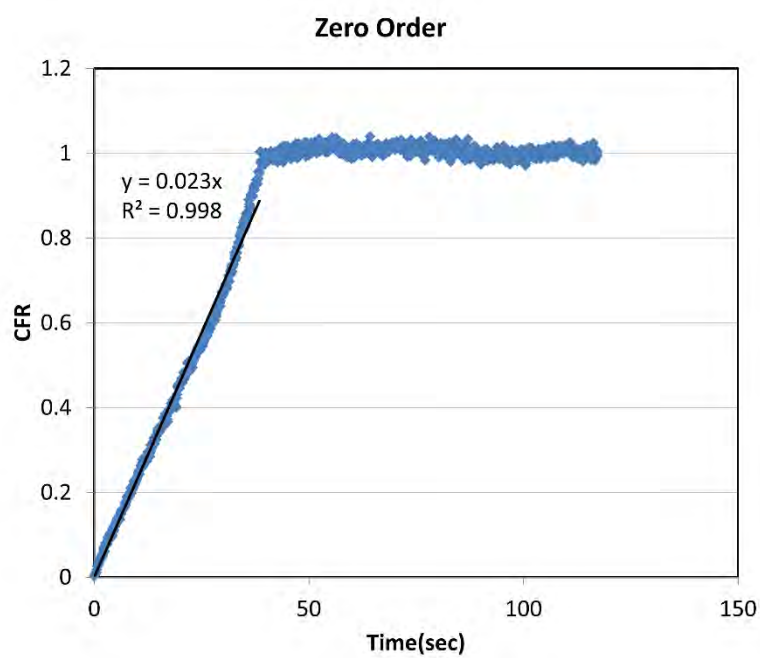
D-12 Calcein release from HER-conjugated eLiposomes (Batch 3) at 9 mW/cm² fitting First-order Model



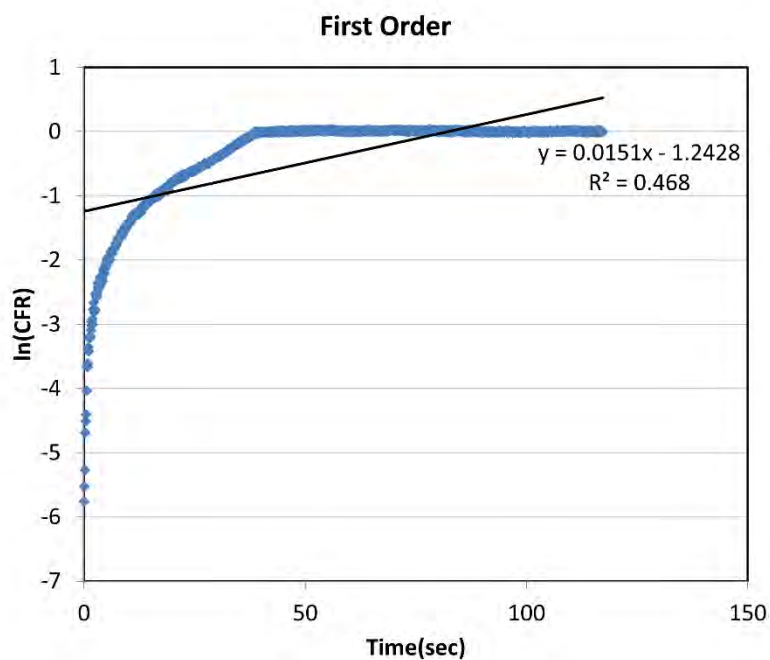
D-13 Calcein release from HER-conjugated eLiposomes (Batch 1) at 10 mW/cm² fitting Zero-order Model



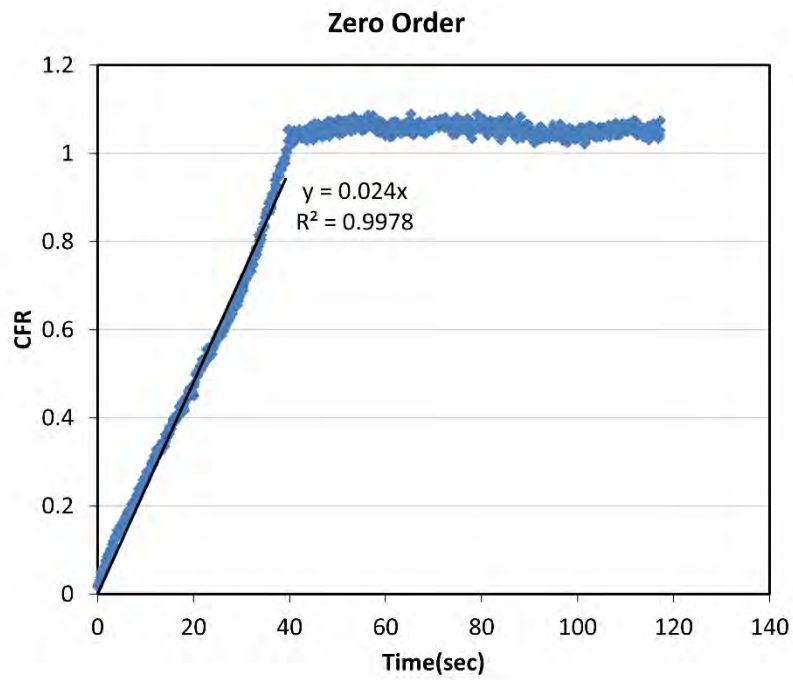
D-14 Calcein release from HER-conjugated eLiposomes (Batch 1) at 10 mW/cm² fitting First-order Model



D-15 Calcein release from HER-conjugated eLiposomes (Batch 2) at 10 mW/cm² fitting Zero-order Model



D-16 Calcein release from HER-conjugated eLiposomes (Batch 2) at 10 mW/cm² fitting First-order Model



D-17 Calcein release from HER-conjugated eLiposomes (Batch 3) at 10 mW/cm² fitting Zero-order Model

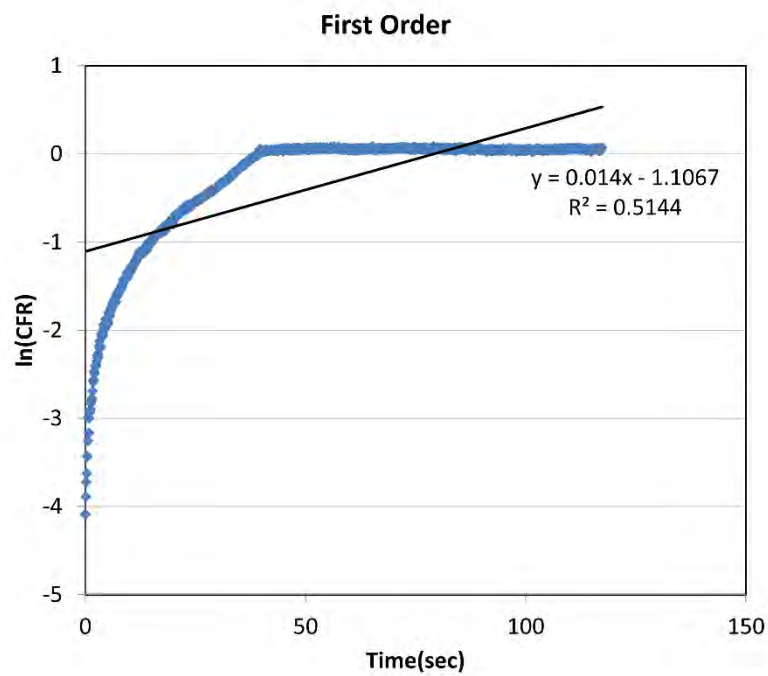


Figure D-18 Calcein release from HER-conjugated eLiposomes (Batch 3) at 10 mW/cm² fitting First-order Model

Vita

Mah Noor Zafar was born in 1992 in Jacobabad, Pakistan. She received her primary and secondary education in Ajman, UAE. She received her B.Sc. degree in Biomedical Engineering from Ajman University in 2015. From 2015 to 2023, she worked as a Biomedical Engineering assistant instructor at Ajman university.

In September 2021, she joined the Biomedical Engineering master's program at the American University of Sharjah as a graduate teaching assistant. During her master's study, she co-authored a journal paper, titled “Acoustically-activated liposomal nanocarriers to mitigate the side effects of conventional chemotherapy with a focus on emulsion-liposomes”.